



NASA CR 165312

NASA CR-165,312

**NASA**

NASA-CR-165312  
19810013548

# The Electric Rail Gun for Space Propulsion

DAVID P. BAUER  
JOHN P. BARBER

INTERNATIONAL APPLIED PHYSICS, INC.

C. JULIAN VAHLBERG

BUSINESS AND TECHNOLOGICAL SYSTEMS, INC.

FEBRUARY 1981

FINAL TECHNICAL REPORT:  
CONTRACT No. NAS3-22475  
NASA-LEWIS RESEARCH CENTER  
CLEVELAND, OHIO

MAY

**IAP**





**INTERNATIONAL APPLIED PHYSICS INC.**

7546 MC EWEN RD. DAYTON, OHIO 45459  
TELEPHONE: (513) 435-8752 • TELEX: 288278 • CABLE: INTALAP

28 April 1981

Dear Sir:

By request of Mr. William Kerlake, NASA-Lewis Research Center, Cleveland, please find enclosed one copy of NASA CR 165312, "The Electric Rail Gun for Space Propulsion." It is the final technical report on contract number NAS3-22475.

Yours truly,

A handwritten signature in cursive script, appearing to read 'David P. Bauer', written in dark ink.

David P. Bauer  
Research Engineer

DPB:nl



NASA CR 165312



# The Electric Rail Gun for Space Propulsion

DAVID P. BAUER

JOHN P. BARBER

INTERNATIONAL APPLIED PHYSICS, INC.

C. JULIAN VAHLBERG

BUSINESS AND TECHNOLOGICAL SYSTEMS, INC.

FEBRUARY 1981

FINAL TECHNICAL REPORT:

CONTRACT No. NAS3-22475

NASA-LEWIS RESEARCH CENTER

CLEVELAND, OHIO



N81-22078#



1. Report No. NASA CR 165312		2. Government Accession No.		3. Recipient's Catalog No.	
4. Title and Subtitle The Electric Rail Gun for Space Propulsion				5. Report Date February 1981	
				6. Performing Organization Code	
7. Author(s) David P. Bauer, John P. Barber, C. Julian Vahlberg				8. Performing Organization Report No.	
9. Performing Organization Name and Address International Applied Physics, Inc. 7546 McEwen Road Dayton, Ohio 45459				10. Work Unit No. YOS0939 RTOP 506-55-32	
				11. Contract or Grant No. NAS3-22475	
12. Sponsoring Agency Name and Address National Aeronautical and Space Administration Lewis Research Center 21000 Brookpark Cleveland, Ohio 44135				13. Type of Report and Period Covered Final Report 24 June 1980 - 30 Jan 1981	
				14. Sponsoring Agency Code	
15. Supplementary Notes  NASA Project Manager: W. R. Kerslake, NASA LeRC, Cleveland, Ohio					
16. Abstract An analytic feasibility investigation of an electric propulsion concept for space application is described in this report. In this concept, quasistatic thrust, due to inertial reaction to repetitively accelerated pellets by an electric rail gun would be used to propel a spacecraft. The study encompassed the major subsystems required in an electric rail gun propulsion system. The mass, performance and configuration of each subsystem was described. Based on an analytic model of the system mass and performance, the electric rail gun mission performance as a reuseable orbital transfer vehicle (OTV) was analyzed and compared to a 30 cm ion thruster system (BIMOD) and a chemical propulsion system (IUS) for payloads with masses of 1150 kg and 2300 kg. For system power levels in the range from 25 kW <sub>e</sub> to 100 kW <sub>e</sub> an electric rail gun OTV would be more attractive (have lower mass) than a BIMOD system for low earth orbit to geosynchronous orbit transfer durations in the range from 20 to 120 days.					
17. Key Words (Suggested by Author(s)) Rail Gun Electric Propulsion Space Systems Electromagnetic Accelerator			18. Distribution Statement  unclassified - unlimited		
19. Security Classif. (of this report) Unclassified		20. Security Classif. (of this page) Unclassified		21. No. of Pages 150	22. Price*

\* For sale by the National Technical Information Service, Springfield, Virginia 22161



## TABLE OF CONTENTS

<u>SECTION</u>		<u>PAGE</u>
1	INTRODUCTION	1
	1.1 SUMMARY OF ANALYSES	3
2	ELECTRIC RAIL GUN PROPULSION SYSTEM ANALYSES	5
	2.1 THE ELECTRIC RAIL GUN THRUSTER CONCEPT	5
	2.2 RAIL GUN PROPULSION SUBSYSTEMS	7
	2.2.1 Primary Power Supply	9
	2.2.2 The Rail Gun Thruster	14
	2.2.2.1 Rail Gun Efficiency	14
	2.2.2.2 Rail Gun Mass	19
	2.2.3 Power Conditioning	23
	2.2.3.1 DC Converter	26
	2.2.3.2 Capacitive Energy Store	29
	2.2.3.3 Solid State Switch	31
	2.2.3.4 Pulse Forming Inductor	34
	2.2.3.5 Performance and Configuration	38
	2.2.4 Propellant Handling System	41
	2.2.4.1 Propellant Handling System Options	42
	2.2.4.2 Mass and Performance	46
	2.2.4.3 Pellet Disposal	53
	2.2.5 Waste Heat Rejection	56
	2.2.5.1 Radiator Performance	57
	2.2.5.2 Radiator Mass and Configuration	64
	2.3 SYSTEM PERFORMANCE	69
3	MISSION ANALYSIS	77
	3.1 ELECTRIC RAIL GUN SYSTEM	79
	3.2 COMPARISON OF ALTERNATIVE PROPULSION SYSTEMS	82
4	CONCLUSIONS AND RECOMMENDATIONS	87
A	ELECTRIC GUN MISSION ANALYSIS RESULTS FOR NASA	A-1

## LIST OF ILLUSTRATIONS

	<u>PAGE</u>
1. A simple parallel rail electric gun.	6
2. The major electric rail gun propulsion subsystem.	8
3. Solar cell electrical characteristics.	11
4. SEPS solar cell array wing.	13
5. Inductively driven rail gun simulation circuit.	16
6. Electric rail gun cycle efficiency.	20
7. Rail gun cross section.	20
8. Major components of power conditioning system.	24
9. Circuit components of power conditioning system.	25
10. Block diagram of DC-DC series resonant converter.	27
11. Series resonant converter specific mass and efficiency (from Reference 13).	29
12. Conceptual configuration of 25 kW <sub>e</sub> power conditioning system.	40
13. Solid propellant pellet former.	51
14. Exhaust velocities which result in pellet stable orbits.	56
15. Meteoroid bumper protected radiator.	62
16. Bumper shielded and unshielded radiator performance comparison.	63
17. Radiator specific mass.	66
18. Rail gun radiator concept.	68
19. Coolant channels in rail gun.	69
20. Electric rail gun propulsion system mass compared to BIMOD.	72
21. Electric rail gun propulsion system efficiency compared to BIMOD.	73

List of Illustrations (cont.)

	<u>PAGE</u>
22. Conceptual configuration of electric rail gun propulsion system.	74
23. Mass requirements to transfer a 2300 kg payload from LEO to GEO with a rail gun OTV.	80
24. Pellet exhaust velocity requirements to transfer a 2300 kg payload from LEO to GEO with a rail gun OTV.	80
25. Effect of reuseable verses one-way missions on rail gun propulsion system mass requirements.	82
26. Effect of payload mass on rail gun propulsion system mass requirements.	83
27. Comparison of alternative propulsion systems for one-way OTV missions.	84

LIST OF TABLES

	<u>PAGE</u>
1. Effect of SEPS Solar Cell Array Characteristics on Propulsion System	10
2. Parameters Effecting Rail Gun Efficiency	18
3. Summary of Capacitive Based Power Conditioning Mass and Performance	39
4. Propellant Handling System Options	43

## NOMENCLATURE

$D_f$	=	outside diameter of solid bar propellant coil
$D_m$	=	mandrel diameter
$E_{ke}$	=	pellet kinetic energy
$E_s$	=	energy required to launch a pellet
$I_o$	=	maximum allowable rail gun current
$L_o$	=	inductance of rail gun drive inductor
$L'$	=	inductance of rail gun per unit length
$M_c$	=	capacitive energy store mass
$M_d$	=	total clamp diode mass
$M_{DC}$	=	DC converter mass
$M_f$	=	propellant mass
$M_{ff}$	=	fluid pellet forming system effective mass
$M_{ft}$	=	fluid propellant transport mass
$M_L$	=	mass of propellant handling/loading system
$M_{LR}$	=	mass of pulse forming coil which satisfies efficiency constraint
$M_m$	=	preformed bar storage mandrel mass
$M_{ps}$	=	solar cell array mass
$M_r$	=	radiator mass
$M_s$	=	total switch/clamp system mass
$M_{sf}$	=	mass of solid pellet shear system
$M_{st}$	=	solid bar propellant transport mass
$M_{sw}$	=	total thyristor switch mass
$M_t$	=	propellant tank mass
$P$	=	output power of solar cell array
$P_{pc}$	=	power input to the power conditioner

Nomenclature (cont.)

- $P_r$  = thermal power to be rejected
- $P_s$  = average power required to shear solid propellant bar
- $P_t$  = propellant storage tank pressure
- $Q$  = heat of fusion
- $R_o$  = resistance of rail gun drive inductor
- $R_r$  = resistance of rail gun per unit length
- $T$  = average radiator temperature
- $T_o$  = effective sink temperature
- $V_s$  = capacitor energy storage voltage
- $a$  = mean radius of Brook's coil
- $d$  = pellet length
- $d_r$  = rail thickness
- $d_s$  = rail gun confining structure thickness
- $\bar{d}$  = average coil mass density
- $h$  = rail gun bore size
- $k_1$  = BIMOD propellant system specific mass
- $k_2$  = specific mass
- $m$  = pellet mass
- $r_e$  = earth radius
- $r_o$  = orbital radius, from center of earth
- $v$  = pellet exhaust velocity
- $v_c$  = pellet exhaust velocity which causes pellet capture by earth during LEO to GEO transfer
- $v_e$  = pellet exhaust velocity which causes earth escape during LEO to GEO transfer
- $v_i$  = pellet exhaust velocity which causes pellet escape during GEO to LEO transfer

## Nomenclature (cont.)

- $w$  = radiator specific radiated power (thermal power per unit surface area)
- $x$  = rail gun length
- $\alpha_{hr}$  = specific mass of radiator
- $\delta$  = electrical skin depth
- $\epsilon$  = fraction of coil cross-section occupied by conductor (coil packing factor)
- $\epsilon_e$  = emissivity
- $\eta_a$  = rail gun efficiency
- $\eta_c$  = capacitive energy store efficiency
- $\eta_r$  = refrigeration system efficiency
- $\rho$  = mass density
- $\sigma$  = stress
- $\sigma_o$  = maximum allowable stress
- $\sigma_{sb}$  = Stefan-Boltzmann constant
- $\tau$  = solid propellant shear strength
- $\tau_a$  = pellet launch time



SECTION 1  
INTRODUCTION

The economical launch of spacecraft to low earth orbit (LEO) will soon be possible with the space shuttle. Many currently contemplated satellites however must be placed in geosynchronous orbit (GEO). Since the shuttle itself cannot effectively reach GEO, alternative propulsion techniques are being examined for the LEO to GEO satellite transfer. In this report we investigate an electric propulsion concept which might be used for the LEO to GEO orbital transfer mission.

Recognition of the potential advantages of electric propulsion has spurred the development of electric thrusters since the early 1960's. Electric propulsion systems feature highly efficient use of propellant relative to chemical rockets. For a given mission therefore, an electric propulsion system would require less propellant and this implies lower costs. In orbital transfer missions the attractiveness of electric propulsion systems is enhanced by the inherent reusability of the propulsion system. With a relatively small additional expenditure of propellant an electric propulsion system may be returned from GEO to LEO, refueled, and the cycle repeated for another payload.

Unfortunately highly developed electric propulsion systems (i.e., ion thrusters) have low thrust relative to propulsion system mass. Ion thruster propulsion systems therefore produce very low spacecraft acceleration and result in long mission durations.

For some planned missions these trip times are unacceptably long. Advanced electric propulsion concepts which combine the characteristics of highly efficient propellant use with improved thrust per unit mass of spacecraft are of ever increasing interest. This report describes the characteristics and performance of an electric rail gun based propulsion system which combines these desirable features.

The objective of this program was to evaluate the feasibility of an electric rail gun based propulsion system as a LEO to GEO orbital transfer vehicle. The study was an analytical investigation encompassing the major subsystems and components which would comprise an electric rail gun based propulsion system configured as a reusable orbital transfer vehicle (space tug) for payloads with mass up to 2300 kg. We analyzed each major subsystem and component from a systems viewpoint. The analysis of the system and each major subsystem began by identifying the parameters which may be used to characterize performance. A detailed performance analysis of each subsystem was conducted. State-of-the-art technology was used to describe the performance, mass and geometrical configuration of an electric rail gun orbital transfer vehicle (OTV). Gaps between state-of-the-art technology and performance projections were identified and assessed. An analytical model describing system mass and performance was assembled from the subsystem analyses. The mission performance of the electric rail gun propulsion system was established and compared to an ion thruster electric propulsion concept (BIMOD) and to a chemical propulsion

system (IUS). The approach and results of the analyses are described in this report.

### 1.1 SUMMARY OF ANALYSES

The analyses reported herein show that:

- (1) State-of-the-art technology and near-term advances can provide the subsystem characteristics required for an electric rail gun OTV with attractive performance.
- (2) The major technology unknown common to most subsystems is component life and reliability.
- (3) An electric rail gun OTV could accomplish a LEO to GEO transfer in approximately one-fourth of the minimum duration obtainable with a BIMOD ion thruster OTV.
- (4) An electric rail gun OTV would have lower total initial mass in LEO than a BIMOD system for all LEO to GEO transfer durations less than 115 days.
- (5) An electric rail gun OTV configured for a 30 day LEO to GEO transfer would have one-half the initial mass in LEO of a IUS system (which would perform the transfer in less than one day). At an initial mass equal to the IUS the electric rail gun OTV could perform the transfer in 15 days.

Generalizing, we conclude that an electric rail gun OTV would have the attractive feature of efficient propellant usage of other electric thrusters, with performance characteristics which permit mission durations intermediate between chemical rockets and ion thrusters.

The study described herein complements an earlier feasibility

study of the electric rail gun propulsion concept as a reuseable OTV for much larger payloads (i.e., payload mass up to 22,700 kg).<sup>1</sup> Much of the analysis developed in Reference 1 was used, with the primary emphasis on evaluating scaled-down characteristics for the various subsystems.

The analysis and results of this electric rail gun propulsion system study are described in the remaining three sections of this report. Section 2 begins with a brief review of the electric rail gun concept and its application to a propulsion system. The major components and subsystems comprising an electric rail gun propulsion system are identified. The performance of each subsystem is described and conceptual sketches showing the essential features of the subsystem are provided. Section 2 concludes with a system mass and performance description assembled from the subsystem analyses. Section 3 describes the mission analyses and performance of the rail gun propulsion system as an orbital transfer vehicle. The mission performance of the electric rail gun propulsion system is compared to that of a BIMOD system and an IUS system. The relative advantages and disadvantages of each system are described. In Section 4 we discuss electric rail gun propulsion system feasibility and outline our conclusions. We also describe the technological developmental requirements and suggest approaches to satisfy these requirements.

---

<sup>1</sup>Bauer, D., Barber, J., Swift, H., and Vahlberg, C., "Electric Rail Gun Propulsion Study (Advanced Electric Propulsion Technology High Thrust)", Air Force Rocket Propulsion Laboratory, AFRPL-TR-81-02, December 1980.

## SECTION 2

### ELECTRIC RAIL GUN PROPULSION SYSTEM ANALYSIS

This section begins with a description of the electric rail gun concept and its application to space propulsion. The major subsystems required in an electric rail gun propulsion system are identified. The mass, performance and conceptual configuration of each subsystem are described. A system mass and performance description is assembled and compared to the BIMOD system.

#### 2.1 THE ELECTRIC RAIL GUN THRUSTER CONCEPT

A simple parallel rail gun consists of a pair of electrodes which form two opposite sides of a rectangular bore accelerator channel. The other two sides which complete the bore are made up of a dielectric material. A rectangular parallelepiped projectile (pellet) is placed in the gun bore as shown in Figure 1. At the rear of the projectile an electrically conducting armature contacts each of the rails. An electrical potential, applied across the rails at the breech, drives current down one rail through the electrically conducting armature and back to the breech through the other rail. Current in the rails produces a magnetic field between the rails. The current flowing in the armature interacts with the magnetic field to produce a force which accelerates the armature and projectile. Projectile velocities of 6 km/s have been demonstrated with electric rail guns and recent experiments may have reached as high as 10 km/s.<sup>2,3</sup> A complete description

<sup>2</sup>Rashleigh, S., and Marshall, R., "Electromagnetic Acceleration of Macroparticles to High Velocities," J. Appl. Phys., March 1978.

<sup>3</sup>Hawke, R., et al, "Results of Railgun Experiments Powered by Magnetic Flux Compression Generators," Lawrence Livermore National Laboratory, UCRL-84875, 1980.

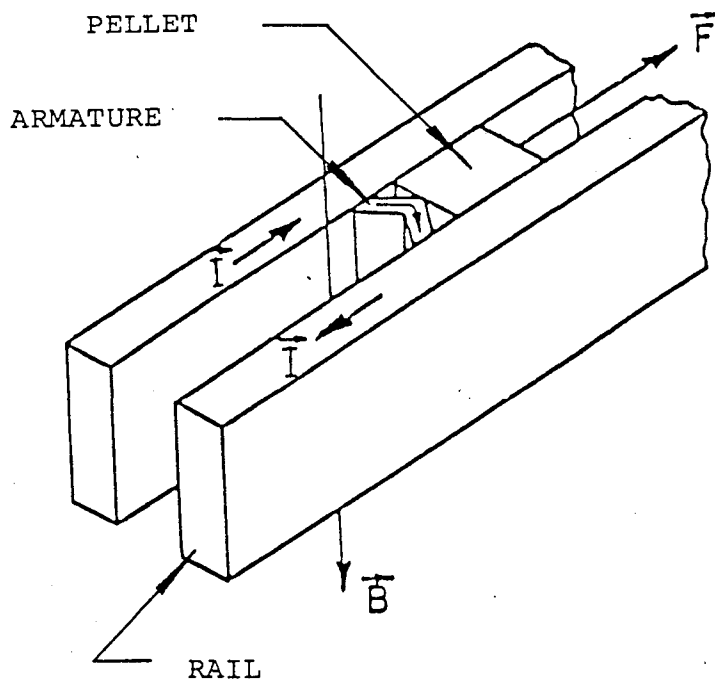


Figure 1. A simple parallel rail electric gun.

of electric rail gun characteristics is provided in Reference 4.

Pellets can be made from almost any material. The pellets must however possess sufficient strength to withstand acceleration stresses. High strength solid phase materials permit efficient high acceleration but low strength solids and liquids within a solid carrier could also be launched.

The current carrying armature behind the pellet would probably be a plasma for an electric rail gun in a spaceborne propulsion system. The plasma would be formed at the initiation of pellet

---

<sup>4</sup>Barber, J., "The Acceleration of Macroparticles in a Hypervelocity Electromagnetic Accelerator", Ph.D. Thesis, The Australian National University, 1972.

launch, by exploding a thin metallic foil. Plasma pressure on the rear of the pellet would cause acceleration. Close pellet conformity to the rail gun bore would be required for plasma obturation.

Inertial reaction to the accelerated pellet (gun recoil) produces a force in the rail gun opposite in direction to the pellet velocity vector. A spacecraft could be propelled with the quasi-static thrust generated by launching pellets repetitively.

## 2.2 RAIL GUN PROPULSION SUBSYSTEMS

In an electric propulsion system the rail gun is the device which converts electrical energy to kinetic energy and propulsive thrust. In addition to the rail gun thruster, several essential subsystems comprise the complete space propulsion system. In the study reported herein our objective was to examine all the subsystems which could effect the feasibility of the electric rail gun propulsion concept. Figure 2 shows the five major subsystems on which the concept feasibility study was based. Each of the five subsystems is associated with major power flow in the propulsion system and/or represents one of the major components of system mass. The primary power source supplies the average system power required for propulsion. A power conditioning system is required to convert the average power from the primary supply to high power, high current pulses required to drive the rail gun. The rail gun itself then converts these high current electrical pulses to pellet kinetic energy. Pellets are loaded into the breech of the rail gun at the required pulse repetition rate from a pro-

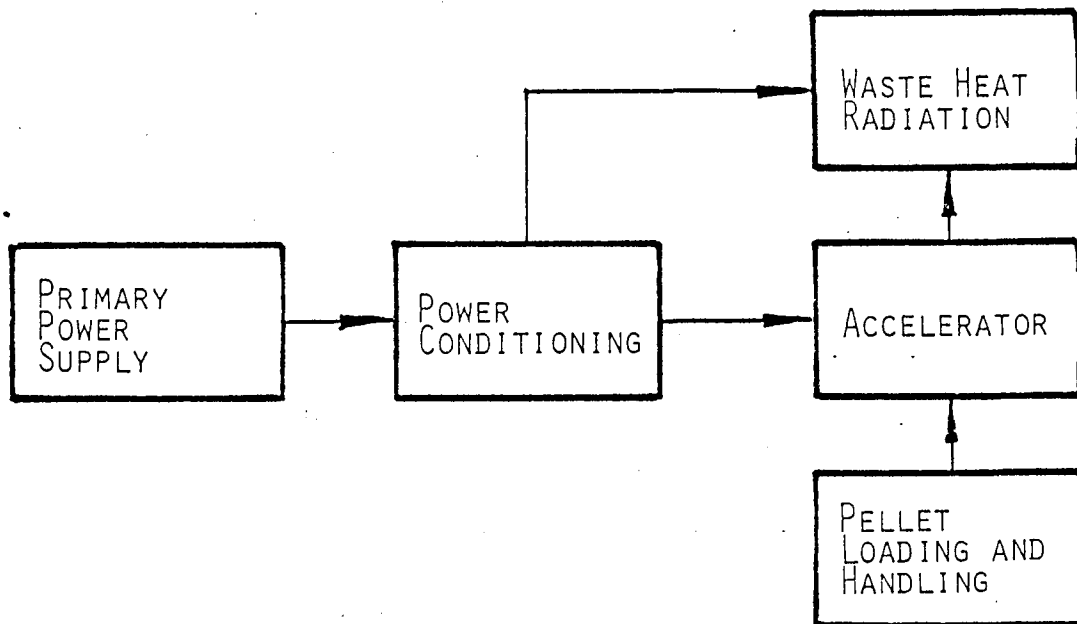


Figure 2. The major electric rail gun propulsion subsystem.

pellant store, by a pellet storage/loading subsystem. Waste thermal energy generated by the electric rail gun and the power conditioning subsystems must be rejected to maintain acceptable operating temperature. An analysis of each of these propulsion subsystems is provided in the following sections.

As discussed in Section 1, the overall objective of this study was to establish the technical feasibility of an electric rail gun propulsion system, and to describe its performance as an orbital transfer vehicle in near-earth space. The objective of the subsystem studies was therefore to evaluate subsystem performance. Expressions defining subsystem mass and efficiency as a function of the independent variables were developed to characterize each subsystem. A conceptual configuration of each subsystem was also

developed in the course of these analyses. The subsystem analyses are described in the following paragraphs.

### 2.2.1 Primary Power Supply

In this study the propulsion system primary power source was assumed to be a solar cell array with SEPS type solar cell array characteristics. SEPS arrays have been designed for ion thruster propulsion applications requiring power levels ranging from 25 kW<sub>e</sub> to 100 kW<sub>e</sub>.<sup>5</sup> Propulsion power levels in this study were limited to 25-100 kW<sub>e</sub>. Most characteristics designed into the SEPS solar cell array for other electric propulsion applications make it attractive for application with the electric rail gun propulsion concept. Details of the array are listed in Table 1. We discuss several of the SEPS array characteristics shown in Table 1 and evaluate SEPS compatibility to the electric rail gun propulsion concept in the following paragraphs.

Solar cell electrical output characteristics influence the power conditioning subsystem design requirements. A solar cell behaves as a voltage limited current generator with internal series resistance. Solar cell current voltage characteristics are shown in Figure 3. These curves show that solar cells and therefore solar cell arrays have a well defined peak output power point. This implies that the array must be connected to a matched

---

<sup>5</sup>Young, L., "Solar Array Technology for Solar Electric Propulsion Missions," AIAA Paper No. 79-3086, Presented at the 14th International Electric Propulsion Conference, Princeton, NJ, October 30 - November 1, 1979.

TABLE 1. EFFECT OF SEPS SOLAR CELL ARRAY CHARACTERISTICS ON PROPULSION SYSTEM

<u>CHARACTERISTICS</u>	<u>EFFECT ON PROPULSION SYSTEM</u>
CELL/ARRAY OUTPUT POWER CHARACTERISTICS	
<ul style="list-style-type: none"> <li>• VOLTAGE LEVEL--300-500 V</li> <li>• MAXIMUM POWER POINT SENSITIVE TO LOAD IMPEDANCE (SEE FIGURE 3)</li> <li>• CHARGED PARTICLE DEGRADATION OF CELL EFFICIENCY BEGINNING-OF-LIFE (BoL)--9-10% END-OF-LIFE (EoL)--6-7%</li> </ul>	<ul style="list-style-type: none"> <li>• POWER CONDITIONING VOLTAGE SCALING REQUIRED</li> <li>• ACTIVE CONTROL OF POWER CONDITIONING INPUT IMPEDANCE REQUIRED</li> <li>• 30-40% ARRAY OVERSIZING REQUIRED</li> </ul>
ARRAY CONFIGURATION/MECHANICAL CHARACTERISTICS	
<ul style="list-style-type: none"> <li>• PLANAR ARRAY GEOMETRY</li> <li>• FLEXIBLE ROLL-OUT SOLAR CELL BLANKETS</li> <li>• SYMMETRIC TWO WING GEOMETRY</li> <li>• HIGH WING ASPECT RATIO--8:1</li> <li>• SPECIFIC POWER (BoL)--125 W/M<sup>2</sup></li> <li>• FUNDAMENTAL VIBRATIONAL MODE--0.02 HZ</li> <li>• SPECIFIC MASS (BoL)--0.0135 KG/W</li> </ul>	<ul style="list-style-type: none"> <li>• SUN TRACKING ACCURACY LESS CRITICAL (THAN CONCENTRATED ARRAY DESIGNS)</li> <li>• COMPACT STORAGE AND STRAIGHT FORWARD DEPLOYMENT</li> <li>• FOR 50 KW<sub>E</sub> OUTPUT EACH WING, 5 M WIDE BY 40 M LONG</li> <li>• ELECTRIC RAIL GUN LAUNCH FREQUENCY MUST BE GREATER THAN 5 HZ</li> <li>• FOR 50 KW<sub>E</sub> OUTPUT TOTAL POWER SUPPLY MASS--675 KG</li> </ul>

impedance load in order to draw the maximum power. Operation of the solar cell array away from the maximum power point reduces overall efficiency and requires array oversizing and increased array mass.

Propulsion system OTV performance would be adversely effected by solar cell array power output degradation. High energy charged particles trapped in near earth space (especially in the Van Allen belts) would impact the solar cell array during a LEO to GEO transfer mission. Impact by these charged particles severely degrades solar cell output power and adversely affects mission performance. As discussed in Appendix A, detailed modeling of

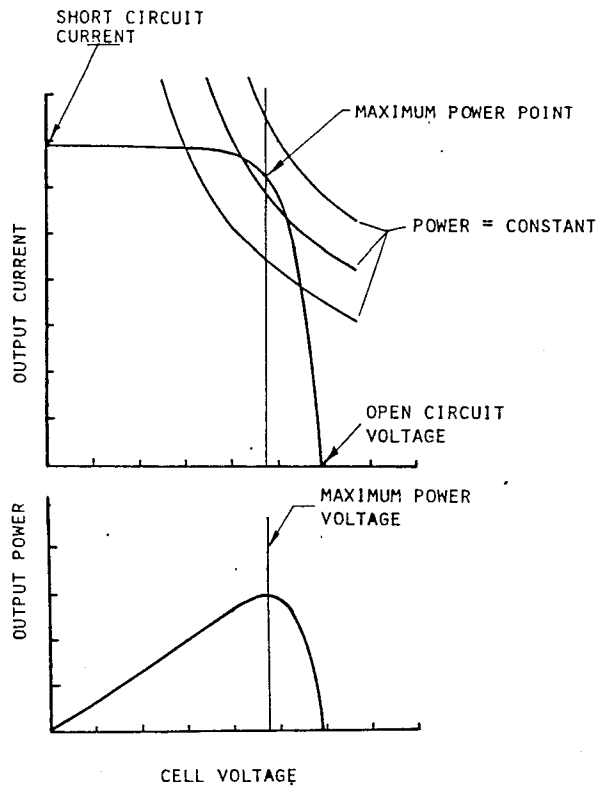


Figure 3. Solar cell electrical characteristics.

the effects of cell degradation on mission performance were beyond the capability of existing mission analysis programs. In Reference 1 simplified calculations of solar cell degradation were performed based on solar cell performance descriptions provided in Reference 6. These estimates showed that SEPS type silicon solar cells would suffer 30-40% reduction in power output for a single LEO to GEO transfer. Power output degradation of this magnitude would be unacceptable for a reusable OTV system. Initial development results for radiation damage resistant solar cells (for example Ga-Al-As),

---

<sup>6</sup>Tada, H., and Carter, J. Jr., "Solar Cell Radiation Handbook," JPL Publication 77-56, Jet Propulsion Laboratory, Pasadena, CA, November 1977.

which could be used in a SEPS type array, indicate that severe degradation can be prevented.<sup>7,8</sup>

The SEPS type solar cell array power supply is a two-winged configuration designed for in-orbit deployment from stowage. Silicon solar cells with electrical interconnections attached to a thin Kapton substrate form the solar cell blanket. This solar cell blanket is stowed during transport from earth to orbit by rolling onto a mandrel or by folding into a box. In orbit the solar cell array is deployed by a self extending truss-type mast. A fold out version of one of these array wings is shown in Figure 4. In addition to the solar cells and the deployment mechanism each wing includes bus strips, slip ring assembly, relays and other hardware necessary to supply power to the spacecraft.

A SEPS type solar cell array would possess adequate mechanical characteristics to make it compatible with an electric rail gun propulsion system. An electric rail gun propulsion system like an ion thruster system would provide low acceleration propulsion with concomitant low inertially induced stress on the array. The pulsed load operation of the electric rail gun would excite harmonic vibrations of the solar cell array. Excitation of the fundamental or low harmonics would result in unacceptably high

---

<sup>7</sup>Hanley, G.M., "Evolution of Satellite Power System (SPS) Concepts," Report No. 78-9403, In Proceedings of the 13th Intersociety Energy Conversion Conference, August 20-25, 1978, San Diego, CA.

<sup>8</sup>Tonelli, A.D., and Nussberger, A.A., "The Design and Evaluation of a 5 GW Ga-Al-As Solar Power Satellite (SPS)," Report No. 78-9404, In Proceedings of the 13th Intersociety Energy Conversion Conference, August 20-25, 1978, San Diego, CA.

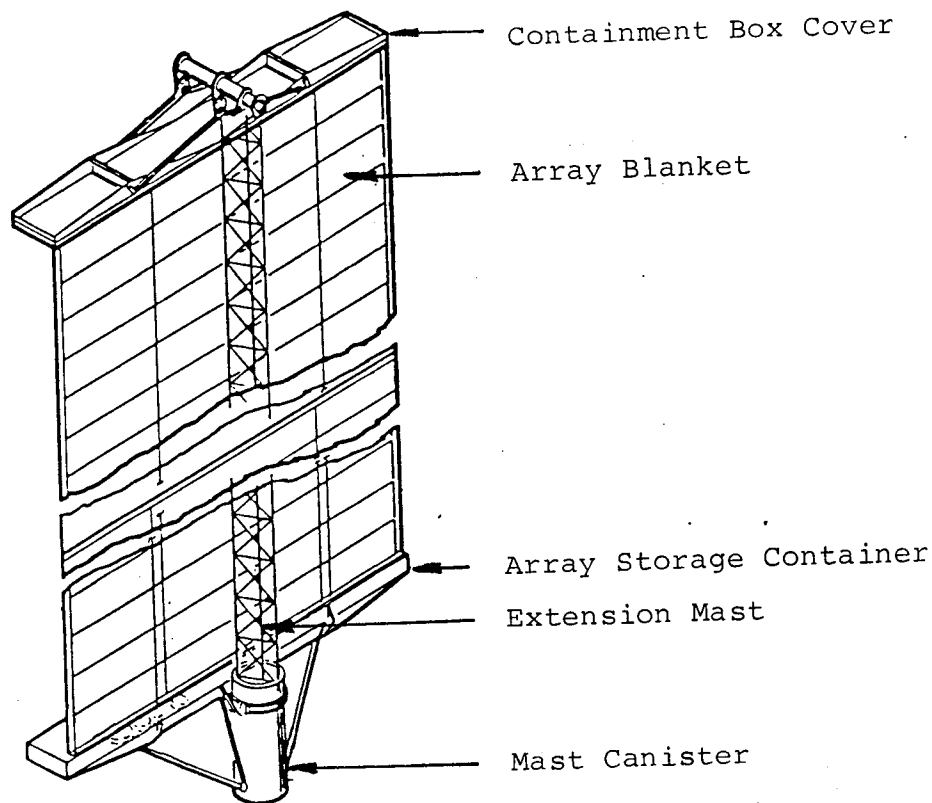


Figure 4. SEPS solar cell array wing.

deflections and dynamic stresses in the array. Fortunately the fundamental vibrational frequency of the SEPS array is 0.02 Hz while the pulse frequency of the electric rail gun would be in the range from about 5-15 Hz. As a result the electric rail gun would excite harmonic modes much higher than the fundamental. At these higher frequencies hysteretic damping throughout the array would effectively dissipate the energy of the harmonic vibrations.<sup>9</sup> Therefore vibration induced stresses and deflections in the solar cell array would not be a serious problem in an electric rail gun propulsion system.

---

<sup>9</sup>Harris, C., and Crede, C., Ed., "Shock and Vibration Handbook", McGraw Hill Book Company, 1976, Chapters 36 and 37.

The mass of a solar cell array is linearly related to output power by a constant of proportionality called the specific mass. In this study we used a specific mass of 13.5 kg/kW<sub>e</sub> for the SEPS solar cell array. The equation relating power supply mass, M<sub>ps</sub>, to array output power, P, may therefore be written as

$$M_{ps} = 0.0135P \quad (1)$$

Equation (1) was used to define power supply mass for the system and mission analyses. The same value was used for both the ion thruster propulsion system and the electric rail gun propulsion system.

#### 2.2.2 The Rail Gun Thruster

In this section we examine the efficiency, mass and configuration of an electric rail gun for a propulsion system. The efficiency with which the electric rail gun converts electric energy to kinetic energy directly effects the size of all other subsystems and therefore is the primary determinant of system performance. The analytical study of single stage inductively driven rail guns described in Reference 1 was extended to the smaller size range under investigation herein.

##### 2.2.2.1 Rail Gun Efficiency

The analysis of rail gun performance was begun by performing an energy balance on the electric rail gun circuit, to determine energy partitioning during a single pellet launch or cycle. The rail gun cycle is defined as the sequence of events beginning with drive inductor current charging and including;

discharging the inductive energy into the rail gun; and accelerating the pellet. The cycle ends when the drive inductor is again ready for recharging. The rail gun cycle efficiency,  $\eta_a$ , is defined as the ratio of pellet kinetic energy (at exhaust velocity) to the sum of the kinetic energy plus energy losses. The pellet kinetic energy,  $E_{ke}$ , is described by the familiar relationship

$$E_{ke} = mv^2/2 \quad (2)$$

where,  $m$ , is the pellet or projectile mass, and  $v$ , is pellet exhaust velocity from the gun. The cycle energy losses may be described by referring to Figure 5. Energy losses during a cycle arise from two sources: resistive energy losses occur during drive inductor charging and during pellet acceleration; and residual magnetic energy stored in the inductor and accelerator at the end of a cycle was assumed to be entirely lost.

Resistive losses during a cycle arise from circuit resistance and rail gun resistance. As shown in Figure 5, a circuit resistance,  $R_o$ , was modelled as a lumped resistance characteristic of the inductor and connecting bus. The resistance of the rail gun,  $R_r$ , was modelled as a varying resistance related to the pellet motion along the gun. The rail resistance also included the "velocity skin effect" which tends to confine current to a thin sheet on the rail surface and significantly increases effective rail resistance.<sup>4</sup>

The magnetic losses at the end of a launch cycle result

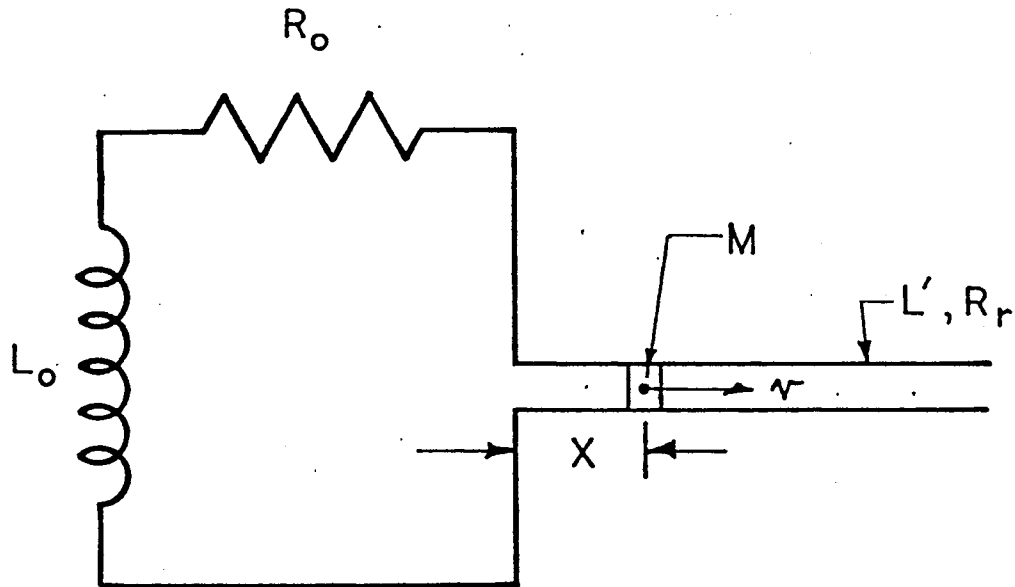


Figure 5. Inductively driven rail gun simulation circuit.

from incomplete magnetic flux expansion. Magnetic flux remains stored in both the drive inductor and the rail gun if current is still flowing in the rail gun circuit as the pellet exits the gun muzzle. If nothing is done to recapture this magnetic energy some of it will be converted to ohmic heating of the rails and a large fraction would be dissipated in an arc at the accelerator muzzle. Conceivably some of the residual magnetic energy could be recaptured by appropriate current clamping and other techniques. However for this analysis we assumed that the residual magnetic energy was an energy loss.

A mathematical model of rail gun pellet acceleration was developed which included the energy loss mechanisms just identified. The modelling resulted in a system of differential equations.

These equations were solved incrementally in a time stepped fashion using finite difference techniques and a digital computer. The rail gun analysis enabled us to identify and analyze the parameters which affect rail gun efficiency.

Strategies were sought which would either maximize efficiency or, due to physical limitations, would lead to constraining conditions for each parameter. The seven major variables which effect efficiency are identified and the effect of each variable on rail gun efficiency is shown in Table 2. In addition, Table 2 also shows the implications of the optimizing or constraining conditions applied to each variable. Finally, the value of each parameter derived and used in the rail gun efficiency model is listed.

When all the possible optimization values of the parameters shown in Table 2 are applied we find that rail gun efficiency remains a function of two free independent variables, pellet exhaust velocity and rail gun bore size (pellet mass). Optimal values cannot be specified for these two parameters independent of mission requirements. To develop an analytical expression relating rail gun efficiency to these two independent parameters, we therefore conducted simulations using the computer model of rail gun efficiency and computed the efficiency for accelerators with the constraints specified in Table 2. The efficiency was calculated for pellets ranging in mass from 0.002 g - 2 g (corresponding to rail gun bore sizes ranging from 1 mm - 10 mm) and for pellet exhaust velocities ranging from 5 km/s to 20 km/s. Based on the data obtained from these efficiency simulations we found that rail gun efficiency

TABLE 2. PARAMETERS EFFECTING RAIL GUN EFFICIENCY

PARAMETER	INCREASING EFFICIENCY RESULTS FROM INCREASING/ DECREASING MAGNITUDE OF PARAMETER	OPTIMIZING VALUE OR PHYSICALLY IMPOSED CONSTRAINT	PHYSICAL IMPLICATIONS	VALUE OF PARAMETERS USED OR DERIVED
RAIL GUN INDUCTANCE PER UNIT LENGTH	INCREASING	OPTIMUM	RAIL GUNS WITH SQUARE BORE ARE OPTIMAL.*	$L' = 0.63 \mu\text{H}/\text{M}$
RAIL GUN LENGTH	INCREASING	OPTIMUM	PRACTICAL OPTIMUM LENGTH, X, IS A FUNCTION OF BORE SIZE AND EXHAUST VELOCITY FOR GIVEN VALUES OF OTHER PARAMETERS.**	$x = 45.6 \times 10^{-6} \text{HV}^2$
RAIL TEMPERATURE	DECREASING	CONSTRAINED	TRADEOFFS REQUIRED, TO OBTAIN PRACTICAL WASTE HEAT RADIATOR SIZE AND ADEQUATE STRENGTH RAILS WITH ACCEPTABLE RESISTIVITY.	$T = 450^\circ\text{K}$
RAIL GUN BORE SIZE	INCREASING	CONSTRAINED	SPECIFIED BY MISSION REQUIREMENTS.	$0.1 \text{ CM} < H < 1.0 \text{ CM}$
PELLET EXHAUST VELOCITY	DECREASING	CONSTRAINED	SPECIFIED BY MISSION REQUIREMENTS. BOUNDS WERE IMPOSED.	$5 \text{ KM/S} < v < 20 \text{ KM/S}$
PELLET ACCELERATING STRESS	INCREASING	CONSTRAINED	ACCELERATING STRESS LIMITED TO MAXIMUM ALLOWABLE STRESS IN PELLET.***	$\sigma_0 = 200 \text{ MN}/\text{M}^2$
PELLET AREAL DENSITY	DECREASING	CONSTRAINED	BOTH PELLET DENSITY, $\rho$ , AND PELLET LENGTH, D, SHOULD BE MINIMIZED. PRACTICAL PELLET DENSITY CHOSEN. PELLET LENGTH IN DIRECTION OF TRAVEL MUST BE LONGER THAN ONE-HALF THE BORE SIZE, TO PREVENT IN-BORE PELLET TUMBLING.*	$\rho = 3000 \text{ KG}/\text{M}^3$ $D = H/2$

\*THE COMBINATION OF A SQUARE BORE AND PELLET LENGTH EQUAL TO ONE-HALF THE BORE SIZE ALLOWS THE PELLET MASS TO BE RELATED DIRECTLY TO BORE SIZE (I.E.,  $m = \rho H^3/2 = 1500H^3$ ). GIVEN THE PELLET DENSITY, PELLET MASS AND BORE SIZE MAY BE USED INTERCHANGEABLY.

\*\*A PRACTICAL OPTIMUM CHARACTERISTIC PELLET ACCELERATION TIME IS THEREFORE IMPLIED AND WAS FOUND TO CORRELATE TO RAIL HEIGHT AND EXHAUST VELOCITY AS,  $\tau_A = 51 \times 10^{-6} \text{HV}$ .

\*\*\*THE COMBINATION OF A DEFINED OPTIMAL RAIL INDUCTANCE,  $L'$ , AND A DEFINED ALLOWABLE STRESS,  $\sigma_0$ , DEFINES THE PEAK RAIL GUN CURRENT,  $I_0$ , AS GIVEN BY,  $I_0 = (2\sigma_0/L')^{1/2} H = 2.52 \times 10^7 H$ .

correlated to a power law relationship as given by

$$\eta_a = 13.67m^{0.104}v^{-0.299} \quad (3)$$

The rail gun simulation data correlated to Equation 3 to better than 5% over the entire range of pellet mass and exhaust velocity. The predicted rail gun efficiency as a function of pellet mass and pellet exhaust velocity is illustrated in Figure 6. Figure 6 shows that efficiency increases as pellet mass (bore size) increases. Efficiency decreases as pellet exhaust velocity increases. Data from Reference 1 are also shown in Figure 6 to show that increasing rail gun bore size (higher pellet mass) increases efficiency. From Figure 6 we see that rail gun efficiency will range from 20% to 45% for pellets with mass of interest in this study.

#### 2.2.2.2 Rail Gun Mass

Rail gun mass was estimated based on a geometrical configuration which satisfies the imposed requirements. The overall rail gun bore size and length are optimally chosen to provide maximum efficiency. The thickness of the current conducting rails must be chosen to carry the high currents. The structure which surrounds the rails must be chosen to have adequate strength to withstand magnetic bursting forces on the rails. A rail gun barrel concept which satisfies these requirements is shown in Figure 7. It consists of a pair of rectangular cross-section copper rails enclosed in a high strength, fiber reinforced composite structure. The mass of the rail gun barrel was computed as the sum of the mass of the rails and the enclosing structure.

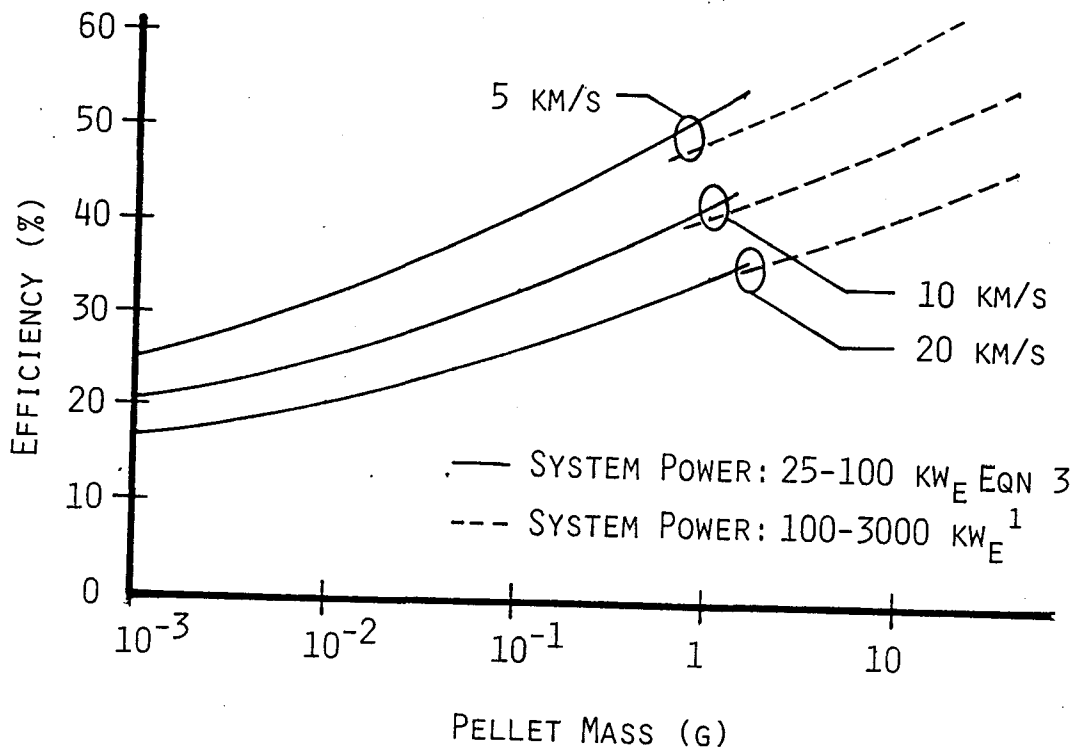


Figure 6. Electric rail gun cycle efficiency.

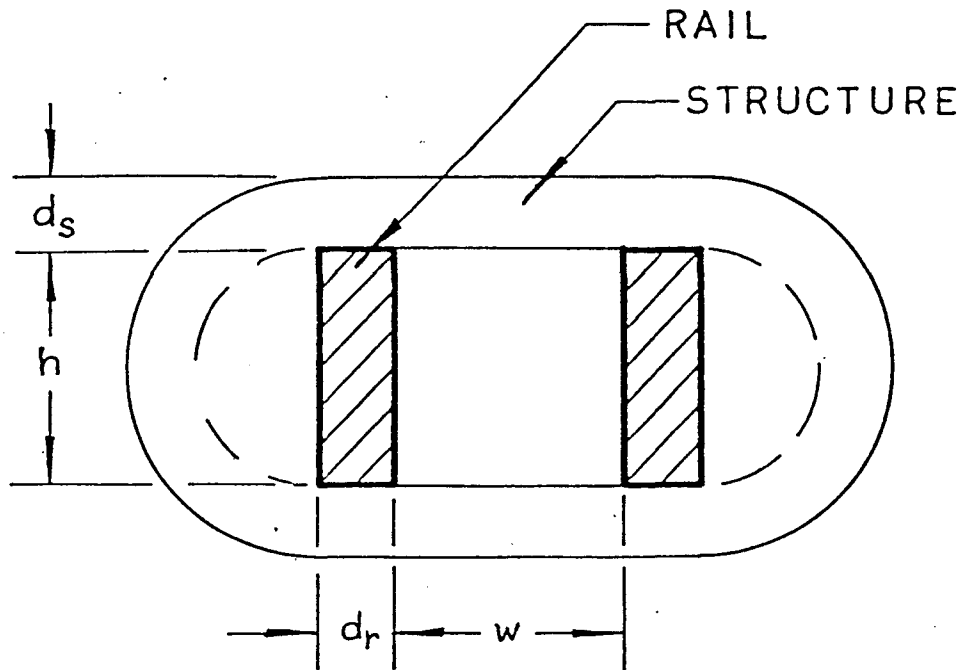


Figure 7. Rail gun cross section.

The rail mass is obtained as the product of rail volume and density. The rail length,  $x$ , is optimally chosen for maximum efficiency (from Table 2) and rail height,  $h$ , is determined based on mission requirements, as described in the previous section. Rail thickness,  $d_r$ , is chosen to be equal to the current diffusion distance into copper (the electrical skin depth  $\delta = (\pi K \tau_a)^{1/2}$  where,  $K$ , is the electrical diffusivity) during the pellet acceleration time,  $\tau_a$ . Based on this criteria for copper rails the rail thickness,  $d_r$ , may be written as

$$d_r = 0.2 \tau_a^{1/2} \quad (4)$$

The mass of the rails,  $M_r$ , is the product of rail volume and rail density and with Equation (4) may be written as

$$M_r = 0.4 h x \tau_a^{1/2} \rho_a \quad (5)$$

By combining the optimal rail gun length and characteristic acceleration time from Table 2 with Equation (5) the mass of copper rails may be written as

$$M_r = 1.17 \times 10^{-3} h^{5/2} v^{5/2} \quad (6)$$

The mass of the structure enclosing the rails is determined based on the allowable stress in the structural material. The principle stress induced in the fiber structure by the

magnetic bursting force on the rails would be tensile. The bursting pressure on the rails is approximately one-half the accelerating pressure on the projectile. A fiber reinforced composite material which could be used in the structure could safely support tensile stresses up to  $600 \text{ MN/m}^2$ . By relating the stress in the structure to the accelerating stress on the pellet we found that the structural wall thickness,  $d_s$ , is related to the bore height by

$$d_s = 0.3h \quad (7)$$

The containment structure cross-sectional area was then computed based on the design shown in Figure 7 and multiplied by the optimum accelerator length,  $x$ , to obtain the volume. Assuming that the average density of the fiber reinforced composite material is  $2000 \text{ kg/m}^3$  the mass of the containment structure may be written as

$$M_s = 0.176h^3v^2 + 1.57 \times 10^4 h^{5/2} v^{5/2} \quad (8)$$

The total mass of the accelerator,  $M_a$ , is obtained by summing the mass of the rails with the mass of the structure. The total mass may be written as a function of pellet mass and exhaust velocity by recalling from Table 1 that pellet mass may be written as a function of bore size ( $m = 1500 h^3$ ). Combining Equations (6) and (8) we obtain;

$$M_a = 1.17 \times 10^{-4} m v^2 + 2.99 \times 10^{-6} m^{5/6} v^{5/2} \quad (9)$$

For most space applications the fineness ratio of the accelerator (the ratio of accelerator length-to-containment structure diameter) would be very high, resulting in unacceptable flexibility of the accelerator. In Section 2.2.5 we show that the rail gun could be integrated with the waste heat radiator structure to provide adequate lateral stiffness.

### 2.2.3 Power Conditioning

The power conditioning system for the rail gun electric propulsion system is comprised of all components required to electrically interface the photovoltaic power supply to the rail gun. The overall purpose of power conditioning is to convert low voltage average power from the solar cell array to high current, high power pulses required by the rail gun for pellet acceleration. Several major components are required to perform power conditioning as shown in Figure 8. The DC converter performs basically as an impedance matching device, providing a constant impedance load to the solar cells while providing constant power variable current, variable voltage charging of the energy store. The energy store provides the means of converting the low average power of the solar cell array to high power pulses required by the rail gun to accelerate pellets to high velocity. To enable repetitive pulse operation of the rail gun switching elements cyclicly open and close to permit energy store charging, followed by rapid discharge into the rail gun. Finally, a pulse forming inductor efficiently transfers the energy pulse to the rail gun at high current

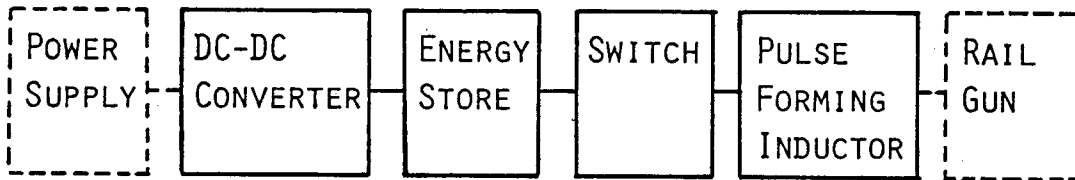


Figure 8. Major components of power conditioning system.

by matching the variable impedance characteristic of the rail gun. In this section we describe an analysis of each power conditioning component. The study objective was to analytically describe the mass and efficiency of the power conditioning components and to develop a geometrical configuration concept for the power conditioning system.

The rail gun propulsion system electrical circuit which was analysed is shown in Figure 9. A DC converter interfaces the solar cell array with a capacitive energy store. The capacitive energy store is charged with sufficient energy to supply the kinetic energy for a single pellet launch. When the capacitive

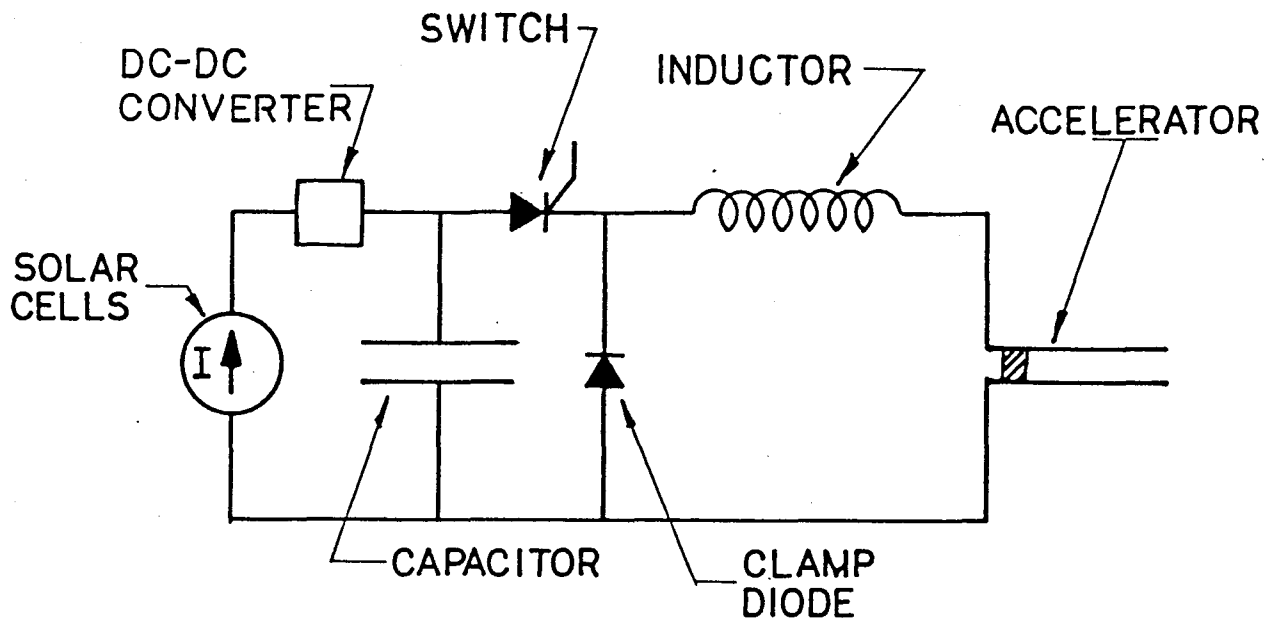


Figure 9. Circuit components of power conditioning system.

energy store reaches the required charge level a solid state switch is closed, transferring the capacitively stored energy to the pulse forming inductor. The pulse forming inductor lengthens the current pulse provided to the rail gun. A solid state clamp diode placed across the inductor-accelerator prevents damaging voltage reversal in the capacitive energy store by providing a short circuit to the energy in the inductor/rail gun circuit. A major advantage of the circuit concept shown in Figure 9 is the low duty cycle of high current components. Reducing the duration of high currents is attractive from the standpoint of reducing losses and simplifying component design. Low duty cycle makes solid state switching practicable. Solid state switching would provide higher reliability than mechanical switching devices.

In addition the capacitive based system concept shown in Figure 9 has lower mass than inductively stored energy concepts at the energy storage levels required for the propulsion system investigated.

#### 2.2.3.1 DC Converter

A DC converter technology which appears attractive for application in an electric rail gun system is an actively controlled series resonant inverter/converter. Series resonant converters are under development for spaceborne electric ion propulsion applications and for aircraft application. Many of the same features are required for the DC converter in an electric rail gun propulsion system.<sup>10,11,12</sup>

A simple block diagram of a series resonant DC converter is shown in Figure 10. Electrical power enters the converter through an input filter which isolates the source and the converter from electrical transients. The input filter consists primarily of diodes and capacitors. In the inverter two switch pairs consisting of thyristors and diodes are used to close and open in alternating succession two series resonant circuits of capacitors and inductors and the primary winding of the transformer.

---

<sup>10</sup>Biess, J., Inouie, J., and Schoenfeld, A., "Thyristor Power Processor for the 30 cm Mercury Electric Propulsion Engine," AIAA Paper 75-433, 1975

<sup>11</sup>Hansen, I., "Description of a 2.2 kW Power Transformer for Space Application," NASA Technical Memorandum 79138, NASA-Lewis Research Center, 1979.

<sup>12</sup>Schwarz, F., "A 10 kW Lightweight DC Converter (Technology Feasibility Study for Lightweight Megawatt Range Converters)," AFAPL-TR-77-45, Air Force Aero Propulsion Laboratory, Wright-Patterson AFB, 1977.

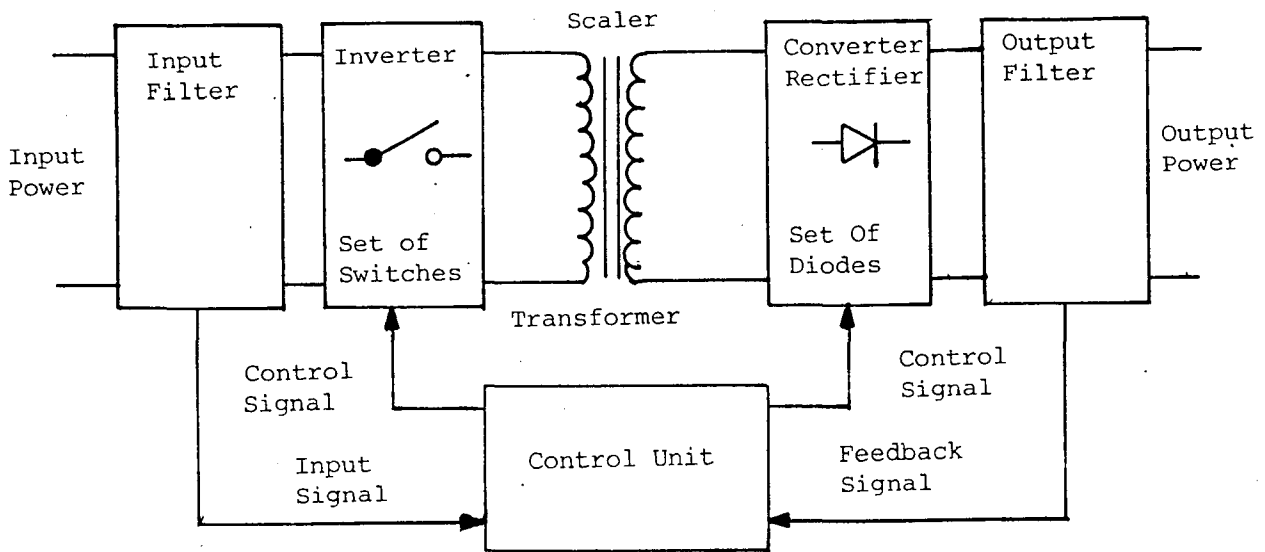


Figure 10. Block diagram of DC-DC series resonant converter.

The high frequency carrier current generated in the inverter is modulated in frequency and amplitude during generation. Active inverter modulation causes the inverter to effectively vary input impedance, enabling maximum power point tracking of the power supply (as described in Section 2.2.1), while providing constant power variable voltage/current energy store charging. The carrier current passes through the high frequency transformer which performs a voltage scaling function. A diode bridge connected to the secondary of the transformer rectifies the scaled current and a high frequency output filter removes the harmonic content. A series resonant converter therefore would satisfy the impedance matching requirements for efficient energy transfer from the solar cell array power supply to the capacitive energy store. State-of-

the-art converters with high internal operating frequencies (10-30 kHz) would satisfy low mass, high efficiency requirements of an electric rail gun converter.

Based on series resonant inverter designs for ion thrusters, Reference 13 presents results of a parametric evaluation which showed that DC converter mass, of state-of-the-art series resonant converter designs is controlled by the converter power input. DC converter mass,  $M_{DC}$ , was found to correlate to converter input,  $P$ , by a power series relationship, as given by

$$M_{DC} = 10 + 0.057P^{1/2} + 0.014P^{3/4} + 10^{-4}P \quad (9)$$

Based on Equation (9), Figure 11 illustrates that specific mass of DC converters significantly decreases as power level rises. Converter mass for power levels ranging from 25 to 100 kW<sub>e</sub>, would range from 49 to 117 kg respectively. We assume that the mass predicted by Equation (9) adequately predicts the DC converter mass for an electric rail gun propulsion system application.

High internal DC converter operating frequencies lead to reduction in the mass of the transformer, and other reactive components involved in the inversion and pulse modulation process. The mass of the components is approximately proportional to the inverse of the inverter frequency. Present resonant converter

---

<sup>13</sup>Byers, D., Terdan, F., and Meyers, I., "Primary Electric Propulsion for Future Space Missions," NASA Technical Memorandum 79141, NASA-Lewis Research Center, Cleveland, Ohio, 1979.

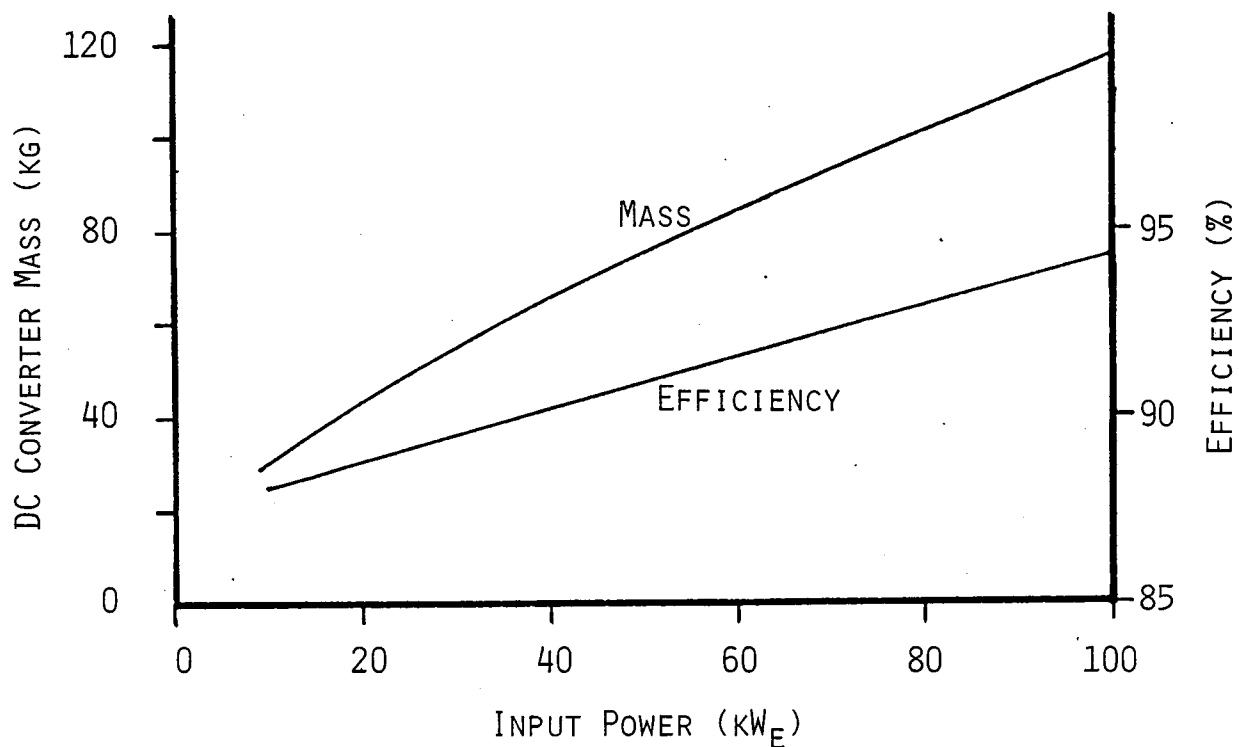


Figure 11. Series resonant converter specific mass and efficiency (from Reference 13).

designs employ internal operating frequencies ranging from 10 kHz - 30 kHz. Developmental efforts should enable operating frequencies to 50 kHz, within the next five years, reducing converter mass by 40%.

Series resonant converter efficiency is a weak function of power level as illustrated in Figure 11, and ranges from 88% to 94%. For the purposes of this report, we assume a non-varying converter efficiency,  $\eta_{DC}$ , equal to 92% for all power levels.

#### 2.2.3.2 Capacitive Energy Store

The capacitive energy store for the rail gun propulsion system would be an assembly of high performance

capacitors configured to provide sufficient energy for a single pellet launch at required voltage and current levels. Capacitor energy storage density and therefore the capacitive energy store mass is related to charge-discharge frequency, life and reliability requirements, and voltage level. The requirements imposed on the capacitive energy store by the rail gun propulsion system largely determine the energy storage density of the capacitors.

The anticipated pulse frequency required of the capacitors is about 10 Hz. The mission duration for an electric rail gun OTV would be in the range from 30 days to 100 days. Assuming continuous thrusting throughout the mission at a pulse repetition rate of 10 Hz the required capacitor life would be in the range from  $10^7$  to  $10^8$  pulses.

The combination of voltage and capacitance must be such that the stored energy is adequate for the acceleration and that the stored energy is transferred to the pulse forming inductor in a time period short relative to the pellet launch time. Too slow an energy transfer would reduce energy transfer and rail gun efficiency. Efficient performance is achieved if the capacitively stored energy is transferred to the pulse forming inductor in less than 10% of the pellet launch time.<sup>1</sup> Applying this criteria the required capacitor voltage,  $V_s$ , is given by

$$V_s = 10\pi E_s / (I_o \tau_a) \quad (10)$$

where,  $E_s$ , is the stored energy,  $I_o$ , is the maximum rail gun current and,  $\tau_a$ , is the pellet acceleration time. For rail gun propulsion systems with power levels in the 25 kW<sub>e</sub> to 100 kW<sub>e</sub> range

the storage voltage specified by Equation (10) ranges from 1800 V to 2200 V.

Capacitors which meet the pulse frequency, life and voltage level requirements specified in the previous paragraphs have been developed and tested in conjunction with other spaceborne electric propulsion programs.<sup>14</sup> The energy storage density of these capacitors is 90 J/kg. Assuming that these state-of-the-art capacitors would be used in the rail gun propulsion system, we can express capacitive energy store mass,  $M_C$ , in terms of the stored energy as

$$M_C = 0.011E_s \quad (11)$$

The capacitors described in Reference 14 have a loss factor less than 0.011. At frequencies of a few Hz this loss factor implies a capacitive energy store efficiency,  $\eta_C$ , of 97%. The energy storage efficiency is the ratio of the energy which can be extracted in a single discharge to the energy initially stored.

#### 2.2.3.3 Solid State Switch

The requirements imposed on the switch and clamp shown in Figure 9 in the high current circuit, include peak voltage standoff and high current conduction. As described in the above paragraphs, the switch and the clamp must be capable of standing off voltages in the range from 2 kV to 2.2 kV, or specifically the voltage,  $V_s$ , given by Equation (10). The peak

---

<sup>14</sup>Ramrus, A., "Development of a High Energy Density Capacitor for Plasma Thrusters," Air Force Rocket Propulsion Laboratory, Report No. AFRPL-TR-80-35, October 1980.

current,  $I_o$ , which the switch must conduct was given in Section 2.2.2 and for the system under investigation may range from 50 kA to 150 kA. The duty cycle (the ratio of on time-to-off time) for the high currents is only about 1.5%. This low duty cycle combined with zero current switch opening implies that low mass, highly reliable solid state switching would be possible.

Solid state switch and clamp elements combine the attractive features of low mass and highly reliable, efficient operation. In addition, solid state devices could be easily actuated with small electrical signals. References 15 and 16 describe the specifications of off the shelf rugged thyristors and rectifiers which could be used in the rail gun circuit. Reference 15 describes the specifications for a fast switching thyristor capable of standing off 2500 V and passing surge currents of up to 13,000 A. The rectifier described in Reference 16 can stand off 3000 V and can pass surge currents of up to 30,000 A. Each of these units has a mass of about 0.95 kg. By suitable series-parallel combinations of these units the required voltage standoff and current conduction required in the rail gun propulsion power conditioning system could be achieved. The number of parallel strings required is obtained by dividing the peak current,  $I_o$ , by the current capability of the solid state device. Similarly, the number of series connected units in each parallel string is

---

<sup>15</sup>Westinghouse, Inc., Data Sheet for Fast Switching Thyristor, SCR-T9GH.

<sup>16</sup>Westinghouse, Inc., General Purpose Rectifiers Data Sheet, R920.

obtained by dividing the maximum capacitor voltage by the standoff voltage capability of an individual device. The total number of units required is obtained by multiplying the number of parallel strings by the number of series connected elements in each string. The mass of the switch array,  $M_{sw}$ , is obtained by multiplying the total number of elements required by the mass per element, and may be written as

$$M_{sw} = 4.21 \times 10^{-8} V_s I_o \quad (12)$$

In a similar manner the mass of the clamp diode array is given by

$$M_d = 1.33 \times 10^{-8} V_s I_o \quad (13)$$

In both of these equations a multiplicative factor of 1.2 was used to account for fault isolation fuses and support structure mass. The thyristors described in Reference 15 have characteristics which would permit each capacitor in the bank to be switched by a single thyristor. Individual capacitor switching would enable a desirable control on energy discharge level.

Since the functional forms of Equations (12) and (13) are the same we can combine the switch mass and the clamp diode mass to obtain one equation describing the total switch system mass,  $M_s$ , as

$$M_s = 5.54 \times 10^{-8} V_s I_o \quad (14)$$

Due to the low switch duty cycle we assumed that the switch losses could be made negligible.

#### 2.2.3.4 Pulse Forming Inductor

The pulse forming inductor in series with the rail gun acts as a choke, lengthening the energy pulse provided to the rail gun. During pellet launch the rail gun appears as a variable impedance load. Impedance is proportional to pellet velocity. A capacitive energy store discharged directly into the rail gun would produce such a high current pulse at the beginning of launch, that the pellet would be destroyed by the acceleration stresses. The inductor is, therefore, a pulse forming device which must be sized to momentarily store the entire energy required for a launch. The required inductance,  $L_o$ , may be related to the stored energy,  $E_s$ , and to the peak allowable current,  $I_o$ , by

$$L_o = 2E_s / I_o^2 \quad (15)$$

A variety of coil geometries could be used to obtain the required inductance and stored energy. The minimum mass geometry, a Brooks coil, is a thick solenoid with square cross-section. The inductance (in MKS units) of a Brooks coil is given by the relationship:<sup>17</sup>

---

<sup>17</sup>Grover, F.W., Inductance Calculations--Working Formulas and Tables, D. Van Nostrand Company, Inc., Copyright 1946.

$$L_o = 1.7 \times 10^{-6} a N^2 \quad (16)$$

where:

N = total number of turns

a = mean radius of the turns

By substituting Equation (15) into Equation (16), we could eliminate  $L_o$  as a parameter and relate the coil dimension,  $a$ , to the number of turns,  $N$ , in the coil. However, in doing so we still cannot specify a unique coil. A unique design will result if the coil satisfies two constraints: acceptable electrical losses; and adequate mechanical strength. Since the coil carries current for only a short period of time it can be made very efficient. We imposed a constraint requiring that the coil efficiency be at least 99%. High current coils containing a high magnetic flux must have adequate strength to resist the induced bursting forces. We chose to limit coil stresses to a conservative level equal to  $25 \text{ MN/m}^2$ .

Imposing the constraint on inductor energy dissipation, implies a maximum allowable coil resistance which is a function of the pellet launch time. By imposing this efficiency constraint and requiring 99% coil efficiency, the coil size is found to be

$$a = 1.29 \times 10^4 (\tau_a \rho / \epsilon)^{1/2} \quad (17)$$

where,  $\rho$ , is the conductor resistivity, and,  $\epsilon$ , is the coil packing factor. The coil mass is given by the product of average coil density times coil volume. Recalling that the cross-section of the windings of a Brook's coil is square, the coil mass,  $M_{LR}$ , may be written as

$$M_{LR} = 6.0 \times 10^{12} \bar{d} (\tau_a \rho / \epsilon)^{3/2} \quad (18)$$

where,  $\bar{d}$ , is the average coil mass density ( $\bar{d} = \epsilon d_c + (1-\epsilon)d_i$ ),  $d_c$ , is the conductor mass density, and  $d_i$ , is the insulation mass density. Aluminum which combines the properties of low resistivity and low density is a good candidate inductor winding material. We assumed the inductor is wound with aluminum conductor with a resistivity equal to  $2.82 \times 10^{-8} \Omega\text{-m}$ , and a density equal to  $2,760 \text{ kg/m}^3$ . The coil packing factor,  $\epsilon$ , is a function of conductor geometry, the voltage, and the dielectric material used between coil windings. We assumed that the packing factor is equal to 0.85. We assumed an insulation with density equal to  $1,200 \text{ kg/m}^3$ . The mass of a Brook's geometry coil is a lower bound estimate of the coil mass. To account for the additional mass (due to support structure; non Brook's geometry and/or shield windings) of an actual coil, we arbitrarily chose to estimate coil mass by multiplying the minimum mass of a Brook's geometry by a factor of two. Substituting for these constants in Equation (18) the coil mass (based on the efficiency criteria) is given by

$$M_{LR} = 2.0 \times 10^5 \tau_a^{3/2} \quad (19)$$

The energy stored in an inductor may be thought of as a two dimensional magnetic pressure which stresses the inductor windings and/or coil former, much as fluid pressure stresses the walls of a tank. For a given stored energy, as the size of the coil is increased the magnetic pressure is decreased. Assuming that the magnetic flux is contained within a cylinder with radius equal to,  $a$ , and length equal to,  $2a/3$  (Brook's coil ), the size of the coil,  $a$ , is related to the stored energy,  $E_s$ , and the coil stress,  $\sigma_y$ , by

$$a = [7E_s / (2\pi\sigma_y)]^{1/3} \quad (20)$$

The mass of the coil may then be written as

$$M_{LS} = 28\bar{d}E_s / (9\sigma_y) \quad (21)$$

where,  $M_{LS}$ , is the coil mass which satisfies the coil strength criteria. Substituting for the density,  $\bar{d}$ , ( $2,700 \text{ kg/m}^3$ ), for the coil stress,  $\sigma_y$ , ( $25 \text{ MN/m}^2$ ), and again using the multiplicative factor of two for the actual coil mass (as discussed in the preceding paragraph), the coil mass may be written as

$$M_{LS} = 6.0 \times 10^{-4} E_s \quad (22)$$

The mass of the pulse forming inductor will be established based on either the resistance criterion or the stress criterion and will always be given by the larger of the

values as calculated from Equation (19) or Equation (22). Using the larger of,  $M_{LR}$  and  $M_{LS}$  guarantees that both the efficiency criterion and resistance criterion are satisfied. For the 25 kW<sub>e</sub> to 100 kW<sub>e</sub> propulsion systems under investigation in this study, we found that the pulse forming inductor is always sized by the resistance criterion and therefore the mass is given by Equation (19).

#### 2.2.3.5 Performance and Configuration

The mass and efficiency of the power conditioning system are obtained by combining the mass and efficiency equations derived for each of the five components. The total mass of the power conditioning system,  $M_{pc}$ , may be expressed as

$$M_{pc} = M_{DC} + M_C + M_S + M_L \quad (23)$$

The power conditioning efficiency,  $\eta_{pc}$ , may be written as

$$\eta_{pc} = \eta_{DC} \eta_C \eta_L \quad (24)$$

The mass and efficiency relationships for the power conditioning system and components are summarized in Table 3.

A concept for a compact geometrical configuration of a 25 kW<sub>e</sub> power conditioning system is shown in Figure 12. Power is input to the DC converter directly from the solar cell array. A coaxial conductor (not shown) could be used to bring power out of the DC converter to the ground and charging plates of the capacitors. Each capacitor would have its own

TABLE 3

Summary of Capacitive Based Power  
Conditioning Mass and Performance

Power Conditioning System Mass:

$$M_{pc} = M_{DC} + M_C + M_L + M_S$$

where:

$$M_{DC} = 10 + 0.057P^{1/2} + 0.014P^{3/4} + 1 \times 10^{-4}P$$

$$M_C = 0.011E_s$$

$$M_S = 1.74 \times 10^{-6}E_s/\tau_a$$

$$M_L = 2 \times 10^5 \tau_a^{3/2}$$

Power Conditioning System Efficiency

$$\eta_{pc} = \eta_{DC}\eta_C\eta_L$$

where:

$$\eta_{DC} = 0.92$$

$$\eta_C = 0.97$$

$$\eta_L = 0.99$$

where:

$M_{pc}$ ;  $\eta_{pc}$  are the total power conditioning mass and efficiency

$M_{DC}$ ;  $\eta_{DC}$  are the DC-DC converter mass and efficiency

$M_C$ ;  $\eta_C$  are the capacitive energy store mass and efficiency

$M_S$  is the switch mass

$M_L$ ;  $\eta_L$  are the pulse-forming inductor mass and efficiency

$P$  is the total average power output of the source

$E_s$  is the stored energy

$\tau_a$  is the characteristic pellet launch time

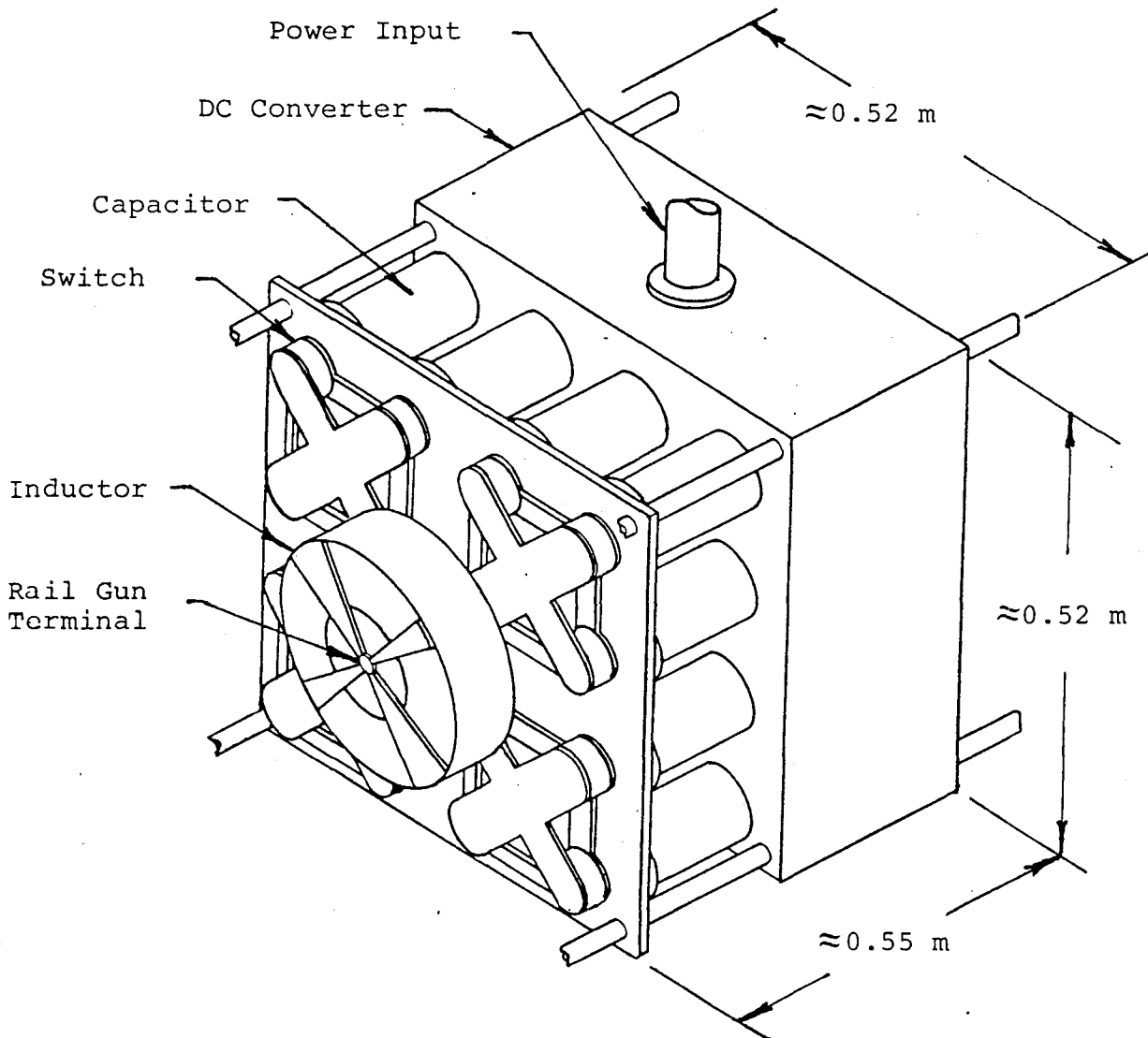


Figure 12. Conceptual configuration of 25 kW<sub>e</sub> power conditioning system.

solid state switch, but a single clamp diode would serve a group of four capacitors. The current from each group of four capacitors would be collected by a plate attached to the switches. The current from each set of four capacitors would be fed into one start of a four start inductor. Current would be collected at the coil terminations by four plates which themselves would be

terminated on one rail of the gun. The other rail of the gun would be connected to the capacitor ground plate by a conductor coaxial with the inductor.

#### 2.2.4 Propellant Handling System

This section describes our assessment of the propellant handling system, required for the electric rail gun propulsion concept under study. Our objective in this analysis was to first identify and then to estimate the mass and performance of technically feasible propellant handling system concepts. As used in this study the propellant handling system includes all components required to repetitively provide the rail gun with a pellet ready for launch. The functions provided by the propellant handling system include: propellant storage, from which a steady supply of pellet material may be drawn; propellant transport, to a pellet forming device which may be physically removed from the propellant store; propellant processing and pellet forming, which may be required to fabricate gun sized pellets; and pellet loading into the rail gun bore.

Several requirements are imposed on the propellant handling system in a rail gun propulsion system. The high pellet accelerating stresses during launch require that the propellant be a solid with considerable strength. The size of the pellet must match the gun bore, which as described in Section 2.2.2 will range from 1 mm to 10 mm. The corresponding pellet masses range from 2 mg to 1 g. The pellet shape must be a half cube, placed in the bore with the shortest dimension in the direction of pellet motion. The pellets must be loaded into the gun at the launch frequency which may range from 5 Hz to 15 Hz.

In the remainder of this section, we first identify a number of propellant handling system concepts. Based on general characteristics we select two of the identified concepts for detailed analysis. We compare the two systems by comparing each concept based on mass and performance estimates. Finally, we briefly review pellet disposal problems and potential solutions to these problems.

#### 2.2.4.1 Propellant Handling System Options

A variety of means are available for accomplishing the four functions (i.e., storage, transport, pellet forming and pellet loading) of the propellant handling system. These four functions provide a convenient means of classifying and describing the various options as shown in Table 4. A major differentiation may be done based on whether the propellant is stored and transported in the fluid state or in the solid state. Sub differentiations are based primarily on pellet forming technique.

Storage and transport of all propellants stored in the fluid state would be accomplished via pressurized tanks, pipes and valves. These storage and transport techniques are well developed and could easily be adapted to the rail gun propulsion system. All three fluid stored propellant concepts could also essentially eliminate pellet loading as an independent operation by forming the pellet directly in the gun bore. The mechanism of phase change from fluid propellant to solid pellet differentiates the fluid propellant concepts and the propellant materials which would be used.

Table 4. Propellant Handling System Options

STORED STATE	FLUID			SOLID			
	PURE LIQUID + FILLER	POLYMER + FILLER	SLURRY	PREFORM PELLETS	PREFORM BAR	PREFORM SHEET	BILLET
PROPELLANT STORAGE	-Tank(s)	-Tank(s)	-Tank(s) (with agitation)	-Tank/Hopper	-Pancake coils on Mandrel	-Coiled on Mandrel	-----
PROPELLANT TRANSPORT	-Pipes/Pressurized Tank(s)/ Valves	-Pipes/Pressurized Tank(s)/ Valves	-Pipes/Pressurized Tank/ Valves	-Conveyor	-Drive Rolls	-Drive Rolls	-----
PELLET FORMING	-Phase Change (Freezing)	-Polymerization	-Extract Transport medium/ consolidate	-Preformed	-Parted Off Bar	-Slice Off Bar/Part Off Pellet	-Extrude Bar/Part Off Pellet
PELLET LOADING	-Formed in Situ	-Formed in Situ	-Formed in Situ	-Mechanical Actuator	-Parted in Situ	-Parted in Situ	-Parted in Situ
ADVANTAGES	<ul style="list-style-type: none"> <li>-Easily stored and transported</li> <li>-Handling technology well developed</li> </ul>			-No pellet forming	<ul style="list-style-type: none"> <li>-Integral armature loading</li> <li>-Transport and pellet formation easy</li> <li>-Low power/ low mass</li> </ul>	<ul style="list-style-type: none"> <li>-Integral fuse loading</li> <li>-Transport and pellet formation easy</li> <li>-Low power/ low mass</li> </ul>	<ul style="list-style-type: none"> <li>-Storage easy</li> <li>-Transport not required</li> </ul>
DISADVANTAGES	<ul style="list-style-type: none"> <li>-Storage tanks are massive (&gt;0.01 mass of propellant)</li> <li>-Many active components (valves, pumps)</li> <li>-Requires refrigeration</li> <li>-Pellet strength limited</li> <li>-Pellet formation rate limited</li> <li>-Separate armature loading</li> <li>-High power required</li> </ul>	<ul style="list-style-type: none"> <li>-Pellet formation rate limited</li> <li>-Requires two liquids</li> <li>-Separate armature loading</li> </ul>	<ul style="list-style-type: none"> <li>-Separation system</li> <li>-High pressure consolidation</li> <li>-Limited pellet strength</li> <li>-High power required</li> <li>-Separate armature loading</li> </ul>	<ul style="list-style-type: none"> <li>-Transport and storage difficult</li> <li>-Pellet de-gradation</li> <li>-Separate armature loading</li> </ul>	<ul style="list-style-type: none"> <li>-Shear required</li> </ul>	<ul style="list-style-type: none"> <li>-Slicer required</li> <li>-Shear required</li> </ul>	<ul style="list-style-type: none"> <li>-High pressure press/high mass</li> <li>-Separate armature loading</li> </ul>

The pellet formation technique for the pure liquid (or a pure liquid with an added filler for increased pellet density) would be by thermal phase change or freezing. In the second fluid propellant concept a monomer, or monomer and catalyst, would be stored as a fluid and pellet formation would be achieved by polymerization of the monomer to form a solid polymer. In the slurry propellant concept, propellant particulates are held suspended in a transport medium. Pellet formation would be achieved by extracting the transport medium from the slurry and consolidating the resultant particulates into a pellet.

The advantages and disadvantages of the three fluid propellant concepts are similar, as shown in Table 4. The advantages are found in the ease of propellant storage and transport via existing technology. The disadvantages include storage tanks which are relatively massive relative to the stored propellant mass (greater than 1%) and many active components. Another disadvantage is the limited pellet strength which could be obtained. All three fluid propellant concepts would also require the complicating feature that the driving armature would require separate loading behind the pellet. Relatively high power would probably be required to operate the refrigeration unit for the pure liquid phase change and high power for the slurry consolidation might also be required. Finally, the polymer fluid propellant concept has the disadvantage of requiring separate storage and transport systems for the monomer and the catalyst.

The solid propellant storage concepts are primarily differentiated by the degree to which the pellet is preformed before being placed aboard the spacecraft. Each of the degrees of preforming imposes somewhat different requirements on the handling functions and only few advantages and disadvantages are common to all.

Preformed pellets have all three dimensions length, width and height, preformed. The pellets would have to be stored in a tank and the transport would be via a conveyor or pressurized pipe system. The pellet loading system would be relatively complex requiring precision mechanical actuators. The

preformed bar would have two dimensions, say length and width preformed to bore dimensions. Bars would be stored by winding them onto coils and loading the coils onto a mandrel. The propellant transport would then be accomplished by unwinding the coiled bar through guides and drive rolls. Pellets would be formed by shearing a pellet of correct length off the end of the bar. This shearing could be done with the pellet in situ eliminating the need for separate pellet loading. The preformed sheet would only have one dimension, say pellet width, preformed. Storage would be accomplished again by coiling onto a mandrel. Drive rolls and guides would again be used for transport. Pellet forming would be accomplished by first slicing bars off the sheet, then shearing pellets off the bar in situ in the gun bore. Propellant stored as a billet would first require extrusion into a bar followed by shearing of the bar into pellets in situ in the gun bore.

The solid propellant concepts share the advantages of freedom of material selection to obtain adequate pellet strength, low power requirements (excepting the billet) and low mass storage and transport (excepting possibly the preformed pellets). The preformed pellets have the major advantage of no pellet forming onboard the spacecraft. However this is obtained at the cost of increased storage and transport difficulty. The preformed bar and the preformed sheet share the advantages of enabling integral armature/fuse attachment to the preformed bar or preformed sheet. Storage and transport are relatively simple but mechanical shears and/or slicers are required. The preformed billet makes storage relatively easy but a high pressure, high mass press would be required

to form the bar and separate armature loading would be required.

Based on the advantages and disadvantages outlined in Table 3, we chose the pure liquid fluid propellant concept and the preformed bar solid propellant concept for further analysis. Our logic for this selection was that the pure liquid fluid propellant concept would provide representative data on the characteristics of all fluid based concepts and that the analysis for the pure liquid concept would be more tractible. The preformed bar solid fuel propellant was selected as representing an optimum balance between pellet loading complexity and pellet forming complexity.

#### 2.2.4.2 Mass and Performance

The mass and performance of the pure liquid fluid propellant and the preformed bar solid propellant fuel handling concepts were estimated by examining each of the four functions or subsystems. The analyses are briefly described in the following paragraphs in the order; storage, transport, pellet forming, and pellet loading. Analytical expressions describing the mass of these alternatives fuel handling systems is then assembled.

We estimated the mass of a tank containing the fluid propellant by assuming a spherical tank. By forming the ratio of the volume of material and the tank wall to the volume enclosed by the tank and multiplying by the density of the tank material and the density of the propellant the ratio of tank mass,  $M_t$ , to propellant mass,  $M_f$ , may be written as

$$M_t/M_f = 3P_t\rho_t/2\sigma\rho_f \quad (25)$$

Where,  $P_t$ , is the tank pressure,  $\rho_t$ , is the tank material density,  $\sigma$ , is the stress in the wall material, and,  $\rho_f$ , is the propellant density. We assumed a tank pressurization of  $0.35 \text{ MN/m}^2$ , a wall stress of  $100 \text{ MN/m}^2$ , a tank wall density of  $3,000 \text{ kg/m}^3$  and a propellant density of  $1,000 \text{ kg/m}^3$ . Substituting these values into Equation (25) we obtain

$$M_t/M_f = 0.0158 \quad (26)$$

Tank hardware, such as flanges, will increase the tank mass-to-propellant mass. The tank mass to propellant mass ratio for an actual system (the BIMOD ion thruster) ranges from 2% to 9%.<sup>18</sup>

The mandrel on which the preformed bar is wound is the solid propellant element comparative to the tank of the fluid propellant concept. To enable our comparison between the solid propellant concept and the fluid propellant concept a ratio of the mandrel mass,  $M_m$ , to propellant mass was derived. We assumed that the outside diameter of the propellant coil,  $D_f$ , is much larger than the diameter of the mandrel,  $D_m$  and the mass ratio was found to be

$$M_m/M_f = \rho_m D_m^2 / \rho_f D_f^2 \quad (27)$$

---

<sup>18</sup>NASA-Lewis Research Center, "30-cm Ion Thrust Subsystem Design Manual," NASA Technical Memorandum 79191, June 1979.

where,  $\rho_m$ , is the effective average density of the mandrel. We assumed the mandrel would be a non-solid, stiffened structure with an average effective density equal to  $300 \text{ kg/m}^3$ . We assumed a solid propellant density equal to  $3,000 \text{ kg/m}^3$  and a ratio of the mandrel diameter-to-propellant diameter equal to 0.1. The mandrel mass-to-propellant mass ratio is then

$$M_m/M_f = 0.001 \quad (28)$$

Comparing Equation (26) with Equation (28) we see that the solid propellant mandrel would be about 10% of the tank mass for a fluid propellant store.

The transport system of pipes, valves, and controls required for a fluid propellant system is very spacecraft design dependent. To estimate fluid propellant transport mass here we scaled the BIMOD ion thruster system design in Reference 18, based on mass flow rate. For a repetitively operated rail gun, the fluid propellant transport mass,  $M_{ft}$ , may be expressed as

$$M_{ft} = k_1 mf \quad (29)$$

where,  $k_1$ , is the specific mass of the BIMOD ion thruster propellant transport system ( $k_1 = 1.2 \times 10^5 \text{ s}$ ),  $m$ , is the mass of each pellet, and,  $f$ , is the launch frequency. The fluid propellant transport mass may then be written as

$$M_{ft} = 1.2 \times 10^5 m_f \quad (30)$$

The mass of the solid propellant transport was estimated based on the power required to unwind the preformed bar off of the coil, propel it along a guide system and insert it into the breech of the rail gun. We assumed that the pellets are roughly cubical and that the transport mechanism must supply peak power of at least ten times the average power required to drive the preformed bar (due to the cyclical operation of the rail gun). The solid bar transport mass,  $M_{st}$ , may be written in terms of an average axial driving stress,  $\sigma$ , in the bar, as given by

$$M_{st} = 10k_2 \sigma f m / \rho_p \quad (31)$$

where,  $k_2$ , is the specific mass of drive motor and,  $\rho_p$ , is the pellet density. The drive motor specific mass,  $k_2$ , may be conservatively estimated based on the specific mass of conventional motors (0.01 kg/W to 0.02 kg/W) and was taken as 0.05 kg/W to approximately account for other components in the system such as drive rolls and guides. We assumed that the preformed bar is driven at a very high, and therefore conservative, value of average stress equal to 100 MN/m<sup>2</sup>. As before the density of the propellant is assumed to be 3,000 kg/m<sup>3</sup>. Substituting these values into Equation (31) the solid propellant transport mass may be written as

$$M_{st} = 1.67 \times 10^4 m_f \quad (32)$$

Equation (32) predicts that the solid propellant transport will be 10% as massive as a fluid transport as predicted by Equation (30).

Forming pellets from the pure liquid (water) propellant is accomplished by freezing in the rail gun breech. The pellet forming mass will be dominated by the refrigeration system required to extract the propellant heat of fusion,  $Q$ . The electrical power input,  $P_r$ , to a refrigerator required to freeze the propellant is given by

$$P_r = mQf/\eta_r \quad (33)$$

where,  $\eta_r$ , is the refrigeration system efficiency. We assumed that the refrigerator operates at 40% of Carnot efficiency, that refrigeration takes place at 250° K, and that heat from the refrigeration system is rejected at 400° K, the efficiency,  $\eta_r$ , will be approximately 67%. We assumed that the mass of the refrigeration system including primary power supply and heat radiators can be related to the electrical power input,  $P_r$ , at a specific mass of 20 kg/kW<sub>e</sub>. The fluid propellant pellet forming mass,  $M_{ff}$ , may then be written as

$$M_{ff} = 1 \times 10^4 m_f \quad (34)$$

Pellet forming from the preformed bar solid propellant is accomplished by shearing the pellet off the end of the bar. A conceptual sketch showing the essential features of this concept is illustrated in Figure 13. The preformed bar would be forced between the rails by a set of drive rolls and a pair of guides. With the end of the propellant bar fully inserted between the rails, a shear would cut the pellet to the required size. To assure containment of the plasma at the beginning of launch, the rail gun could be fired with the shear blade extended across the top of the rails.

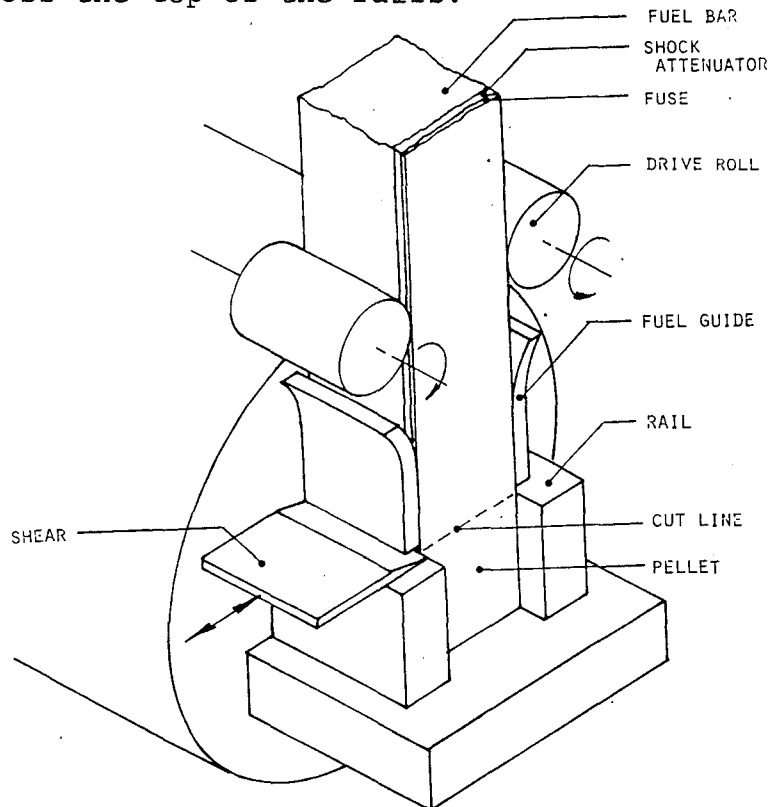


Figure 13. Solid propellant pellet former.

The average power,  $P_s$ , required to repetitively shear pellets from the propellant bar may be written as

$$P_s = \tau mf / \rho_p \quad (35)$$

where,  $\tau$ , is the propellant shear strength. We have assumed that the propellant is cubical. We assume that the propellant shear strength is equal to  $100 \text{ MN/M}^2$ , and that pellet density is  $3,000 \text{ kg/m}^3$ . We also assumed that the mass of the pellet forming system is linearly related to the shear power,  $P_s$ , by the constant specific mass of  $0.02 \text{ kg/W}_e$  to account for the power supply and waste heat radiator required to operate the shear (the specific mass of the shear itself is therefore  $0.08 \text{ kg/W}_e$ ). The mass of the solid propellant pellet former system is obtained by substituting for the constants in Equation (35) and multiplying by the specific mass to obtain

$$M_{sf} = 3.33 \times 10^3 mf \quad (36)$$

Pellet loading is accomplished simultaneously with the pellet forming function in-situ in the bore of the rail gun for both the fluid and solid propellant concepts. No additional mass is therefore identified for the pellet loading function.

The total mass,  $M_1$ , of the propellant handling system is obtained by summing the mass of each of the individual components associated with propellant storage, transport, and pellet forming. The mass of the fluid propellant handling system is given by

$$M_1 = 1.6 \times 10^{-2} M_f + 1.3 \times 10^5 m_f \quad (37)$$

Mass of the preformed bar solid propellant handling system is given by

$$M_1 = 1 \times 10^{-3} M_f + 2.0 \times 10^4 m_f \quad (38)$$

We can see that the mass,  $M_1$ , of the propellant handling system is a function of the total stored propellant mass at the beginning of a mission, pellet mass, and the launch frequency. The solid propellant handling system has a lower mass over all ranges of performance.

#### 2.2.4.3 Pellet Disposal

Each pellet in the exhaust stream from an electric rail gun thruster would have a kinetic energy ranging from about 1 kJ to 20 kJ. Impact of any one of these pellets on other spacecraft in near earth orbit poses a substantial hazard. The probability of a pellet impact on another spacecraft would be greatly increased if the pellets are inserted into stable earth orbits. Repetitively operating the rail gun thruster as an OTV could establish artificial meteoroid belts in which the probability of impact on a spacecraft would be unacceptably high. It is therefore apparent that the pellets cannot be permitted to attain stable earth orbits.

We have identified two potential methods which can be used to prevent pellet disposition in stable earth

orbits. One approach is to control the pellet exhaust velocity to prevent pellet disposition in stable earth orbits. The velocity would be controlled such that the pellet would either enter the earth's atmosphere or leave earth orbit. The second approach involves using pellets made of a material which would "decompose" into a state harmless to other spacecraft. One material, for example, might be water launched as ice and sublimed to harmless water vapor after launch.

Final pellet orbital disposition is a function only of pellet velocity with respect to the earth's reference frame. The objective is to arrange for the pellet to intersect the earth's surface at or before perigee or to escape earth orbit at apogee. The pellet velocity and therefore orbital characteristics in the earth's reference frame is the vector sum of the spacecraft velocity in the earth's reference frame and the pellet launch velocity in the spacecraft reference frame. Assuming that the spacecraft orbit remains nearly circular during the orbital transfer, we examined the conditions under which pellet "safe" disposal would be accomplished.<sup>1</sup>

We examined the pellet disposal requirements for the thrusting strategy which produces optimal mission performance (i.e., for coplanar orbital transfers, holding the thrust vector tangent to the orbit is optimal; see Appendix A). Under these conditions the pellet exhaust velocity relative to the spacecraft,  $v_c$ , which causes earth capture of the pellet may be written in terms of the ratio of the orbital radius from the center of

the earth,  $r_o$ , to the radius of the earth,  $r_e$ . For the LEO to GEO outbound transfer this velocity is given by

$$v_c \leq 7742 [(2/(r_o/r_e+1))^{1/2} + 1] (r_e/r_o)^{1/2} \quad (39)$$

The pellet exhaust velocity,  $v_e$ , which causes the pellet to escape earth orbit during outbound transfer is given by

$$v_e \geq 7742 (2^{1/2}+1) (r_e/r_o)^{1/2} \quad (40)$$

For the inbound transfer from GEO to LEO the spacecraft orbit velocity and the pellet exhaust velocity are in the same direction and therefore the pellet exhaust velocity,  $v_i$ , which will cause pellet escape is given by

$$v_i \geq 7742 (2^{1/2}-1) (r_e/r_o)^{1/2} \quad (41)$$

Together Equations (39)-(41) define regions of stable pellet orbit as illustrated in Figure 14. During an outbound transfer the exhaust velocity could be adjusted to prevent any pellets from attaining stable orbits. During the inbound transfer, practically all exhaust velocities of interest would result in pellets escaping earth orbit. Figure 14 illustrates that controlling pellet exhaust velocity is a feasible approach to prevent pellets from attaining stable earth orbits.

Using a sublimable pellet material, such as water ice, appears to be another alternative which could be

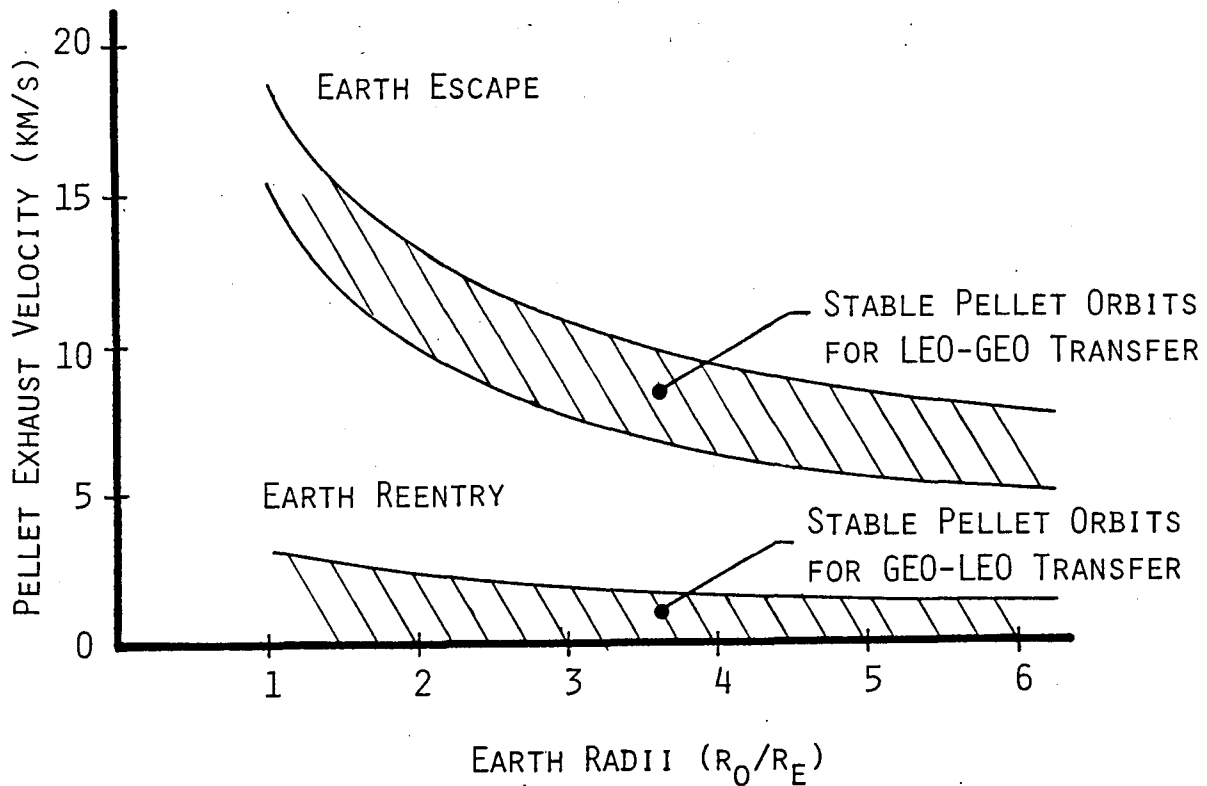


Figure 14. Exhaust velocities which result in pellet stable orbits.

used to prevent pellet impact on other spacecraft. Solar radiation would provide the sublimation energy. We performed a calculation to find the surface recession rate of a pellet sublimating in the solar flux. Assuming an 80% absorption, the surface recession of ice would be approximately 2 mm/hr. (The absorption could in principle be controlled with dyes). This implies that for the pellets of interest in this study (2 mm - 5 mm cubes) the pellet would be totally sublimed in approximately 1 hour. For most altitudes this would be less than the orbital period. Assuming that the ice could be made strong enough to survive launch (which appears feasible), this represents a second alternative for preventing damaging pellet-spacecraft impact.

### 2.2.5 Waste Heat Rejection

In this section we examine the waste heat radiators

required to reject the propulsion system power losses appearing as heat. The rail gun is the primary source of waste heat. This analysis therefore, concentrates on rail gun radiators. The power conditioning system is the other major source of waste heat and the DC converter is the major contributor within the power conditioning system. We assume that the waste heat radiators for the BIMOD DC converters could also be used for the electric rail gun propulsion system.<sup>18</sup> The objective of the analysis was to determine the mass, and a feasible configuration for the waste heat radiators required to reject rail gun losses. Before estimating mass we examine the effects of requirements imposed on the radiator by operation with the electric rail gun in the space environment.

#### 2.2.5.1 Radiator Performance

Three factors which significantly effect spaceborne radiator performance include: radiator operating temperature; effective sink temperature; and life and reliability.

Spacecraft heat rejection by radiation is governed by a fourth-power temperature dependence as derived from Planck's equation and given by:

$$w = \sigma_{sb} \epsilon_e (T^4 - T_o^4) \quad (42)$$

where  $w$  is the rejected thermal power per unit radiator surface area (referred to as specific radiated power),  $\sigma_{sb}$ , is the Stefan-Boltzmann constant ( $5.67 \times 10^{-8} \text{ w m}^{-2} \text{ } ^\circ\text{K}^{-4}$ ),  $\epsilon_e$ , is the radiator surface emissivity,  $T$ , is the radiator surface temperature, and,

$T_0$ , is the effective temperature of the sink. Equation (42) illustrates that spacecraft specific radiated power increases rapidly as the difference between radiator rejection temperature,  $T$ , and the effective space sink temperature,  $T_0$ , increases. Heat rejection temperature,  $T$ , is established by a tradeoff between improved specific radiated power and higher rail gun ohmic losses implied by the higher rejection temperatures.

Due to its size, a rail gun radiator would interchange radiant energy with all other sources/sinks in its surroundings including the sun, earth, deep space and other spacecraft components (especially the solar cell array). The effective sink temperature,  $T_0$ , (in Equation (42)) is therefore a function of radiator geometry, orientation, and the spectral properties of the radiator surface. Sink temperature can be effectively minimized by minimizing the radiant flux absorbed by the radiator surface. Minimizing flux absorption is accomplished by: configuring the radiator to minimize the radiant interchange with the spacecraft (i.e., by orienting the radiator so that the minimum practicable surface area can "see" the solar cell array); and by employing radiator surface coatings with low solar absorptance and high thermal emissivity. Effective sink temperature minimization is specific to overall spacecraft design. The effective sink temperature,  $T_0$ , for several spacecraft designs for near earth space missions with multikilowatt heat rejection requirements

ranges from 190°K to 230°K.<sup>19,20,21</sup> For the rail gun propulsion system we assume an effective sink temperature of 230°K.

Meteoroid impact damage poses a severe threat to radiators. Highly reliable, long radiator life necessitates that redundant radiator components be provided or that the radiator be adequately protected. The meteoroids comprising the flux in the vicinity of the earth range in mass from  $10^{-12}$  grams to 1 gram. The particle mass density is usually taken as  $0.5 \text{ g/cm}^3$  for all particle sizes. The average particle velocity is often assumed to be 20 km/s. Particles with mass ranging from  $10^{-6}$  grams to 1 gram have the greatest probability of damaging a radiator. Smaller particles have insufficient kinetic energy to puncture the radiator while larger particles are not sufficiently numerous to have an appreciable encounter probability. Based on a general meteoroid flux model developed by NASA,<sup>22</sup> a radiator for a 50 kW<sub>e</sub> rail gun OTV would have a probability approaching 1 of being impacted by a meteoroid with mass  $5 \times 10^{-6}$  grams in a hundred day mission, and would have a probability approaching 1 of being impacted by a meteoroid with mass  $3 \times 10^{-5}$  grams in a three year life time.

---

<sup>19</sup>Leach, J., and Stalmach, D., "Optimum Design of Spacecraft Radiators for Large Capacity or Long Duration Mission Applications," Paper No. 79-ENAS-10, American Society of Mechanical Engineers, 1979.

<sup>20</sup>Nelson, W., and Howell, H., "Orbital Service Module Thermal Control System Design," Paper No. 79-ENAS-22, American Society of Mechanical Engineers, 1979.

<sup>21</sup>Filippi, F., Nervegna, N., and Zarotti, G., "Modularity and Optimization in Fluid Loop Radiator Systems," Paper No. 79-ENAS-37, American Society of Mechanical Engineers, 1979.

<sup>22</sup>Weidner, D., "Space Environment Criteria Guidelines for Use in Space Vehicle Development (1969) Revision)," NASA-TM X-53957, 1969.

The radiator for the rail gun OTV must therefore, be designed to survive impact by meteoroids with mass at least up to  $5 \times 10^{-5}$  grams.

Either one of two general design approaches are used to protect against radiative failure due to meteoroid impacts. Radiator component redundancy is used to reduce the probability that meteoroid damage will cause complete radiator failure. Redundancies of 100%-200% are usually required to obtain radiator reliabilities greater than 99%.<sup>2 3</sup> Radiators designed with redundancy therefore, have a mass ranging from 2 to 3 times the radiator mass required to reject design heat loads.

A second design approach used to reduce the mass penalty of redundant systems is to use little or no redundancy and to surround critical radiator components with a thin sacrificial shell called a "meteoroid bumper." The bumper, physically spaced several centimeters away from the protected radiator surface, is designed to fragment and/or vaporize high velocity meteoroids. The energy density of the debris plume of meteoroids which perforate the shield is sufficiently low to prevent damage of the critical radiator component surfaces. As predicted from equations in Reference 19, the radiator bumper thickness required to protect a rail gun radiator against damage by meteoroids with mass of approximately  $5 \times 10^{-5}$  grams ranges from 0.08 mm to 0.5 mm. While

---

<sup>2 3</sup>Wright, J., "Optimization of Large Heat Pipe Radiators for Long Life Space Heat Rejection Systems," Paper No. 79-ENAS-25, American Society of Mechanical Engineers, 1979.

meteoroid bumper design optimization is specific to the spacecraft design, these bumper thicknesses imply that satisfactory rail gun OTV radiator reliability can be obtained with a meteoroid bumper radiator design at much lower mass than with a redundant component radiator design. The attractiveness of meteoroid bumper design is however somewhat mitigated by the reduction in specific radiated power caused by the meteoroid bumper.

For purposes of analyzing the effects of a meteoroid bumper on radiator performance the meteoroid bumper and the radiator surface are assumed to be two plain parallel surfaces, thermally connected by radiative interchange as shown in Figure 15. We assume that both surfaces of the meteoroid bumper are at a constant temperature,  $T_2$ . The meteoroid bumper reflects part of the radiation emitted by the radiator surface and absorbs part. The absorbed radiation is then emitted to the surroundings at an intermediate temperature between the radiator surface temperature and the temperature of the surroundings. The effect of the meteoroid bumper on overall radiant heat transport may be determined by conservation of energy considerations at plane A and plane B. An equivalent emissivity,  $\epsilon$ , for use in Equation (42) can then be found. Assuming that the radiator surface and the inner and outer surfaces of the meteoroid bumper have independent emissivities of  $\epsilon_1$ ,  $\epsilon_2$ ,  $\epsilon_3$  respectively, the equivalent emissivity of the radiator-meteoroid bumper combination may be written as

$$\epsilon_e = (\epsilon_1^{-1} + \epsilon_2^{-1} + \epsilon_3^{-1} - 1)^{-1} \quad (43)$$

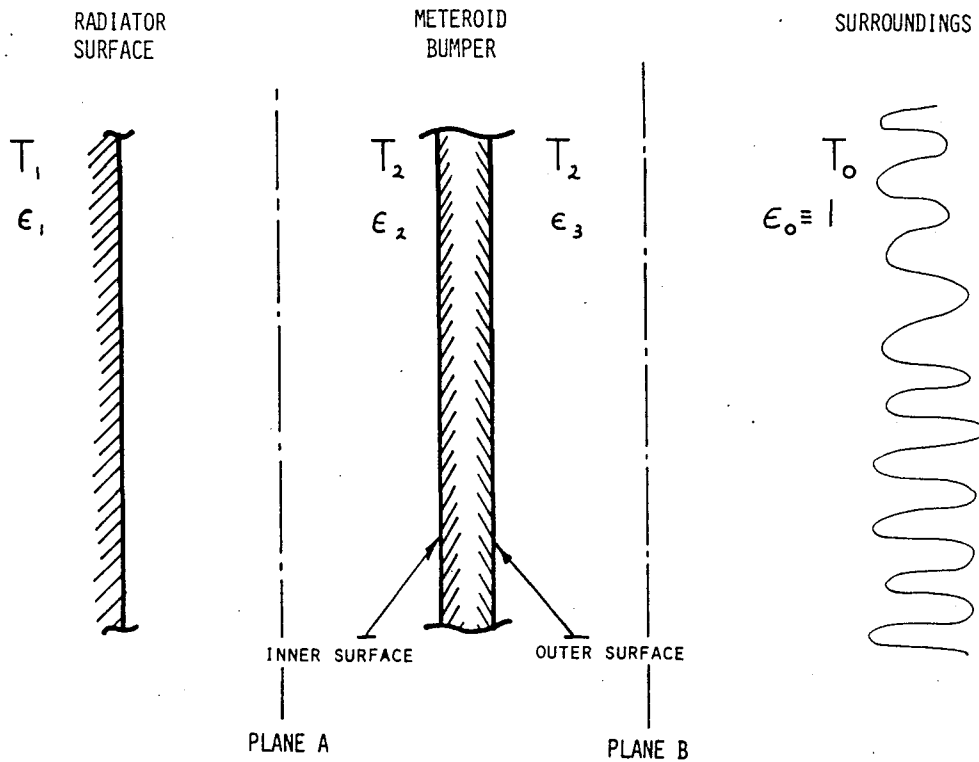


Figure 15. Meteoroid bumper protected radiator.

where,  $\epsilon_e$ , is the equivalent emissivity of a radiator with no meteoroid bumper. Assuming that the radiator surface and the meteoroid bumper surfaces are all spectrally black (i.e.,  $\epsilon_1 = \epsilon_2 = \epsilon_3 = 1$ ) Equation (43) shows that a meteoroid bumper protected radiator has an emissivity of only one-half of an unprotected black radiator surface. Emissivities of practical surface coatings range from 0.85 to 0.95. The corresponding equivalent emissivity of a meteoroid bumper protected radiator ranges from 0.39 to 0.44. The specific radiated power of a meteoroid bumper protected radiator with  $\epsilon_1 = \epsilon_2 = \epsilon_3 = 0.9$ , is compared to the specific radiated power of an unshielded radiator in Figure 16, for an effective sink temperature,  $T_o$ , of 230°K. Recalling that an unshielded redundant element radiator must be oversized

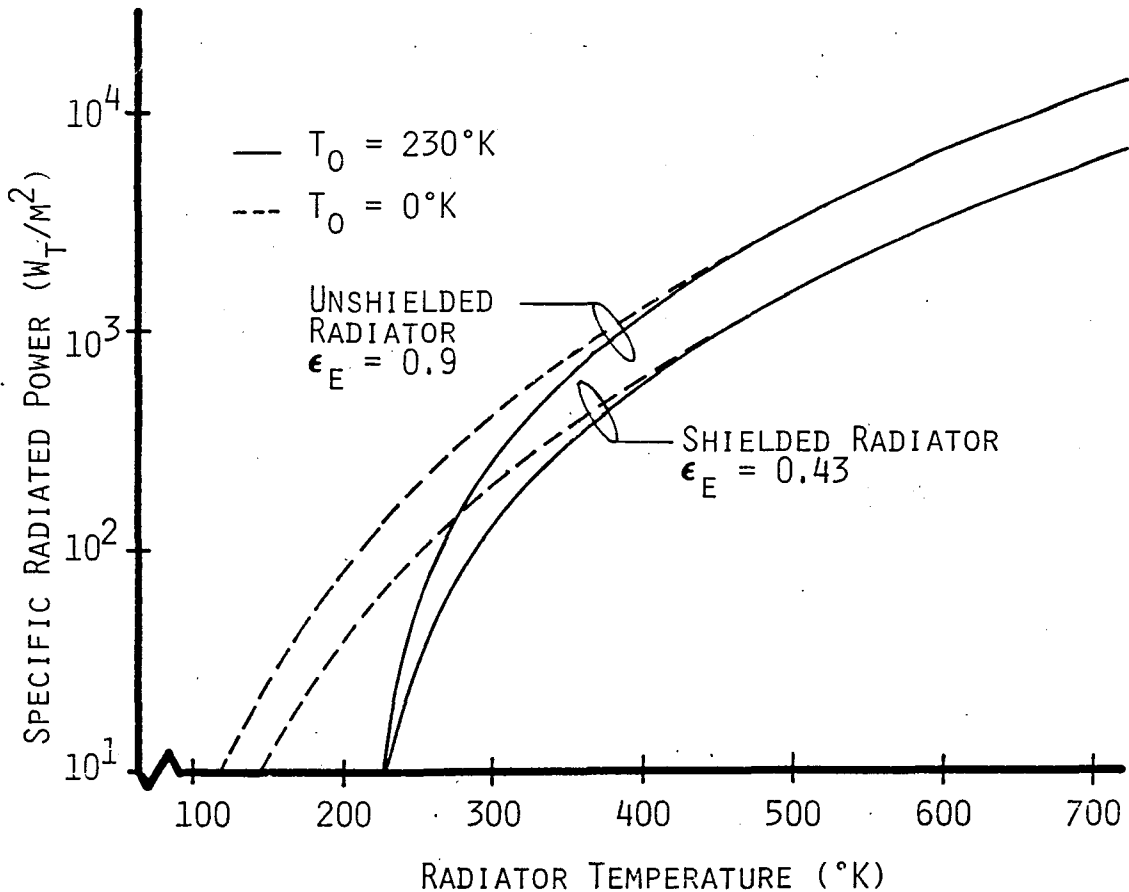


Figure 16. Bumper shielded and unshielded radiator performance comparison.

by a factor of approximately 2 to 3, and that the meteoroid bumper of the shielded radiator design is a small fraction of radiator mass, the alternative design concepts will have approximately equal mass. Selection between the two alternatives must be made on specific spacecraft design requirements.

A second characteristic apparent from Figure 16, is that below a radiator surface temperature of  $230^{\circ}K$  no heat can be rejected from the spacecraft. A radiator surface temperature above approximately  $375^{\circ}K$ , would practically eliminate the effect on heat rejection, of radiation absorbed from the sun, earth, and other parts of the spacecraft.

As illustrated in Figure 16, elevated temperature heat rejection is desirable. Higher operating temperatures however, increase rail gun resistive losses and decrease rail mechanical strength due to thermal softening of the rails. Copper alloys (for example, zirconium-copper) permit elevated temperature ( $\approx 650^\circ\text{K}$ ) rail gun operation with only modest increase in rail resistivity and decrease in rail strength.<sup>24</sup> For this analysis, we chose radiator/rail gun operating temperatures in the range from  $375^\circ\text{K}$  to  $450^\circ\text{K}$ . From Figure 16, the corresponding specific radiated power for a shielded radiator ranges from  $400 \text{ W/m}^2$  to  $900 \text{ W/m}^2$  with an average specific radiated power equal to  $625 \text{ W/m}^2$ . For a  $25 \text{ kW}_e$  rail gun propulsion system at 30% efficiency, the required radiator surface area is equal to  $28 \text{ m}^2$ .

#### 2.2.5.2 Radiator Mass and Configuration

Specific radiator system design and therefore radiator system mass is a function of the operating temperature, life and reliability. Radiator system design may be categorized according to the method employed for thermal transport from the heat source to the radiator. Heat pipe radiators are passive, requiring no mechanical pumping for thermal transport. Pumped fluid radiators on the other hand require a pump for active thermal transport. Heat pipe radiators are inherently more reliable than pumped coolant systems. High source heat flux at moderate temperature (less than  $500^\circ\text{K}$ ) such as found in the rail

---

<sup>24</sup>American Metal Climax, Inc., "AMZIRC," AMAX Publication No. OF/66-2791, 1966.

gun usually requires a pumped coolant system. New design concepts propose hybrid radiators comprised of pumped coolant components to remove heat from the source and transport it to the radiator which is a heat pipe unit. The selection among heat pipe, pumped coolant, and hybrid radiator systems appears to be spacecraft dependent. Trade-off studies have shown that minimum radiator system mass depends more on mission life and reliability requirements and overall spacecraft compatibility than radiator design type.<sup>19-22,25</sup> We assume that for the rail gun propulsion system under study radiator life would be 2 to 3 years and 0.90 reliability would be adequate (assuming an unmanned vehicle).

The mass of conventional heat pipe, pumped coolant, and hybrid radiator systems was approximated by relating radiator system specific mass (i.e., mass per unit radiated power) to a fourth power temperature relationship, for radiators with similar life and reliability. Based on data in References 19, 20, 21, 22, 25, 26 and 27 we found that radiator specific mass,  $\alpha_{hr}$ , can be related to radiator temperature, T, by

$$\alpha_{hr} = 2 \times 10^8 T^{-4} \quad (44)$$

---

<sup>25</sup>Alario, J. and Haslett, R., "Modular Heat Pipe Radiators for Enhanced Shuttle Mission Capabilities," Paper No. 79-ENAs-17, American Society of Mechanical Engineers, 1979.

<sup>26</sup>Ellis, W., "Radiator Heat Rejection Options for Shuttle Payloads," Paper No. 79-ENAs-18, American Society of Mechanical Engineers, 1979.

<sup>27</sup>Koenig, D., Ranken, W., and Salmi, E., "Heat Pipe Reactors for Space Power Applications," AIAA Paper No. 77-491, American Institute of Aeronautics and Astronautics, 1977.

as illustrated by the uppermost line in Figure 17. The data in these references spans the temperature range from 290°K to 900°K and spans heat rejection requirements ranging from 600 W thermal to 1 MW thermal. Most of these designs would be constructed from aluminum or titanium materials.

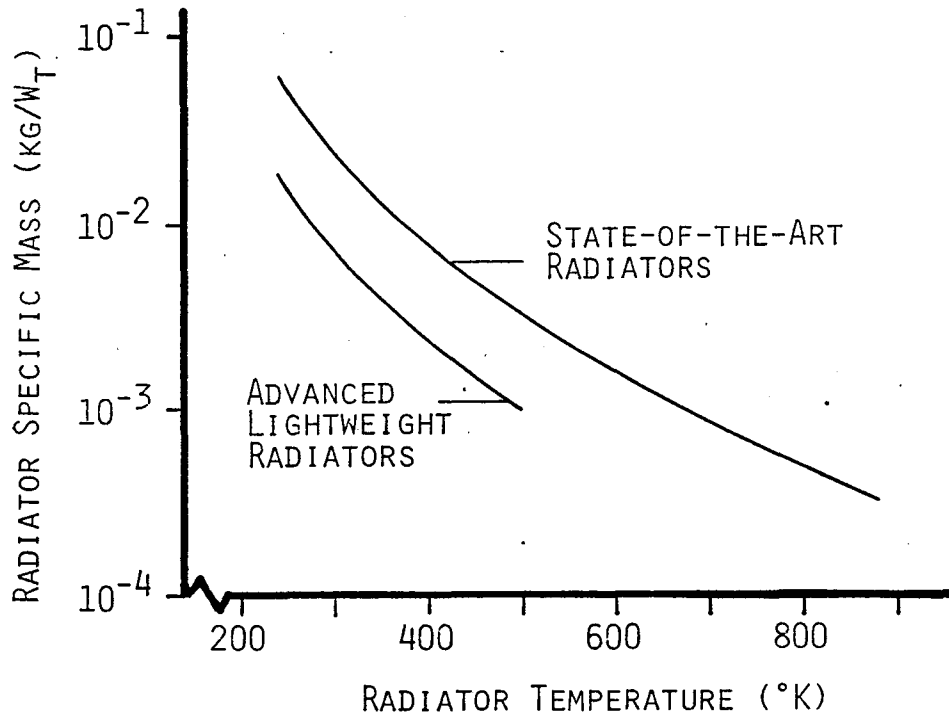


Figure 17. Radiator specific mass.

Advanced lightweight radiator concepts currently being developed employ lightweight plastic construction concepts (for example, FEP teflon).<sup>26</sup> These radiators would be flexible and would be roll-out deployed by inflatable extension members. Pumped coolant is the only practicable thermal transport concept thus far developed. We estimated the mass of lightweight

radiators based on the design concepts described in Reference 26 for the various components required in a lightweight radiator system protected by a meteoroid bumper. Lightweight radiator mass is scalable by a fourth power temperature relationship as given by

$$\alpha_{hr} = 6 \times 10^7 T^{-4} \quad (45)$$

and is illustrated in Figure 17. The plastic materials employed in the lightweight radiator permit a maximum operating temperature of less than 500°K. The lightweight radiator would be less than half as massive as a conventional radiator, due largely to the decrease in material density. Assuming that the lightweight radiator design would be compatible with the electric rail gun, radiator system mass,  $M_r$ , in the temperature range from 375°K to 450°K is given by

$$M_r = 0.0018 P_r \quad (46)$$

where,  $P_r$ , is the thermal power rejected.

An attractive configuration of the lightweight radiator is to integrate it with the rail gun along the entire gun length as shown in Figure 18. A major advantage of this concept is to minimize thermal transport distance. The lightweight radiator loop would be supported on a truss structure which would also serve to rigidify the rail gun barrel. The coolant would

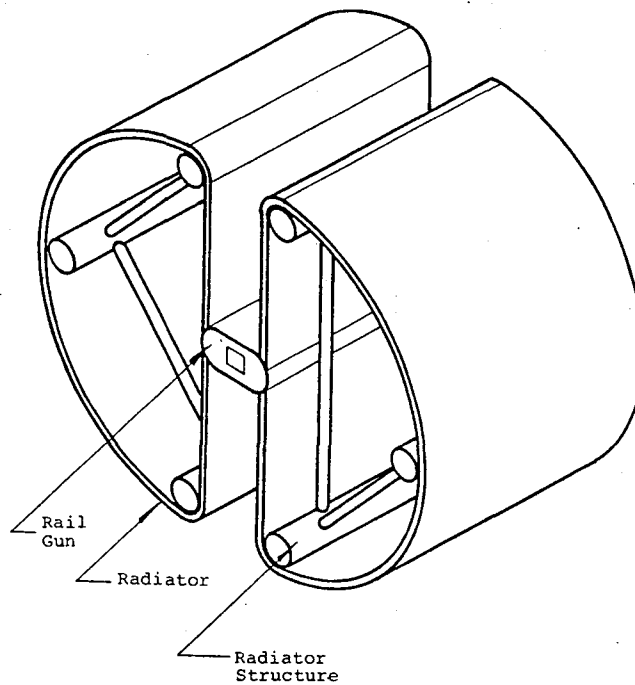


Figure 18. Rail gun radiator concept.

be pumped through channels on the backside of each rail as shown in Figure 19, and through the radiator loop. The overall diameter of the radiator loop shown in Figure 18 would be approximately 0.8 m for a 25 kW<sub>e</sub> propulsion system and approximately 1.5 m for a 50 kW<sub>e</sub> propulsion system. Liquid coolant would probably be used to provide the most effective heat removal of the high thermal power density in the rails. Flow velocities in the coolant loop would be on the order of 1 to 2 m/s. Convective heat transfer coefficients ranging from 6000 W/m<sup>2</sup>/°K to 12,000 W/m<sup>2</sup>/°K (assuming water or water-like coolant properties)<sup>28</sup> could be achieved.

---

<sup>28</sup>Kreith, F., Principals of Heat Transfer, Intext Educational Publishers, New York, 1973, pg 14.

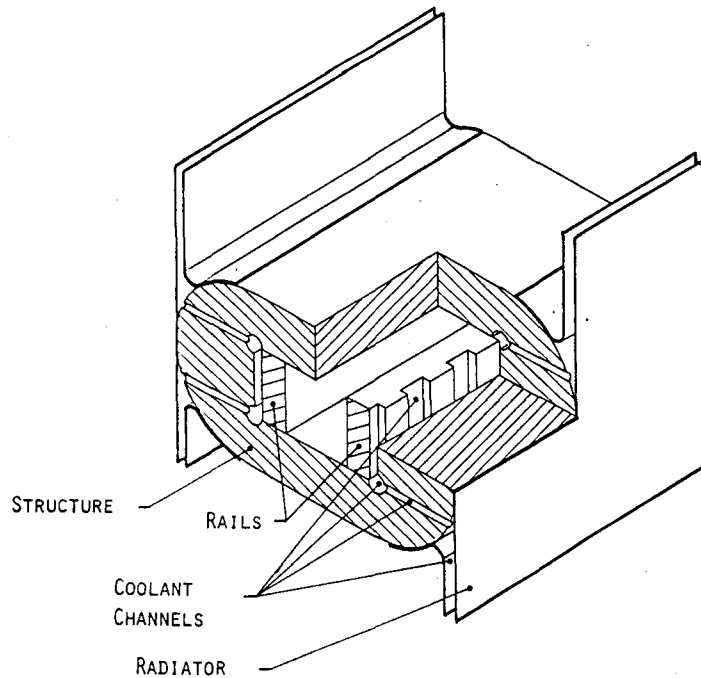


Figure 19. Coolant channels in rail gun.

Assuming a  $25 \text{ kW}_e$  propulsion system and a 2 mm rail gun bore size, the coolant temperature rise would range from  $40^\circ\text{K}$  to  $80^\circ\text{K}$ . Detailed radiator system design would be required to determine trade-offs among temperature rise, pumping power requirements, and radiator mass.

### 2.3 SYSTEM PERFORMANCE

Analytical expressions describing propulsion system mass and performance were developed to enable analytical mission performance analyses. Earlier system and mission analyses demonstrated that system mass and efficiency, pellet exhaust velocity, and system power level are the important parameters required to describe the propulsion system. The steps required to formulate

the system model in terms of these variables is briefly described in the following paragraphs.

The rail gun propulsion system mass,  $M_e$ , is obtained by summing the mass of the five subsystems described in Section 2.2

$$M_e = M_{ps} + M_{pc} + M_a + M_l + M_r \quad (47)$$

The system electrical efficiency,  $\eta_e$ , is equal to the product of rail gun efficiency and power conditioning efficiency and may be written as

$$\eta_e = \eta_a \eta_{pc} \quad (48)$$

Examining the expressions for subsystem mass and efficiency developed in Section 2.2, the system mass and efficiency are found to be a function of system power, pellet exhaust velocity, pellet mass, stored energy, pellet launch time, and launch frequency. The independent parameter set can be reduced to pellet mass, exhaust velocity, and launch frequency by noting that: stored energy is equal to the pellet kinetic energy divided by accelerator efficiency and therefore can be related to pellet mass and exhaust velocity; system power is proportional to the product of pellet kinetic energy and launcher frequency; and that pellet launch time and rail gun efficiency are a function only of pellet mass and exhaust velocity as described in Section 2.2.2.

Rather than perform the algebraic manipulations required to relate mass and efficiency to the three independent variables

a digital computer was used to facilitate the evaluation numerically. All equations for subsystem mass developed in Section 2.2 along with Equations (47) and (48) were programmed, and the independent parameters were systematically varied. Data for the mass and efficiency for each of the subsystems was output in terms of system power, exhaust velocity and frequency.

We found that, for a given power level and pellet exhaust velocity, system mass was minimized at a particular launch frequency. Power levels ranging from 25 kW<sub>e</sub> to 100 kW<sub>e</sub> and exhaust velocities ranging from 5000 to 20,000 m/s were examined. We found that the optimizing frequency is relatively insensitive to both power level and exhaust velocity and ranges from 8 to 10 Hz for all combinations of power level and exhaust velocity investigated.

Frequency was eliminated as an explicit independent variable by correlating the system mass and efficiency at optimal frequency to power level and exhaust velocity using a numerical non-linear regression analysis. We found that the frequency minimized system mass, M<sub>e</sub>, can be expressed as a simple linear function of system power given by

$$M_e = 25 + 0.0178P \quad (49)$$

which is illustrated in Figure 20. The major components comprising the optimized system mass are also shown in Figure 20. The solar cell array power supply obviously dominates system mass

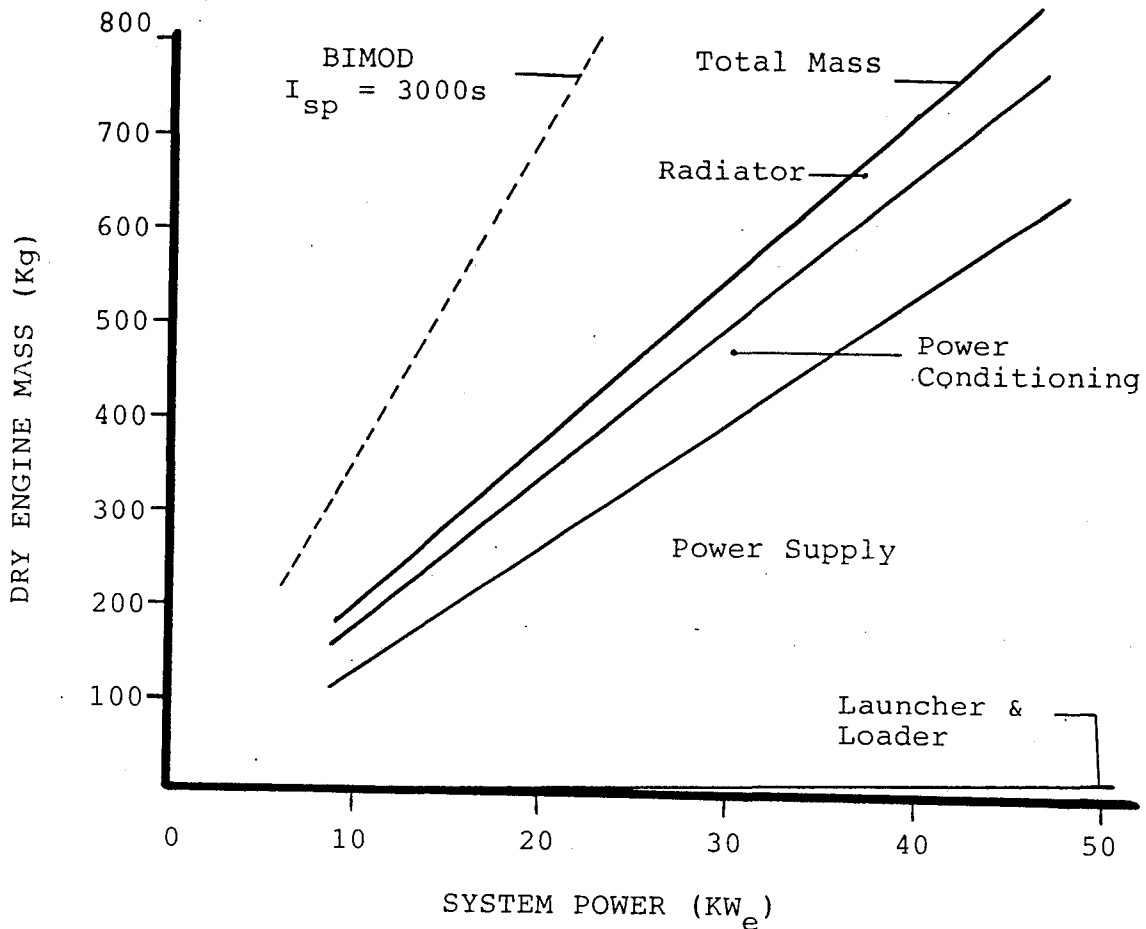


Figure 20. Electric rail gun propulsion system mass compared to BIMOD

followed by power conditioning and radiator mass. Figure 20 also compares BIMOD ion thruster propulsion system mass<sup>18</sup>, to the optimized rail gun propulsion system mass and shows that BIMOD mass is higher throughout the power range.

At optimal frequency the rail gun propulsion system efficiency,  $\eta_e$ , was found to be described by

$$\eta_e = 14.4v^{-0.566}P^{0.116} \quad (50)$$

which is illustrated in Figure 21. The inverse relationship of rail gun system efficiency to pellet exhaust velocity (specific impulse) contrasts with the direct proportionality relationship between BIMOD system efficiency and specific impulse as shown in Figure 21.

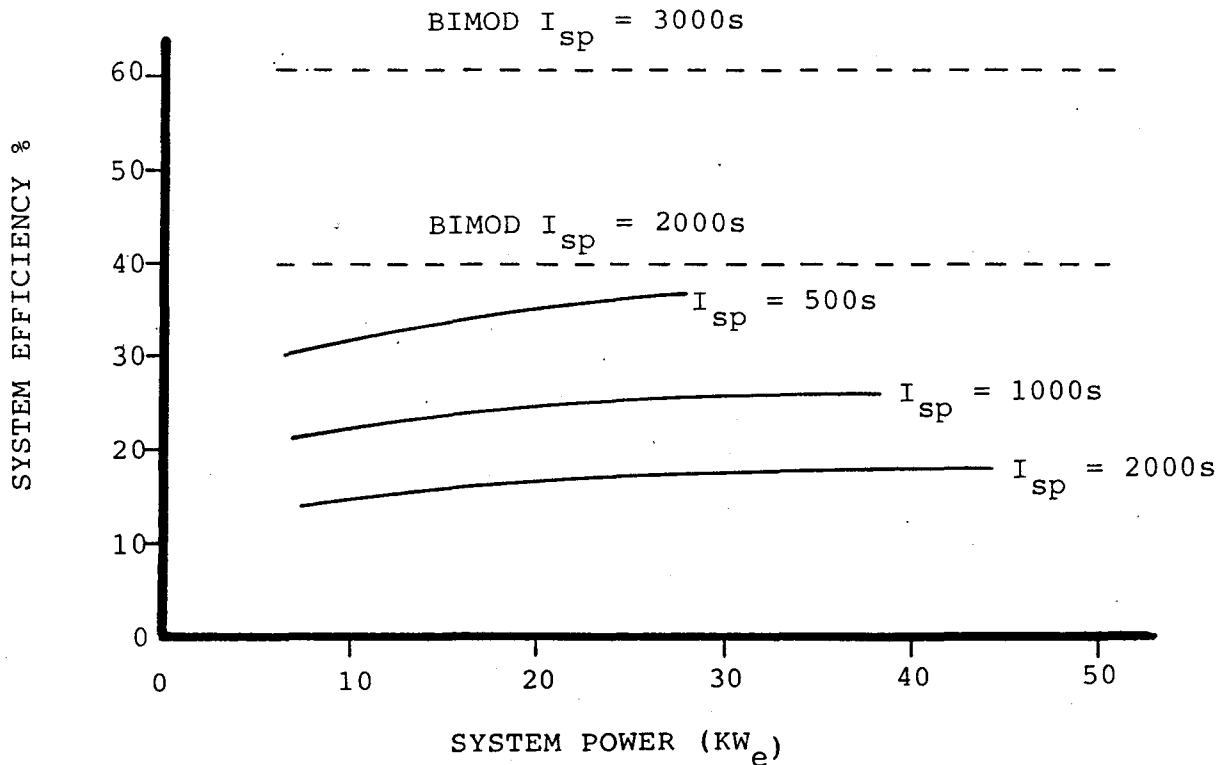


Figure 21. Electric rail gun propulsion system efficiency compared to BIMOD

The expressions describing optimized rail gun propulsion system mass and efficiency described by Equations (49) and (50), were used to examine rail gun propulsion system OTV mission performance. Pellet exhaust velocity was constrained in the range from 5,000 m/s to 20,000 m/s and system power level was constrained in the range from 25  $kW_e$  to 100  $kW_e$ .

A sketch showing a conceptual configuration of the electric rail gun propulsion system is shown in Figure 22. All major sub-systems and components can be seen in this figure except for the pellet loader. The payload was simply chosen to be representative of the payload size which could be attached to the rail gun propulsion system.

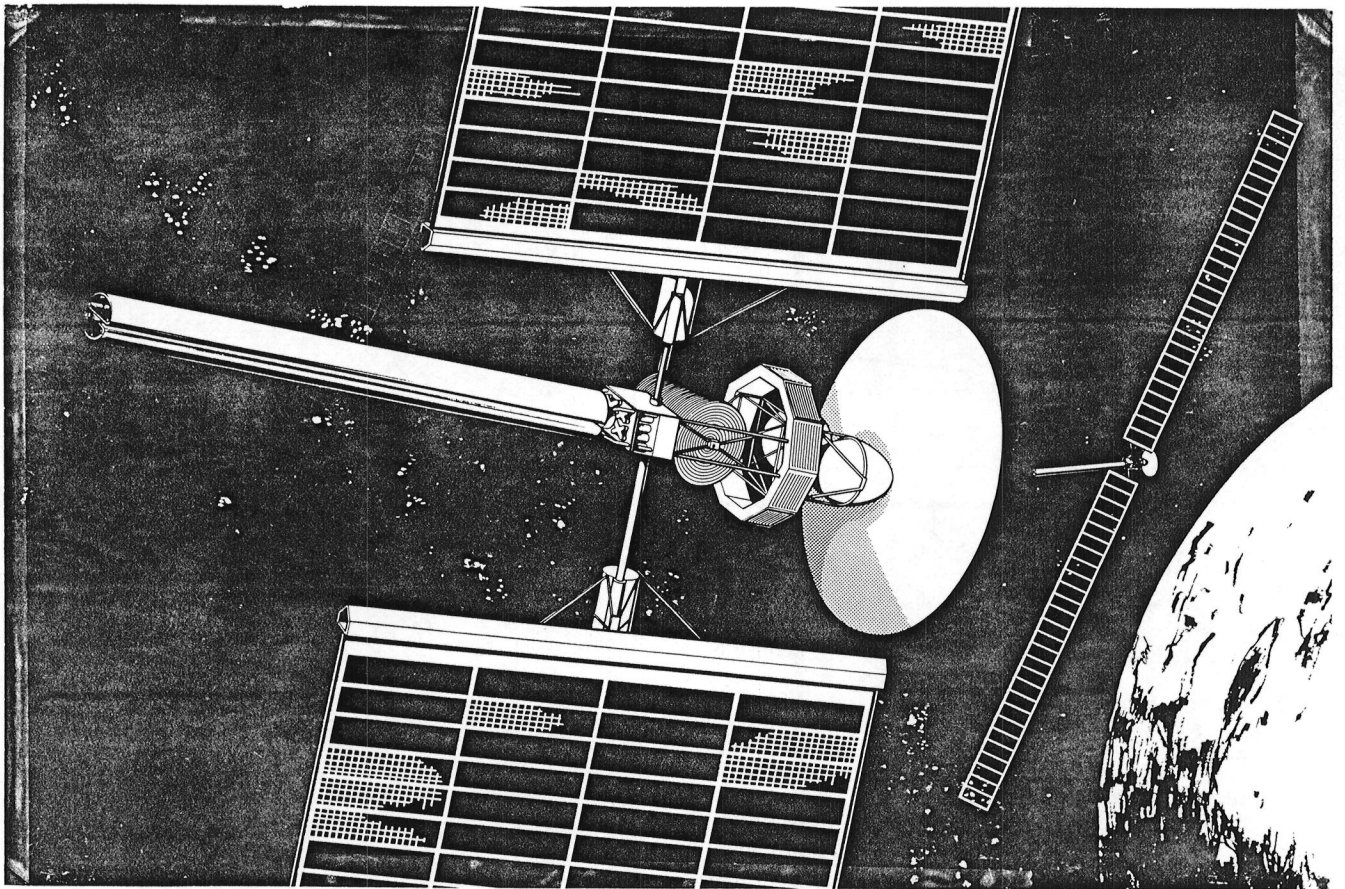


Figure 22. Conceptual configuration of electric rail gun propulsion system.

Two areas of subsystem interaction can be identified by observing Figure 22. As discussed in Section 2.2.5 the waste heat radiator integral with the rail gun could operate at elevated temperatures. During certain portions of every orbit the solar cell array would be subjected to this elevated temperature radiation. The amount of thermal radiation received and the effect on the solar cell array is difficult to estimate at this point. Elevated temperature self annealing solar cells (such as GaAlAs cells) may actually benefit from the thermal radiation. The electro-magnetic radiation emitted due to the high current pulsing of the pulse forming inductor may effect system electronics. This effect is difficult to evaluate, but must be considered in detailed design. We feel that these subsystem interactions do not significantly effect system feasibility.



SECTION 3  
MISSION ANALYSIS

The mission performance of an electric rail gun propulsion system was analysed for coplaner payload transfer from low earth orbit (LEO) to geosynchronous orbit (GEO). The mission examined included payload transfer from LEO to GEO followed by the return of the propulsion system to LEO for reuse. One way transfer from LEO to GEO of the propulsion system and payload was examined. The rail gun mission performance was compared to two alternative orbital transfer propulsion devices; a 30 cm BIMOD ion thruster propulsion system, and the inertial upper stage (IUS) chemical propulsion unit. Mass was the single parameter used to characterize payloads. Payload masses of 1150 and 2300 kg were considered.

The mission performance of the electric propulsion systems was analyzed based on low thrust, spiral-up orbital mechanics. The IUS mission performance was analyzed based on the classical two impulse Hohmann transfer. Electric rail gun system performance characteristics used in the mission analysis were derived from Equations (49) and (50). BIMOD system performance data were obtained from Reference 18. Two-staged IUS system performance data was obtained from Reference 29.

The objective of the mission analyses was to establish the conditions which minimize propulsion system initial mass in LEO

---

<sup>2</sup> NASA, "NASA Space Systems Technology Model," To Be Published

for a given LEO to GEO trip time and subject to power supply size constraints. The assumptions in all cases included propulsion system operation at the full available power of the power supply, and constant exhaust velocity throughout the LEO to GEO transfer. For the rail gun system, an optimization is required to find the exhaust velocity which minimizes the initial propellant or system mass. The approach in the mission analysis was therefore to select a trip time and solve the orbital transfer equations to determine the exhaust velocity which results in the lowest initial mass or the lowest propellant mass. Mission analysis details are fully described in Appendix A.

Due to the directly proportional relationship of BIMOD system efficiency to exhaust velocity, there is no advantage in orbital transfer missions to operate the ion thruster at less than the maximum obtainable exhaust velocity. System mass and trip time are therefore uniquely related with no optimization required.

The effect of solar shadowing on electric propulsion OTV performance is included in all mission analyses as described in Appendix A. The system mass and propellant mass requirements are both increased by solar shadowing and these effects are included in all the results presented in this report. The trip time is also increased by solar shadowing (by  $\approx 25\%$ ), however, this effect is not included in the results displayed (i.e., the trip times assume continuous thrusting). The effect of solar cell array degradation due to charged particle bombardment in near earth space could not be adequately handled by the analysis programs available. Due to the high solar cell degradation, the numerical optimization

computer code was unable to iterate to optimal solutions with the available machine resources (Appendix A). For both electric propulsion alternatives therefore we calculated mission performance assuming no solar cell array degradation during the mission.

In the following paragraphs, we first summarize the results describing electric rail gun OTV mission performance. We then compare the electric rail gun system with the BIMOD ion thruster and the IUS. These results are fully described in Appendix A.

### 3.1 ELECTRIC RAIL GUN SYSTEM

The mass elements (at LEO) of an electric rail gun OTV configured for a 2300 kg payload transfer from LEO to GEO followed by the return of the propulsion system to LEO are shown in Figure 23. For a given LEO-GEO transfer time Figure 23 illustrates optimal total spacecraft mass, subject to one of three constraints: minimum initial mass; 50 kW<sub>e</sub> power supply; or 25 kW<sub>e</sub> power supply. The minimum initial mass curve represents the minimum spacecraft mass that could be employed for a given LEO-GEO transfer time. Limiting the size of the solar cell array to 50 kW<sub>e</sub> output results in only a small change from the optimal minimum initial mass condition for outbound transfer times longer than 60 days. At 110 days the 50 kW<sub>e</sub> power level is optimal. The 50 kW<sub>e</sub> propulsion system could accomplish the transfer in trip times as short as about 45 days. However, the propellant mass required to accomplish the transfer would become quite large. A 25 kW<sub>e</sub> propulsion system could accomplish the transfer in an outbound time as short as 70 days, but would be far from optimal at trip times shorter than about 120 days. In all cases as the trip times become shorter propellant mass begins to dominate total system mass.

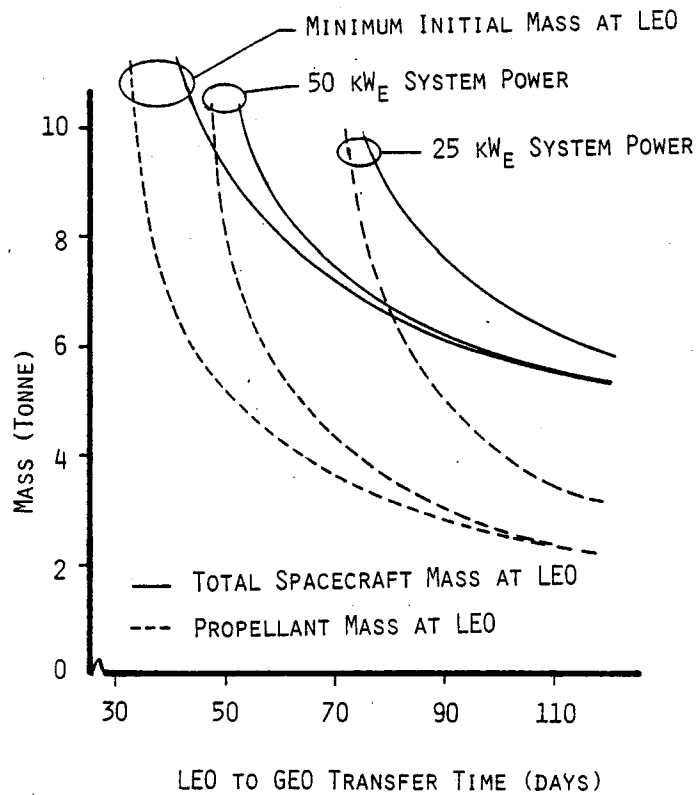


Figure 23. Mass requirements to transfer a 2300 kg payload from LEO to GEO with a rail gun OTV.

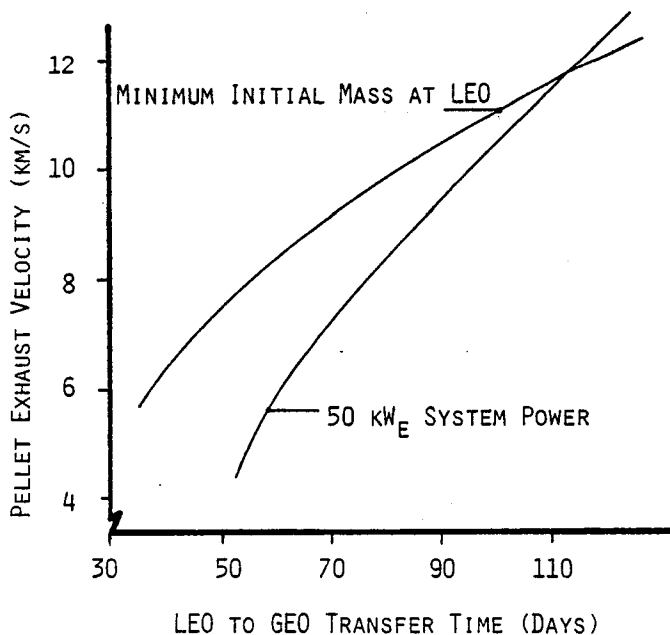


Figure 24. Pellet exhaust velocity requirements to transfer a 2300 kg payload from LEO to GEO with a rail gun OTV.

Pellet exhaust velocities which result in optimal mass conditions (as shown in Figure 23) are illustrated in Figure 24 for the minimum initial mass constraint and the 50 kW<sub>e</sub> power supply constraint. The optimal pellet exhaust velocity during the inbound trip from GEO to LEO is very similar to the outbound pellet exhaust velocity shown in Figure 24 (see Appendix A). Requirements on pellet exhaust velocity do not exceed 13 km/s at 110 days outbound trip times and at 50 days are only around 5 to 6 km/s (which is near demonstrated rail gun capability<sup>2</sup>).

Figures 23 and 24 illustrate that an electric rail gun would provide an enabling capability to effectively trade-off shorter trip durations with increased propellant requirements. The trade-off is obtained by adjusting pellet exhaust velocity while operating at constant power. Many mission options would become available with this enabling trade-off. For example, a single reuseable electric gun OTV could be used in one mission for rapid LEO to GEO payload transfer and for highly efficient propellant usage in a subsequent transfer.

For payloads which require high power and/or station keeping in GEO it may be advantageous to construct the rail gun propulsion system as an integral part of the payload, and not return the propulsion system to LEO for reuse. We examined the effect of one way trips on rail gun propulsion system operation (see Appendix A). The effect on mass of one way trip operation is shown in Figure 25 for a 2300 kg payload and a power supply limited to 50 kW<sub>e</sub> output. The initial mass for one way transfers is significantly less than about 90 days. A 50 kW<sub>e</sub> rail gun reuseable propulsion system could accomplish the LEO-GEO transfer in 60 days while for one way use the transfer could be accomplished in as little

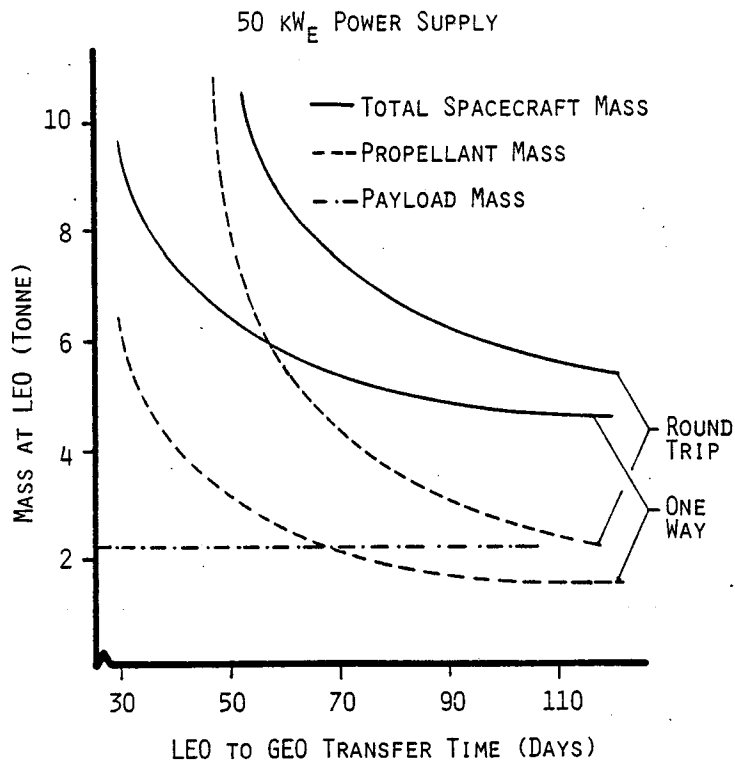


Figure 25. Effect of reusable versus one-way missions on rail gun propulsion system mass requirements.

as 30 days. The advantage in mass of one way transfers increases at lower trip times due to the reduction in propellant required.

The effect of payload mass scaling on propulsion system mass is shown in Figure 26. Data from Reference 1 were used for the larger payload masses. As illustrated the mass scales approximately linearly. The apparent discontinuity between the results of this study and those of Reference 1 arises from the much higher solar cell array mass used in this study. (i.e., 13.5 kg/kW<sub>e</sub> compared to 5 kg/kW<sub>e</sub>).

### 3.2 COMPARISON OF ALTERNATIVE PROPULSION SYSTEMS

Uniform comparison of performance among the electric rail gun propulsion system, the BIMOD ion thruster system, and the IUS chemical propulsion system requires that only one way LEO

60 DAY LEO-GEO TRANSFER

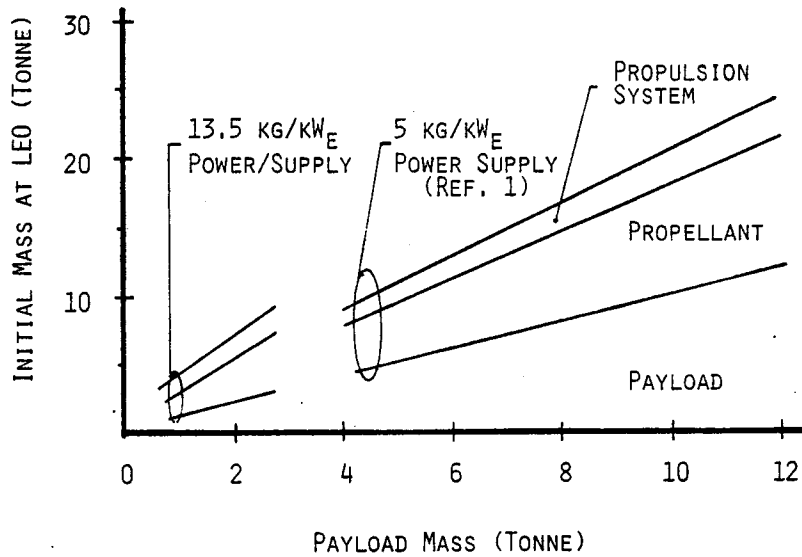


Figure 26. Effect of payload mass on rail gun propulsion system mass requirements.

to GEO transfers be considered since the IUS cannot return from GEO to LEO. The comparisons may be done based on the initial total propulsion system mass as a function of LEO to GEO transfer time characteristics for a 2300 kg payload as shown in Figure 27. The performance of the IUS is represented by a single point since there is little freedom in varying the transfer characteristics. The BIMOD performance is represented by a single curve, since there is no advantage to operating the BIMOD at less than full specific impulse capability.\* Selecting a trip time therefore defines the BIMOD power requirement and the system mass. The three curves for electric rail gun system mass representing the optimal configuration (min  $M_0$ ) and two constrained power level

\*Comparing a specific BIMOD at a single specific impulse

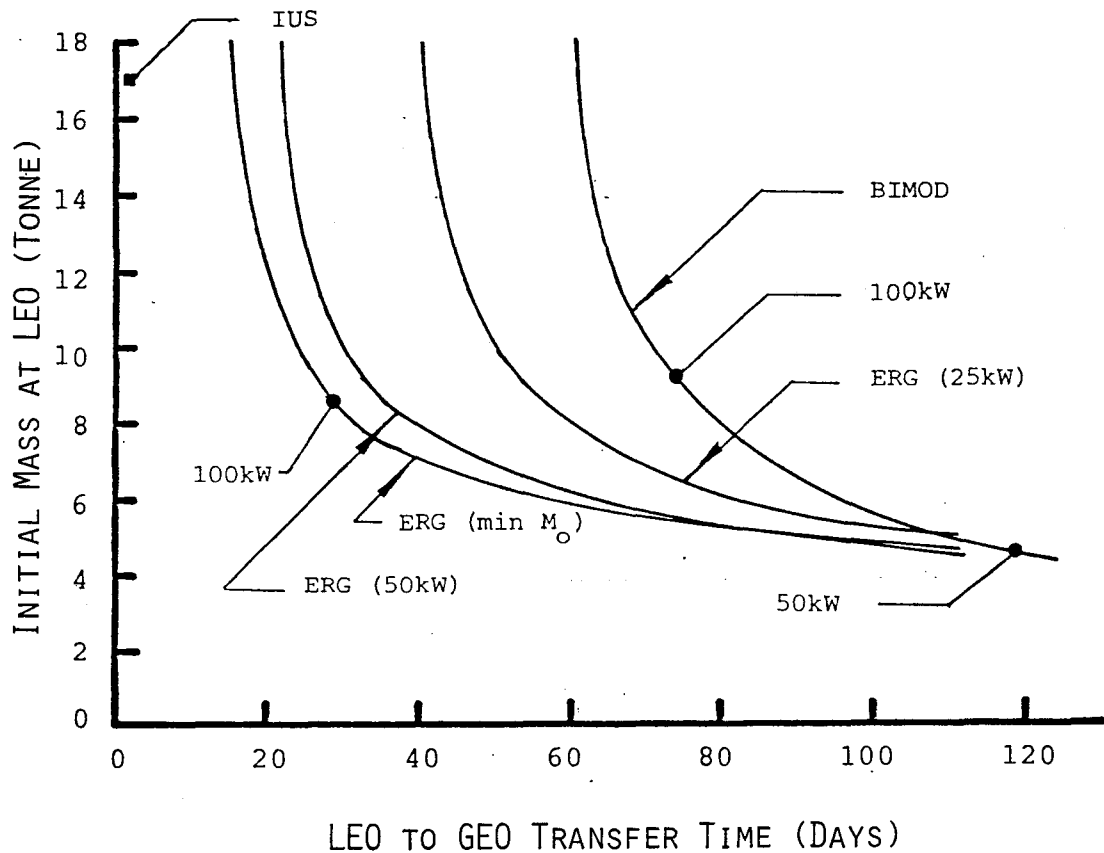


Figure 27. Comparison of alternative propulsion systems for one-way OTV missions.

configuration.

A number of comparisons can be made based on Figure 27. Comparing the three systems at an initial mass equal to 17 tons, the IUS can complete the transfer in less than 1 day, the electric rail gun can complete the transfer in the range from 15 days to 40 days depending on the system power level while the BIMOD can complete the transfer in approximately 60 days. Obviously if 1 day transfers are required chemical propulsion is the only alternative. For initial system mass ranging from 4.2 to 17 tons the

electric rail gun system can complete the transfer in the range from 15 to 130 days depending on the power level. The BIMOD in this mass range always has a longer trip time than the rail gun and ranges from 60 days to 130 days. For initial mass less than 4.2 tons both electric propulsion systems have trip times longer than 130 days but the higher specific impulse of the BIMOD makes it more attractive (i.e., lower mass).

The two electric propulsion alternatives may also be compared by imposing constraints on the system power level. Limiting the power to  $100 \text{ kW}_e$  the electric rail gun system could accomplish the transfer in times as short as 15 days, albeit with a severe mass penalty. If we constrain the power to  $100 \text{ kW}_e$  and the electric rail gun system mass is about equal to BIMOD system mass. The rail gun system can complete the transfer in 25 days while the BIMOD could accomplish the transfer in approximately 75 days. If the power level is constrained to  $50 \text{ kW}_e$ , the electric rail gun could complete the mission in as short as 22 days. If the mass is constrained to the same mass as the BIMOD at  $50 \text{ kW}_e$  the rail gun could complete transfer in 110 days while the BIMOD could complete the transfer in 120 days. At  $25 \text{ kW}_e$  the electric rail gun can complete the transfer in as short as 40 days. However at trip times longer than about 110 days the superior specific impulse of the BIMOD makes it more attractive.

In general comparing the two electric propulsion systems, for transfer times less than 130 days the electric rail gun system is more attractive than the BIMOD while at trip times greater than 130 days the BIMOD is more attractive than the electric rail gun.



## SECTION 4

### CONCLUSIONS AND RECOMMENDATIONS

A system concept has been developed for an electric rail gun based propulsion system for space applications. The subsystems and components associated with the major power flow on an electric rail gun system have been identified and the performance analysed. State-of-the-art or near term advancements in component technology have been assumed in the subsystem and system evaluation. In this section, we describe our conclusions about the electric rail gun propulsion concept. We also describe our assessment of the technology development requirements and make recommendations for further development of the electric rail gun propulsion concept.

We conclude that an electric rail gun propulsion system is technically feasible. We found no problems which in principle would block technical accomplishment. In fact, most of the required technology is largely developed. We also conclude that an electric rail gun propulsion OTV system would be most attractive for missions requiring orbital transfers in less than 120 days. In the 20 to 120 day mission transfer regime the electric rail gun system would have both lower initial deployed mass and lower propellant requirement than a BIMOD ion thruster system and the IUS chemical propulsion system. At transfer times less than 20 days the IUS system is the only alternative and at transfer times greater than 120 days the superior efficiency and specific impulse of the BIMOD make it more attractive (i.e., lower mass). Finally, the electric

rail gun OTV system becomes increasingly attractive as payload mass increases. Both the ratio of propellant mass-to-payload mass and initial system mass-to-payload mass decrease with increasing payload mass. The attractive performance characteristics of an electric rail gun system will require, however, substantial investment in system development.

In the course of our subsystem investigations we assessed the state of current technology compared to the technology requirements of the electric rail gun propulsion system. We conclude that each subsystem requires important developmental work.

The SEPS type solar cell array would be compatible with an electric rail gun OTV. The domination of electric propulsion system mass by the power supply, however, places a premium on low specific mass power supplies. Successful development of such supplies would improve the attractiveness of all electric propulsion systems. In addition, the severe radiation degradation of current silicon solar cells implies that alternative technologies must be developed for LEO to GEO missions. Efforts to develop advanced spaceborne power supplies which overcome these problems (GaAlAs solar cell arrays; and nuclear electric power supplies) are already under way as part of other technology development programs.

Power conditioning components suitable for the electric rail gun system are also being developed in conjunction with other spaceborne and airborne systems. Advanced resonant DC converters, capacitors, inductors, and switches are currently under development. Improvements in specific mass of these components are desirable, but compatibility to electric rail gun circuits is required. Life

and reliability of DC converters, capacitors and switches must also be demonstrated.

The electric rail gun is obviously the key to the rail gun propulsion concept and it is the least developed component. Two major development milestones are required. First, rail gun pellet exhaust velocity must be demonstrated in the range from 5 km/s to 20 km/s. The second major milestone is demonstration of long life, high reliability operation at these high exhaust velocities. Successful solutions to barrel erosion, thermal fatigue and mechanical fatigue will require substantial developmental work. In addition, rail gun efficiency and performance scaling must be proven experimentally in the ranges of interest for electric rail gun propulsion.

Waste heat radiator technology is relatively well developed. The major development areas specific to electric rail gun propulsion include demonstration of long life radiators which are compatible to electric rail guns. Low mass, low power heat removal at high thermal power density from the rails must also be demonstrated.

Several options appear to be available for propellant handling and pellet loading. The major developmental requirement is demonstration of reliable, long life operation of the mechanical components.

Safe pellet disposal after launch is of critical importance to technical acceptability of an electric rail gun OTV system (or any other pellet launching concept). Pellet orbital control or pellet material selection (for sublimation) appear to be

feasible approaches to this problem. However for near earth space further analyses are required to investigate the pellet hazard to other spacecraft during the pellet disposal process.

An important step in any advanced electric propulsion concept development is the establishment of mission requirements for the propulsion device. In particular, the importance of orbital transfer time must be quantified and the benefits identified.

The development of the rail gun propulsion system should take a number of specific steps.

We feel that a development program should first address the development of the electric rail gun. The acceleration of pellets in the size range and to the velocities required for propulsion system operation must be demonstrated. Launcher life and reliability demonstrations would be the second major developmental goal. Power conditioning, pellet loading and waste heat removal specific to repetitive rail gun operation could be performed in parallel, after basic rail gun velocity and performance capabilities are proven.

Pellet disposal problems should receive further detailed treatment early in propulsion system development. Spacecraft safety hazards and/or political constraints must be satisfied early for overall concept acceptance.

## LIST OF REFERENCES

1. Bauer, D., Barber, J., Swift, H., and Vahlberg, C., "Electric Rail Gun Propulsion Study (Advanced Electric Propulsion Technology High Thrust)", Air Force Rocket Propulsion Laboratory, AFRPL-TR-81-02, December 1980.
2. Rashleigh, S., and Marshall, R., "Electromagnetic Acceleration of Macroparticles to High Velocities," J. Appl. Phys., March 1978.
3. Hawke, R., et al, "Results of Railgun Experiments Powered by Magnetic Flux Compression Generators," Lawrence Livermore National Laboratory, UCRL-84875, 1980.
4. Barber, J., "The Acceleration of Macroparticles in a Hypervelocity Electromagnetic Accelerator," Ph.D. Thesis, The Australian National University, 1972.
5. Young, L., "Solar Array Technology for Solar Electric Propulsion Missions," AIAA Paper No. 79-3086, Presented at the 14th International Electric Propulsion Conference, Princeton, NJ, October 30 - November 1, 1979.
6. Tada, H., and Carter, J. Jr., "Solar Cell Radiation Handbook," JPL Publication 77-56, Jet Propulsion Laboratory, Pasadena, CA, November 1977.
7. Hanley, G.M., "Evolution of Satellite Power System (SPS) Concepts," Report No. 78-9403, In Proceedings of the 13th Intersociety Energy Conversion Conference, August 20-25, 1978, San Diego, CA.
8. Tonelli, A.D., and Nussberger, A.A., "The Design and Evaluation of a 5 GW Ga-Al-As Solar Power Satellite (SPS)," Report No. 78-9404, In Proceedings of the 13th Intersociety Energy Conversion Conference, August 20-25, 1978, San Diego, CA.
9. Harris, C., and Crede, C., Ed., "Shock and Vibration Handbook," McGraw Hill Book Company, 1976, Chapters 36 and 37.
10. Biess, J., Inouie, J., and Schoenfeld, A., "Thyristor Power Processor for the 30 cm Mercury Electric Propulsion Engine," AIAA Paper 75-433, 1975.
11. Hansen, I., "Description of a 2.2 kW Power Transformer for Space Application," NASA Technical Memorandum 79138, NASA-Lewis Research Center, 1979.
12. Schwarz, F., "A 10 kW Lightweight DC Converter (Technology Feasibility Study for Lightweight Megawatt Range Converters)," AFAPL-TR-77-45, Air Force Aero Propulsion Laboratory, Wright-Patterson AFB, 1977.

13. Byers, D., Terdan, F., and Meyers, I., "Primary Electric Propulsion for Future Space Missions," NASA Technical Memorandum 79141, NASA-Lewis Research Center, Cleveland, Ohio, 1979.
14. Ramrus, A., "Development of a High Energy Density Capacitor for Plasma Thrusters," Air Force Rocket Propulsion Laboratory, Report No. AFRPL-TR-80-35, October 1980.
15. Westinghouse, Inc., Data Sheet for Fast Switching Thyristor, SCR-T9GH.
16. Westinghouse, Inc., General Purpose Rectifiers Data Sheet, R920.
17. Grover, F.W., Inductance Calculations--Working Formulas and Tables, D. Van Nostrand Company, Inc., Copyright 1946.
18. NASA-Lewis Research Center, "30-cm Ion Thrust Subsystem Design Manual," NASA Technical Memorandum 79191, June 1979.
19. Leach, J., and Stalmach, D., "Optimum Design of Spacecraft Radiators for Large Capacity or Long Duration Mission Applications," Paper No. 79-ENAS-10, American Society of Mechanical Engineers, 1979.
20. Nelson, W., and Howell, H., "Orbital Service Module Thermal Control System Design," Paper No. 79-ENAS-22, American Society of Mechanical Engineers, 1979.
21. Filippi, F., Nervegna, N., and Zarotti, G., "Modularity and Optimization in Fluid Loop Radiator Systems," Paper No. 79-ENAS-37, American Society of Mechanical Engineers, 1979.
22. Weidner, D., "Space Environment Criteria Guidelines for Use in Space Vehicle Development (1969) (Revision)," NASA-TM X-53957, 1969.
23. Wright, J., "Optimization of Large Heat Pipe Radiators for Long Lift Space Heat Rejection Systems," Paper No. 79-ENAS-25, American Society of Mechanical Engineers, 1979.
24. American Metal Climax, Inc., "AMZIRC," AMAX Publication No. OF/66-2791, 1966.
25. Alario, J. and Haslett, R., "Modular Heat Pipe Radiators for Enhanced Shuttle Mission Capabilities," Paper No. 79-ENAS-17, American Society of Mechanical Engineers, 1979.
26. Ellis, W., "Radiator Heat Rejection Options for Shuttle Payloads," Paper No. 79-ENAS-18, American Society of Mechanical Engineers, 1979.

27. Koenig, D., Ranken, W., and Salmi, E., "Heat Pipe Reactors for Space Power Applications," AIAA Paper No. 77-491, American Institute of Aeronautics and Astronautics, 1977.
28. Kreith, F., Principals of Heat Transfer, Intext Educational Publishers, New York, 1973, pg 14.
29. NASA, "NASA Space Systems Technology Model," To Be Published.



APPENDIX A

ELECTRIC GUN MISSION ANALYSIS  
RESULTS FOR NASA

C. JULIAN VAHLBERG  
BUSINESS AND TECHNOLOGICAL SYSTEMS, INC.



TABLE OF CONTENTS

	<u>Page</u>
1.0 INTRODUCTION.....	A-5
2.0 ENGINE MODELING AND MASS DIFFERENTIAL EQUATIONS.....	A-7
3.0 ORBITAL OPTIMIZATION EQUATIONS.....	A-11
3.1 Basic Orbital Transfer Equations.....	A-11
3.2 Optimal Exhaust Velocity Results.....	A-13
3.4 Constraint Upon Exhaust Velocity.....	A-14
4.0 INITIAL AND PROPELLANT MASS FOR SPECIFIC MISSIONS.....	A-17
4.1 Missions Being Considered.....	A-17
4.2 Analytic Results for the Missions.....	A-20
5.0 MISSION ANALYSIS RESULTS.....	A-23
5.1 Electric Rail Gun Performance Evaluation.....	A-23
5.2 Comparison with BIMOD.....	A-33
5.3 Comparison with Inertial Upper Stage (IUS).....	A-40
6.0 CONCLUSIONS AND RECOMMENDATIONS.....	A-45
7.0 REFERENCES.....	A-47
APPENDIX AA.....	A-49
APPENDIX AB.....	A-53
APPENDIX AC.....	A-55



## 1.0 INTRODUCTION

The electric rail gun (Reference 1) has been recognized as a potentially important space propulsion system. Pellet exhaust velocities have already been demonstrated which are higher than current chemical rocket exhaust velocities. Even higher exhaust velocities are probably achievable. Thus, the specific impulse is higher, hence propellant consumption lower than for chemical rockets. However, power must be provided by solar cell or nuclear power systems.

Ion thrusters such as BIMOD (Reference 2), which also require separate power systems, have an even higher specific impulse than probably achievable using a rail gun. However, they are much heavier relative to the thrust developed than the rail gun. Thus, past mission analyses using ion thrusters are not applicable due to the differences in propulsion system mass.

The rail gun has a significant advantage over ion propulsion systems since it can provide very high thrust levels, albeit at a low acceleration (relative to gravity) due to the relatively small mass of the power supply. These high thrust levels offer NASA an alternative to ion thrusters which require longer transfer times and chemical rockets which require large propellant masses.

This report provides documentation on studies investigating the implication upon mission planning of the rail gun concept. It is a continuation of the effort documented in Reference 3 which was based upon Air Force desires to raise 5, 12.5 and 25 ton payloads from low earth orbit (LEO) to geosynchronous orbit (GEO), then return the propulsion system to LEO. This effort has focused upon the smaller payloads which are of interest to NASA (1150 kg and 2300 kg).

The effort has been divided into analytic studies to size the system and determine basic tradeoffs, followed by numerical studies to determine

the effects of some of the more important effects of space flight in earth orbit. The report is organized as follows. Chapter 2 presents the analytical mass differential equations applicable to any propulsion system. Chapter 3 presents the optimal orbital differential equations applicable to transfers for which the propulsion acceleration is smaller than the gravitational acceleration. Some specific expressions for initial and propellant mass are presented in Chapter 4 which are applicable to this mission for which the power plant must be returned to LEO. Results of numerically minimizing those expressions are presented in Chapter 5 along with a comparison with the currently available BIMOD and Inertial Upper Stage (IUS). Conclusions and recommendations for further studies are presented in Chapter 6.

The effects of solar shadowing, as determined using the SECKSPOT Computer program, are given in Appendix A. Appendix B presents the form of equations used for the propulsion system mass and efficiency. Appendix C contains a glossary of symbols used in this report.

## 2.0 ENGINE MODELING AND MASS DIFFERENTIAL EQUATIONS

This chapter presents the models and equations for propellant mass depletion used for this analysis. They are derived from the fundamental physics which represent railgun performance. Similar expressions were derived in Reference 4. From the conservation of momentum we have:

$$m |A| = - \dot{m} c \quad (2-1)$$

where

$m$  = total spacecraft mass

$A$  = spacecraft acceleration

$\dot{m}$  = rate of depleting fuel  $\leq 0$

$c$  = fuel exhaust velocity  $\geq 0$ .

However, since the power is provided by a solar or nuclear power supply the power is limited. We, therefore, have the constraint:

$$\eta P = \frac{1}{2} \dot{m} c^2 \quad (2-2)$$

where

$P$  = total power provided by power supply

$\eta$  = propulsion system efficiency.

In general, it is assumed that all available power is being used. Combining equations (2-1) and (2-2) yields:

$$\dot{m} = - \frac{m^2 A^2}{2\eta P} \quad (2-3)$$

Alternatively:

$$\dot{m} = - \frac{2\eta P}{c^2} \quad (2-4)$$

as the expression for the fuel depletion as a function of either spacecraft, acceleration,  $A$ , or the exhaust velocity,  $c$ . Either one equation or the other will be used in other analyses depending upon what assumptions are made on the acceleration or exhaust velocity.

The relationship between acceleration and exhaust velocity is given by equation (2-5):

$$A = \frac{2\eta P}{mc} \quad (2-5)$$

A general solution to equation (2-3) is given by:

$$m(t) = \frac{m_0}{1 + \frac{m_0}{P} L_1^2 \frac{t}{t_f}} \quad (2-6)$$

where

$$L^2(t) = \frac{1}{2} \int_0^t \frac{A^2(s)}{\eta(s)} ds \quad (2-7)$$

In the special case of constant acceleration,  $A$ , and engine efficiency,  $\eta$

$$L^2(t) = L_1^2 \frac{t}{t_f} \quad (2-8)$$

where

$$L_1^2 = \frac{\Delta u^2}{2\eta t_f} \quad (2-9)$$

$\Delta u$  = equivalent change in linear velocity caused by A

$$= \int_0^{t_f} |A| dt$$

$t_f$  = total transfer time.

The propellant used to accomplish this change in velocity is given by:

$$m_p = m_0 - m(t_f) = \frac{m_0^2 L_1^2}{P + m_0 L_1^2} \quad (2-10)$$

The power and hence the power plant mass have not been specified yet. However, they will have a very critical effect upon the propellant used or equivalently, the initial mass,  $m_0$ , since it would be a critical component of  $m_0$ . In addition, obviously, the final mass must always be greater than the sum of the payload and propulsion system masses. The means for determining the optimal P will be given in a later section.

For the special case of constant exhaust velocity,  $c$ , the solution to equation (2-4) is given by:

$$m(t) = m_0 - \frac{2\eta P}{c^2} t \quad (2-11)$$

Alternatively, equation (2-1) can be rewritten as:

$$\frac{\dot{m}}{m} c = - |A| \quad (2-12)$$

and integrated in combination with:

$$\dot{u} = |A| \quad (2-13)$$

to yield:

$$m(t) = m_0 \left[ 1 - \left( 1 - e^{\frac{-\Delta u}{c}} \right) \frac{t}{t_f} \right] \quad (2-14)$$

$$m(t_f) = m_0 e^{\frac{-\Delta u}{c}} \quad (2-15)$$

The propellant used is, thus, given by:

$$m_p = m_0 - m(t_f) = m_0 \left( 1 - e^{\frac{-\Delta u}{c}} \right) \quad (2-16)$$

For this case, there are three (assumed) constant parameters:  $P$ ,  $c$ ,  $t_f$ . The choice (specification) of any two of these implies a value for the third. Alternatively, if less than two are specified then the excess parameters can be optimally chosen to minimize some other parameter of interest.

### 3.0 ORBITAL OPTIMIZATION EQUATIONS

The basic orbital equations of interest are derived in numerous places. Reference 5 has results which are closest to the transfer desired here. However, those results are extended and clarified in References 6 and 7.

The following are presented in the nomenclature of this report without derivation. The reader is referred to appropriate derivations in the above references. The orbital elements of interest are the mean orbital speed,  $v$ , and the inclination,  $i$ . The speed is related to semimajor axis,  $a$ , by

$$v = \sqrt{\frac{\mu}{a}} \quad (3-1)$$

where  $\mu$  is the gravitational constant. Another orbital element of potential interest is eccentricity. However, in the interest of keeping equations as simple as possible, eccentricity is not included since eccentricity does not change along an optimal transfer between circular orbits with an inclination change of less than  $36^\circ$ .

#### 3.1 Basic Orbital Transfer Equations

The differential equations for change in orbital elements are:

$$\frac{dv}{dt} = -A \cos \beta \quad (3-2)$$

$$\frac{di}{dt} = \frac{1}{v} A \sin \beta \cos \theta \quad (3-3)$$

where

$A$  is the thrust acceleration

$\theta$  is the mean anomaly (position angle)

$\beta$  is the angle between the thrust vector and the orbital plane.

The optimum choice of  $A$  and  $\beta$  over one orbit are shown in Reference 5 to be given by

$$\tan \beta = \sqrt{2} \tan k \cos \theta \quad (3-4)$$

$$A = \bar{A} \sqrt{1 + \sin^2 k \cos 2\theta} \quad (3-5)$$

where

$$\sin k = \frac{v_0}{v(t)} \sin k_0 \quad (3-6)$$

$$\sin k_0 = \frac{v_0}{\Delta u} \sin \sqrt{2} \Delta i \quad (3-7)$$

$$\Delta u^2 = v_0^2 - 2v_0 v_f \cos \sqrt{2} \Delta i + v_f^2 \quad (3-8)$$

Note that

$$L_1^2 = \frac{1}{2n} \int_0^{t_f} A^2(t) dt = \frac{1}{2n} \bar{A}^2 t_f \quad (3-9)$$

Using the above results for the optimal thrust-direction and magnitude leads to:

$$\frac{dv}{dt} = -\bar{A} \cos k \quad (3-10)$$

$$\frac{di}{dt} = \frac{\bar{A}}{\sqrt{2}v} \sin k \quad (3-11)$$

$$\frac{dm}{dt} = -\frac{m^2}{2\eta P} \bar{A}^2 \quad (3-12)$$

as the differential equations relating the change in average orbital elements to the (low) thrust acceleration. The solution to equations (3-10) and (3-11) is dependent upon the form of  $\bar{A}$ . In either event, equation (2-6) or (2-14) are still possible solutions to equation (3-12).

### 3.2 Optimal Exhaust Velocity Results

If  $\bar{A}$  is free to be chosen, the optimal choice is

$$\bar{A} = \text{constant.}$$

In that case,  $c$  is time varying,  $m(t)$  is given by equation (2-6), and the solution to equations (3-10) and (3-11) is given by:

$$v^2(t) = v_0^2 - 2\Delta u v_0 (\cos k_0) \frac{t}{t_f} + \left( \Delta u \frac{t}{t_f} \right)^2 \quad (3-13)$$

$$i(t) = i_0 + \frac{1}{\sqrt{2}} (k(t) - k_0) \quad (3-14)$$

$$\bar{A} = \frac{\Delta u}{t_f} \quad (3-15)$$

$$c(t) = \frac{2nPt_f}{\Delta u m(t)} \quad (3-16)$$

where  $k, k_0, \Delta u$  are given by equations (3-6) to (3-8) respectively. The power,  $P$  required to accomplish this transfer has not been determined by this solution. Rather, it is free to be chosen by other means.

### 3.3 Constant Exhaust Velocity Results

If  $c$  is constrained to be a constant, the solution to equations (3-2) and (3-3) over one orbit requires elliptic integrals and is, therefore, not amenable to further analytic investigations. It turns out that the solution of equations (3-10) and (3-11) under the assumption of constrained  $\bar{A}$  (but not  $A$ ) is a very good approximation --

despite the rather large deviations of  $A$  from  $\bar{A}$ . A constant  $c$  leads to a time varying  $A$  as given by equation (2-5). The mass,  $m(t)$  is given by equation (2-14) and the solutions to equations (3-10) and (3-11) are given by:

$$v^2(t) = v_0^2 + 2c v_0 (\cos k_0)y + (cy)^2 \quad (3-17)$$

$$i(t) = i_0 + \frac{1}{\sqrt{2}} (k(t) - k_0) \quad (3-18)$$

where

$$y = \ln \left( \frac{m(t)}{m_0} \right) \quad (3-19)$$

and  $k, k_0, \Delta u$  are given by equations (3-6) to (3-8), respectively. Among the three parameters,  $P, c,$  and  $t_f$ , only two are free to be chosen. The third is determined by simultaneous solution of equations (2-11) and (2-14) at  $t = t_f$ .

### 3.4 Constraint Upon Exhaust Velocity

The expended pellets from the electric gun present a hazard not present for more conventional propulsion systems. The pellets go into an orbit of their own and are large enough to present a hazard to this and other spacecraft. At the very least, steps must be taken to ensure that no pellets remain in earth orbit. This is accomplished either by the pellets falling into the earth (small exhaust velocity) or by the pellets escaping from the earth (large exhaust velocity).

For outbound transfers between coplanar circular orbits, these limits are easily given by:

$$c < \sqrt{\frac{1}{a}} \left( 1 + \sqrt{\frac{2}{a+1}} \right) \quad (3-20)$$

and

$$c > \sqrt{\frac{\mu}{a}} (1 + \sqrt{2})$$

respectively. Numerical values for these limits are shown in Figure 3-1. The pellets always escape from the earth for inbound trajectories of interest.

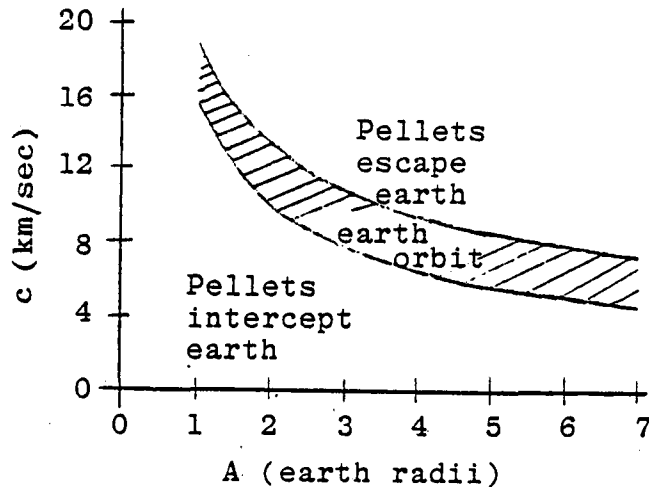


Figure 3-1 Final Orbit of Pellets for Transfers Between Coplanar Circular Orbits

The final orbit of the pellets is not answered so easily for transfers involving a plane change. The problem is simple for coplanar transfers since the pellet exhaust velocity and spacecraft velocity are colinear allowing the summation of scalars. As shown in Section 3.1 by equation (3-4) the optimal thrust direction is out of plane for part of the orbit in order to accomplish the plane change. Thus, the vectors must be summed and there would be a variation in pellet orbit over one orbit of the spacecraft.

The effect upon the masses of constraining the exhaust velocity could be easily determined for coplanar transfers since the optimal thrust directions would still be the same (tangential). However, for plane

changes, the constraint on exhaust velocity certainly would change the thrust directions. It is possible that the penalty in propellant mass would be quite small. Further investigations are, unfortunately, beyond the scope of this effort.

#### 4.0 INITIAL AND PROPELLANT MASS FOR SPECIFIC MISSIONS

This chapter presents the missions being considered along with analytic equations for initial mass and propellant mass under various assumptions about pellet exhaust velocity. The equations presented can be minimized by choice of  $P$  or  $c$ . Results of numerical minimization of these equations are presented in Chapter 5.

##### 4.1 Missions Being Considered

The electric gun is being considered as the propulsion system to accomplish the following mission:

- Go from low earth orbit (LEO) to geosynchronous orbit (GEO) in the specified time  $t_{f1}$
- Leave the payload,  $m_{\pi}$ , there
- Return to LEO in the minimum time possible given the available propulsion system
- The final mass in LEO will be the reusable power plant and propulsion system.

A second mission being considered consists simply of the LEO to GEO transfer in the specified time  $t_{f1}$ . The parameters describing these orbital transfers are given in Table 4-1. The basis for the equivalent  $\Delta u$ , taking shadowing and other non-ideal effects into account, is presented in Appendix A. The propulsion system mass,  $m_e$ , as derived in Appendix B from the data in Reference 9, is a function of the output power,  $P$

$$m_e = 17800 P + 25 \quad (4-1)$$

Table 4-1  
Missions Being Considered

	Low Earth Orbit (LEO)	Geosynchronous Earth Orbit (GEO)
Semi-major axis, a (earth radii)	1.	6.36
Mean orbital speed (km/sec)	7.75	3.07
$\Delta u$ (ideal)	4.674	
$\Delta u$ (accounting for effect of shadowing)	4.810	

The propulsion system efficiency, also derived in Appendix B, is given by

$$\eta = 1.552 P^{0.1161} C_{\max}^{-0.566} \quad (4-2)$$

For all transfers considered under this study, the exhaust velocities have been constrained to be constant during any mission phase. However, the outbound and inbound exhaust velocities were allowed to be different constants. There is some variation in results depending upon how the propulsion system size,  $P$ , is chosen and upon how the one or two constant exhaust velocities will be chosen. Table 4-2 presents the five cases of interest, the choice of  $P$ , and the mass being minimized. The basis for these choices is discussed below.

Table 4-2  
Case Designation Description

Case	Round Trip	Choice of $P$	Choose $c_1, c_2$ to optimize
I	yes	optimum	$m_o$
II	yes	optimum	$m_p$
III	yes	fixed	$m_o$ or $m_p$
IV	no	optimum	$m_o$
V	no	fixed	no free parameter

An electric propulsion system has the advantage of lower propellant mass than chemical rockets, yet there is a penalty for the large propulsion system mass. Thus the first three cases assume that the propulsion system is returned to LEO for reuse. For comparison, the last two cases assume an outbound transfer only to determine whether more propellant is required to return the power plant than the mass of the power plant itself.

Clearly, it is possible to reduce the mass requirements if more system parameters are free to be chosen. Thus Cases I, II, and IV seek the optimum propulsion system size and exhaust velocities in order to minimize some choice of mass. The minimization of initial mass (Cases I and IV) reflects the cost of putting the total system in LEO. On the other hand, minimization of propellant mass (Case II) reflects only the cost of the new fuel required to reuse a spacecraft. For outbound-only transfers (Cases IV and V) there is no relevance to minimizing propellant alone, since the system is not returned for reuse.

The optimum choice of propulsion system size and exhaust velocities may not be practical since it is possible that only certain standard systems will be available. However, the optimum results yield interesting insight into how much mass reduction is possible by a different choice of parameters. For comparison, two cases (III and V) considered a fixed propulsion system size. Since  $P$  is fixed for Case III, there is no difference between minimizing  $m_0$  and  $m_p$ , the result is the same. For Case V, with  $P$  fixed there is no free parameter. The outbound exhaust velocity must be chosen so that the transfer is accomplished in the specified time.

#### 4.2 Analytic Results for the Missions

The mass time history for both the outbound and inbound legs of the transfer is given by Equation (2-14). The initial mass for the inbound leg is the final mass from the outbound leg minus the payload. The final mass from the inbound leg is the power plant mass. In order

to satisfy these constraints, simultaneous solution of the following equations is required.

$$m_o = E_1^2(m_\pi + m_e E_2^2) \quad (4-3)$$
$$= \frac{2\eta P t_{f_1}}{c_1^2(1-E_1^{-2})}$$

where

$$E_1 = e^{\frac{\Delta u}{2c_1}} \quad (4-4)$$

$$E_2 = e^{\frac{\Delta u}{2c_2}}$$

$c_1$  = outbound exhaust velocity

$c_2$  = inbound exhaust velocity

The propellant mass is given by

$$m_p = m_o - m_e - m_\pi \quad (4-5)$$

Simultaneous solution of Equations 4-3 and 4-4 must be obtained numerically. The results of those numerical studies are presented in Chapter 5. If  $P$  is free to be chosen, it can be varied to satisfy the equations. Then,  $c_1$  and  $c_2$  can be varied to minimize either Equation 4-3 (Case I) or Equation 4-5 (Case II). If  $P$  is fixed, as in Case III, Equations 4-3 and 4-4 must be satisfied by choice of  $c_1$  leaving only  $c_2$  free to minimize  $m_0$  or equivalently  $m_p$  (since  $m_e$  is fixed).

Since the exhaust velocity for the return leg is determined by one of the above criteria, the return time of flight is not free to be chosen. It is given by

$$t_{f_2} = \frac{m_e}{P} \frac{c_2(E_2^2 - 1)}{2\eta} \quad (4-6)$$

Note that the return time is independent of outbound time if the propulsion system mass,  $m_e$ , is linearly proportional to power output and if the efficiency is the same for the different transfers. Some reduction in mass is possible for larger times of flight if the thrust is not provided continuously. Those small improvements have not been calculated since timeliness of the return was considered to be more important.

For outbound-only transfers (Cases IV and V), Equations 4-3 and 4-4 can be used by setting  $E_2 = 1$  and eliminating  $c_2$  as a parameter. Case IV seeks the minimum initial mass by choice of  $c_1$  with  $P$  constrained by the simultaneous solution of Equations 4-3 and 4-4. When  $P$  is chosen to be some fixed value (Case V), then  $c_1$  must be chosen to satisfy the two equations and there are no free parameters for an optimization.

## 5.0 MISSION ANALYSIS RESULTS

The results of numerically minimizing the mass expressions presented in Chapter 4.0 are presented in this chapter. An evaluation of electric rail gun performance for the five cases of interest are presented in Section 5.1. Electric gun performance is compared with BIMOD in Section 5.2 and the Inertial Upper Stage (IUS) in Section 5.3.

Based upon the results of an earlier study (Reference 3), the higher values of  $\Delta u$  (presented in Table 4-1) representing the effect of solar shadowing were used in this solution of the analytic equations. Thus, the results in this chapter represent the masses and power plant sizes which would be required considering the effect of solar shadowing. The times of flight, however, are the ideal times. Shadowing lengthens the transfers by about 25 percent.

### 5.1 Electric Rail Gun Performance Evaluation

The power plant size in kilowatts, initial and propellant masses in kg, and relevant exhaust velocities in km/sec are given in Tables 5-1 and 5-2 for missions to raise 2300 kg and 1150 kg payloads, respectively. The results are plotted in Figures 5-1 through 5-9 for the 2300 kg case. Similar shaped curves were obtained for the smaller payload. Some observations on these curves (and companion numbers in Table 5-1) are appropriate.

As shown in Figures 5-1 and 5-2, minimizing  $m_0$  (Case I) results in a slightly lower initial mass than if  $m_p$  is minimized (Case II). The converse is also true. Yet, as shown in Figure 5-3, there is a large difference in the required propulsion system size,  $P$ . This demonstrates the extent to which the minimum is relatively flat and comparable results can be obtained over a range of parameters.

The optimum choice of  $P$  is for Cases I and II is larger than the specified range (10 to 50 KW). The Case II results for  $P = 50$

Table 5-1  
Mission Parameters - 2300 kg Payload

Case		Outbound Time (Days)				
		30	50	70	90	110
I	Power	177	93	68	57	50
	Initial Mass	17605	9399	7165	6124	5523
	Propellant Mass	12123	5419	3631	2790	2305
	Outbound $c_1$	5.7	7.8	9.5	10.7	11.8
	Inbound $c_2$	9.5	9.6	9.7	10.7	11.8
II	Power	229	140	114	99	92
	Initial Mass	18178	9929	7704	6639	6029
	Propellant Mass	11776	5114	3355	2544	2074
	Outbound $c_1$	6.4	9.4	12.1	14.5	16.5
	Inbound $c_2$	11.3	12.8	14.2	15.3	16.5
III (power=50)	Initial Mass	Transfer not Possible	11897	7401	6146	5523
	Propellant Mass		8682	4186	2931	2308
	Outbound $c_1$		4.8	7.7	9.9	11.8
	Inbound $c_2$		5.7	7.8	9.9	11.8
IV	Power	93	68	56	49	44
	Initial Mass	8007	6163	5381	4933	4636
	Propellant Mass	4026	2631	2056	1733	1522
	Outbound $c_1$	6.8	8.6	9.9	11.1	12.0
V (power=50)	Initial Mass	9650	6349	5400	4933	4650
	Propellant Mass	6435	3134	2185	1718	1435
	Outbound $c_1$	4.4	7.1	9.3	11.2	13.0

Power in KW, masses in kg, velocity in km/sec

Table 5-2  
Mission Parameters - 1150 kg Payload

Case	Outbound Time (Days)					
	30	50	70	90	110	
I	Power	103	52	37	30	27
	Initial Mass	10244	5159	3857	3259	2918
	Propellant Mass	7233	3062	2018	1551	1265
	Outbound $c_1$	5.4	7.4	9.0	10.2	11.4
	Inbound $c_2$	9.6	9.7	9.9	10.4	11.5
II	Power	132	76	62	54	49
	Initial Mass	10593	5435	4147	3546	3195
	Propellant Mass	7069	2906	1875	1409	1142
	Outbound $c_1$	6.0	8.8	11.3	13.7	15.8
	Inbound $c_2$	11.6	13.0	14.4	15.6	16.5
III (power=25)	Initial Mass	Transfer not Possible	8231	4107	3297	2919
	Propellant Mass		6611	2487	1677	1299
	Outbound $c_1$		3.8	7.0	9.1	10.9
	Inbound $c_2$		5.2	7.2	9.2	11.0
IV	Power	50	36	30	26	23
	Initial Mass	4247	3228	2802	2559	2399
	Propellant Mass	2189	1414	1099	923	809
	Outbound $c_1$	6.6	8.3	9.6	10.7	11.7
V (power=25)	Initial Mass	5461	3374	2824	2560	2377
	Propellant Mass	3841	1754	1204	940	757
	Outbound $c_1$	4.0	6.6	8.7	10.5	12.5

Power in KW, masses in kg, velocities in km/sec

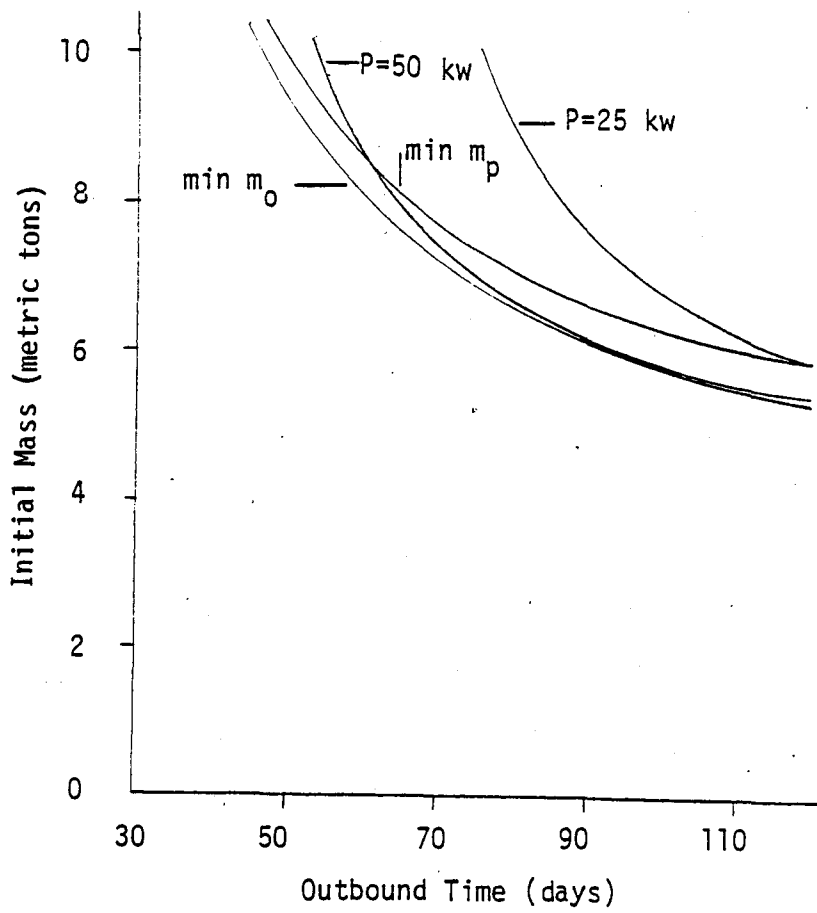


Figure 5-1 Initial Mass Required in LEO to Raise 2300 kg to GEO

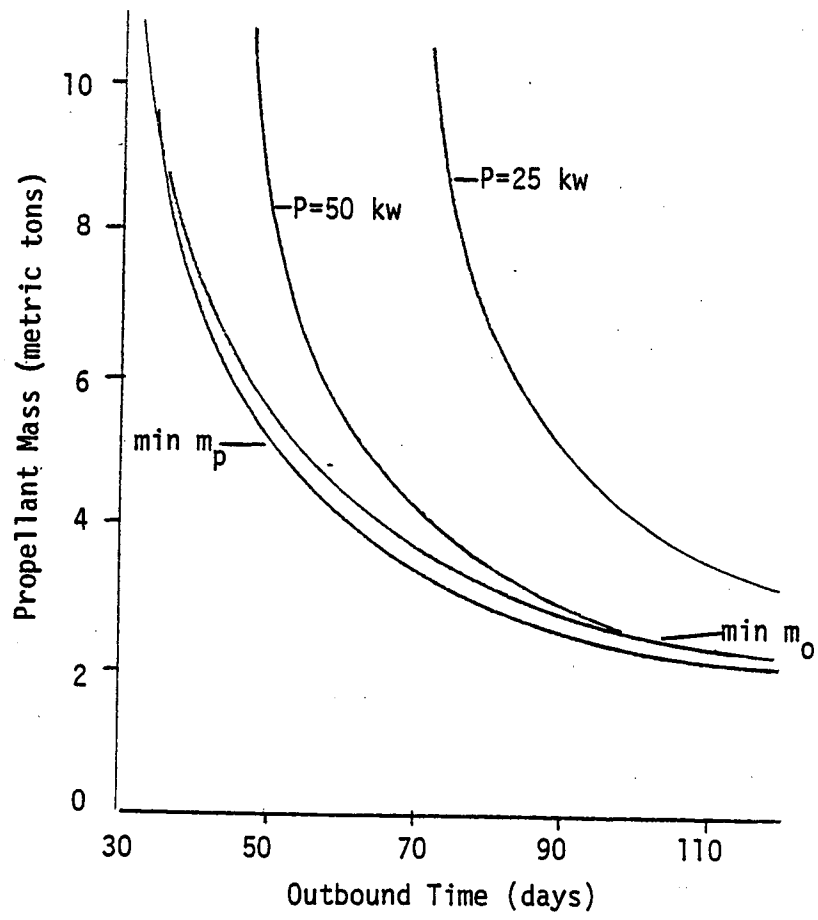


Figure 5-2 Propellant Mass Requirements to Raise 2300 kg to GEO

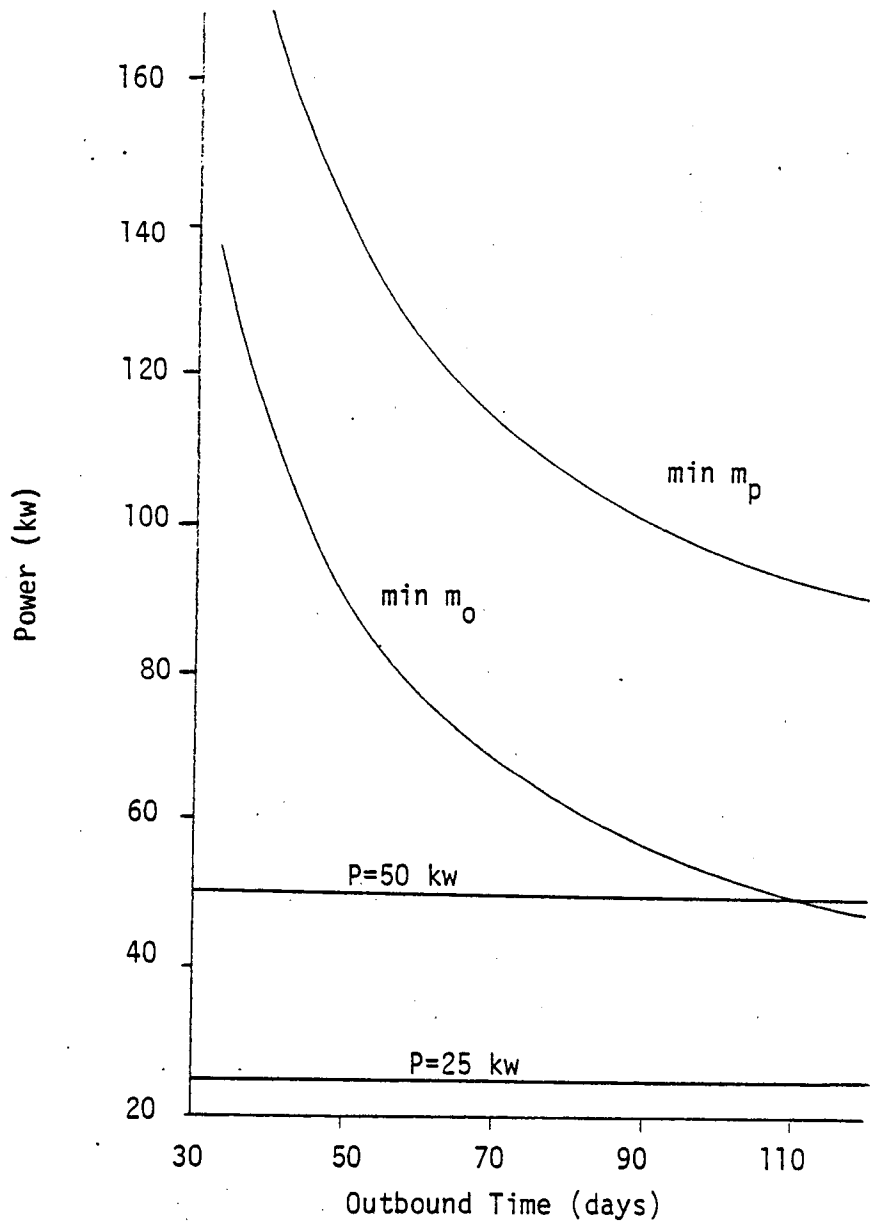


Figure 5-3 Propulsion System Size Required to Raise 2300 kg to GEO

KW shows that there is not much of an initial mass penalty for using the non-optimal  $P$ , but there is a large difference in propellant mass required. However, the Case III results for  $P = 25$  KW are much worse and clearly outside the realm in which the initial mass is insensitive to choice of  $P$ .

The primary power plant requirements are shown in Figure 5-3 under the same set of assumptions about exhaust velocity. Note that when propellant mass is minimized, the power plant size is much larger than if initial mass is minimized. The difference, of course, is that in the former case, the power plant mass only indirectly affects the cost function (since propellant is required to move it), whereas in the latter case, the power plant mass is included in the cost function.

Pellet exhaust velocities are shown in Figures 5-4, 5-5 and 5-6 for Cases I, II, and II respectively. The Case I inbound pellet velocity is very low in order to maximize efficiency, hence minimizing the power plant size which must be larger if the rail gun is less efficient. The Case II inbound exhaust velocity is larger since it is propellant mass that is being minimized and the power plant mass only enters indirectly, the same as for the above discussion about Figure 5-3. The Case III exhaust velocities are lower than either of the above. Since the Case III available power is lower than the optimum, the exhaust velocity (hence specific impulse) must be smaller in order to get the necessary thrust level.

Thus there is a tradeoff between power plant mass and propellant mass. The exact choice for any specific mission will be dependent upon the number of times the propulsion system could be reused, the mass which would have to be replaced periodically and the availability of propellant (such as empty shuttle tanks).

Any electric propulsion system has a relatively large mass for the power source and propulsion system. Although logic indicates that it would be desirable to reuse the propulsion system, the results presented in Figure 5-7 indicate that, from a mass requirements point of view, that

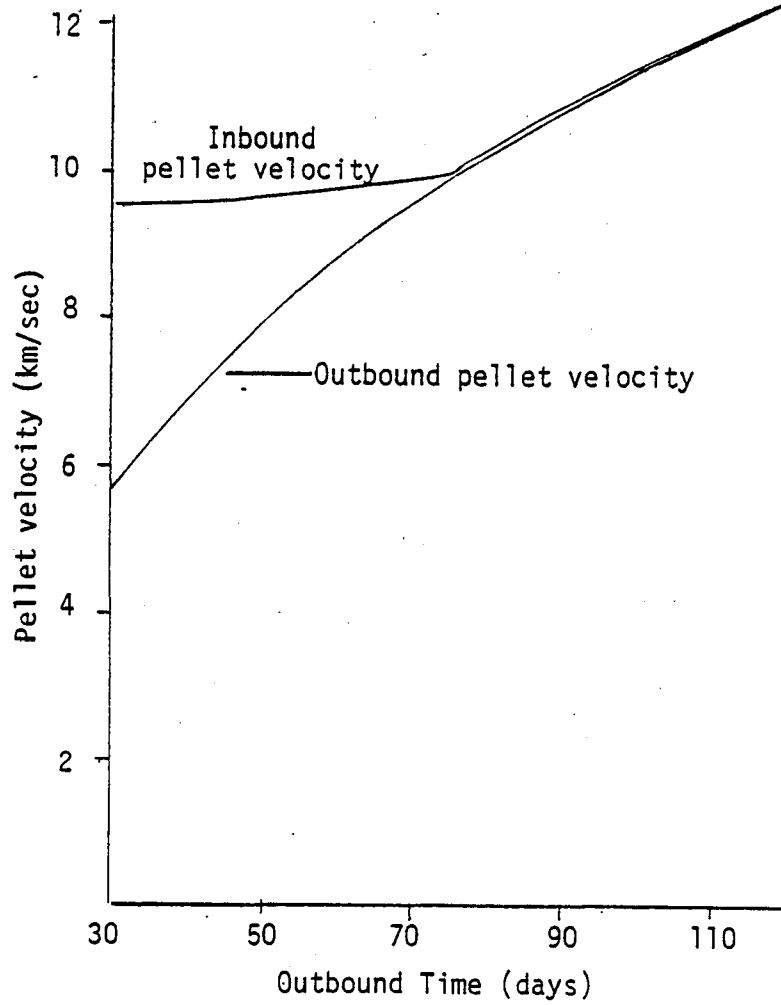


Figure 5-4 Pellet Exhaust Velocities  
Required for Case I. ( $\min m_o$ )

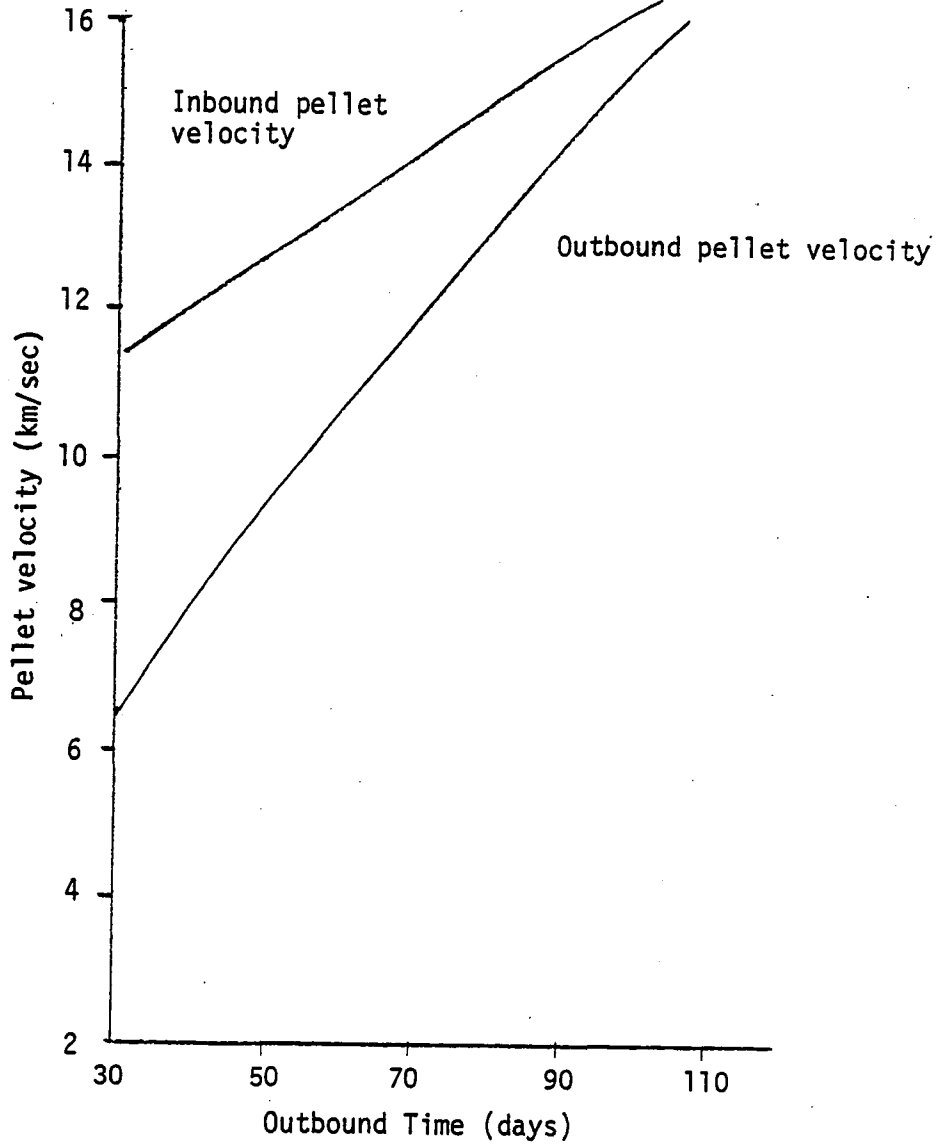


Figure 5-5 Pellet Exhaust Velocities  
Required for Case II ( $\min m_p$ )

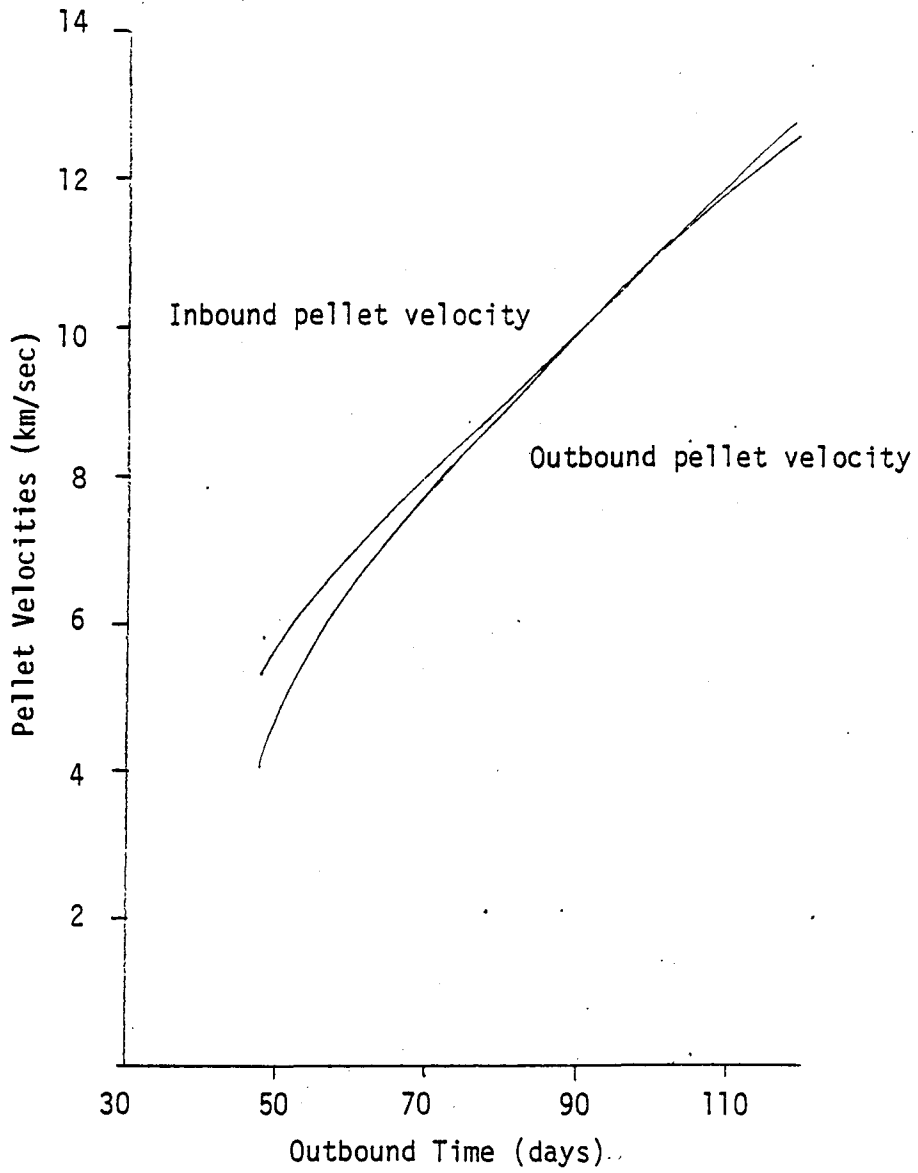


Figure 5-6 Pellet Exhaust Velocities  
Required for Case III (P=50 kw)

more propellant mass is required to return the system to LEO than the mass of a new (smaller) system for a one-way transfer. Figure 5-7 compares the propellant mass requirement for the round trip (Cases II and III) with the propellant plus propulsion system masses ( $m_p + m_e$ ) for the one-way trip (Cases IV and V). Both optimum (Cases II and IV) and fixed P (Cases III and V) results are shown. For shorter times of flight, there is a clear advantage for the one-way transfer.

The propulsion system sizes and exhaust velocities corresponding to Figure 5-7 are shown in Figures 5-8 and 5-9 respectively. Less power is required for the one-way transfer since the propellant for the return trip does not have to be moved out and then back. This also means that the exhaust velocities can be higher to make more efficient use of the fuel. The requirements on P for outbound-only transfers have the additional feature that they are closer to the specified constraints (10-50 KW).

## 5.2 Comparison with BIMOD

It is interesting to compare the electric gun performance and requirements with the BIMOD thruster which is an ion propulsion system currently available for mission planning. The power plant mass for BIMOD is given by

$$m_e = 35,429 \left( \frac{\text{kg}}{\text{MW}} \right) P ,$$

which corresponds to one BIMOD thrusters for each 6252 watts. BIMOD operates at constant exhaust velocity

$$C = 29.6 \text{ km/sec}$$

and efficiency

$$\eta = .610 .$$

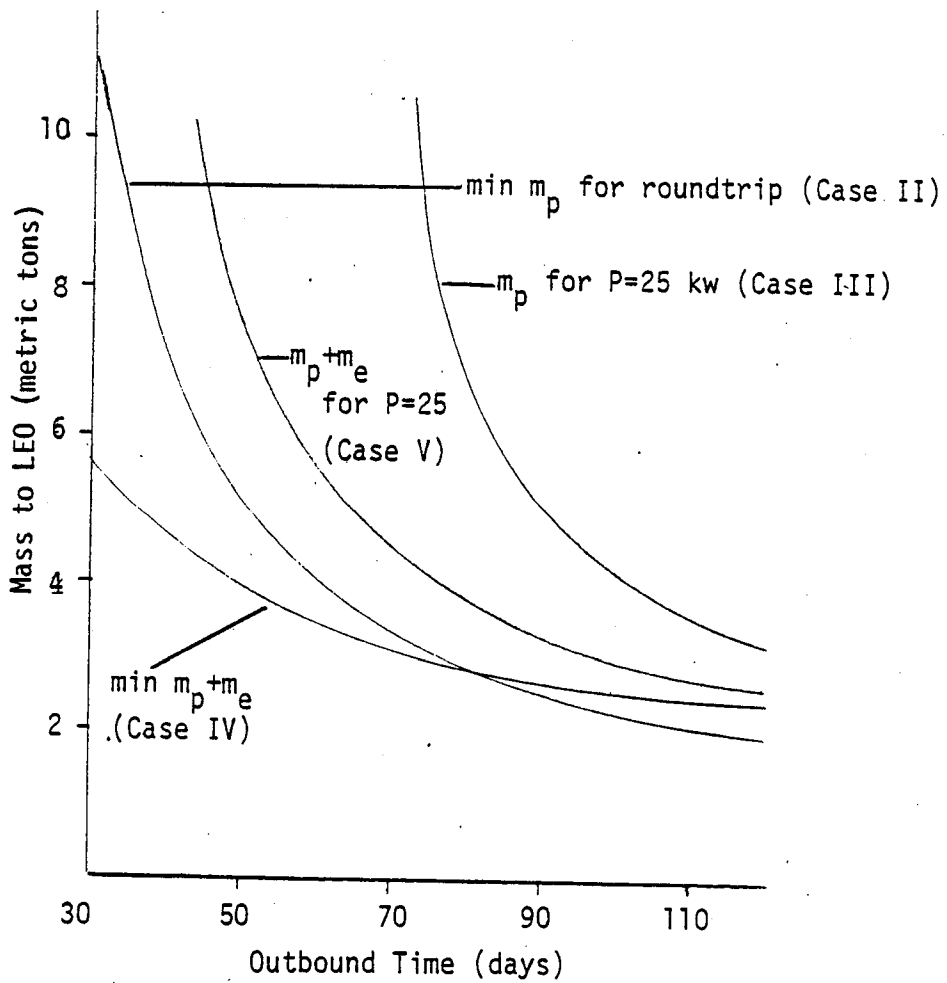


Figure 5-7 Comparison of Required Mass to LEO--Roundtrip vs. One-way

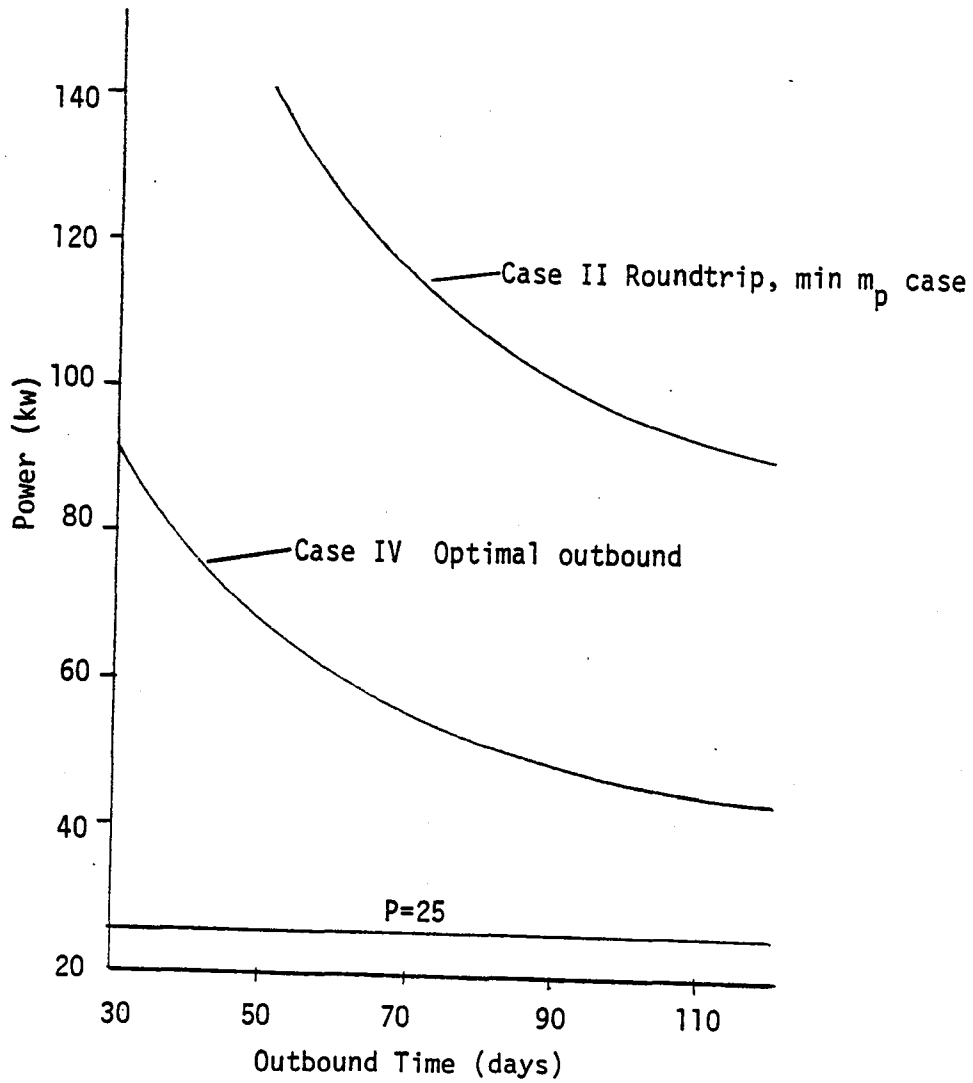


Figure 5-8 Propulsion System Size Comparison

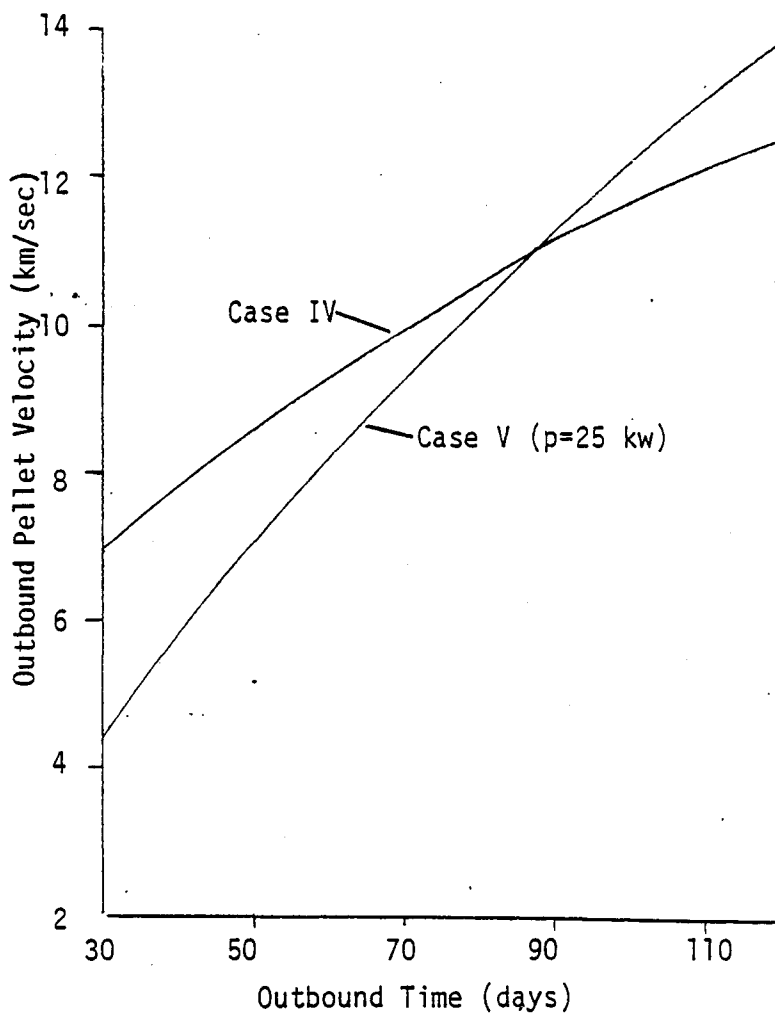


Figure 5-9 Pellet Exhaust Velocities  
Required for Outbound Only Missions

The BIMOD operates more efficiently at a higher exhaust velocity than the electric gun\*. However, it has a much heavier power plant which must be moved.

The comparison between electric gun and BIMOD initial mass and power requirements are shown in Figures 5-10 and 5-11 respectively for outbound-only transfers. The BIMOD, with its higher efficiency and exhaust velocity, can accomplish the transfer with a smaller mass only for very long transfers. For shorter transfer, the electric gun is clearly superior. Whereas, the electric gun could accomplish the transfer in less than twenty days, the BIMOD cannot accomplish the transfer in less than sixty days. The results presented here have assumed that any size system with the BIMOD characteristics could be used. The fact that integral numbers of individual BIMOD units must be selected is reflected in the stair-step curve alongside the ideal power requirement in Figure 5-11.

Since BIMOD has a fixed exhaust velocity, constraining the power plant size implies the transfer time. With 50 KW (8 BIMOD units) the transfer could be accomplished in 120 days. With 25 KW (4 BIMOD units) it would take 185 days.

The rail gun has an additional advantage over BIMOD in that its propellant is "less expensive". As pointed out by O'Neill (Reference 10), the space shuttle tanks can be carried into low earth orbit with the shuttle, at the expense of reducing the shuttle payload by an amount equal to less than four percent of the tank mass. Thus, even though the rail gun uses more propellant mass than BIMOD for longer times of flight, it is still superior since its reaction mass can be put in low earth orbit at a "lower cost". In order for BIMOD or any other ion propulsion system to be competitive with the rail gun, the propulsion system would have to be as light as the rail gun with the high efficiencies of the best ion propulsion system and very high (by current standards) exhaust velocities (specific impulse).

---

\* There is no advantage in decreasing the BIMOD exhaust velocity since the efficiency also decreases such that thrust is also lower. Decreasing electric gun exhaust velocities results in higher thrust--when it is needed.

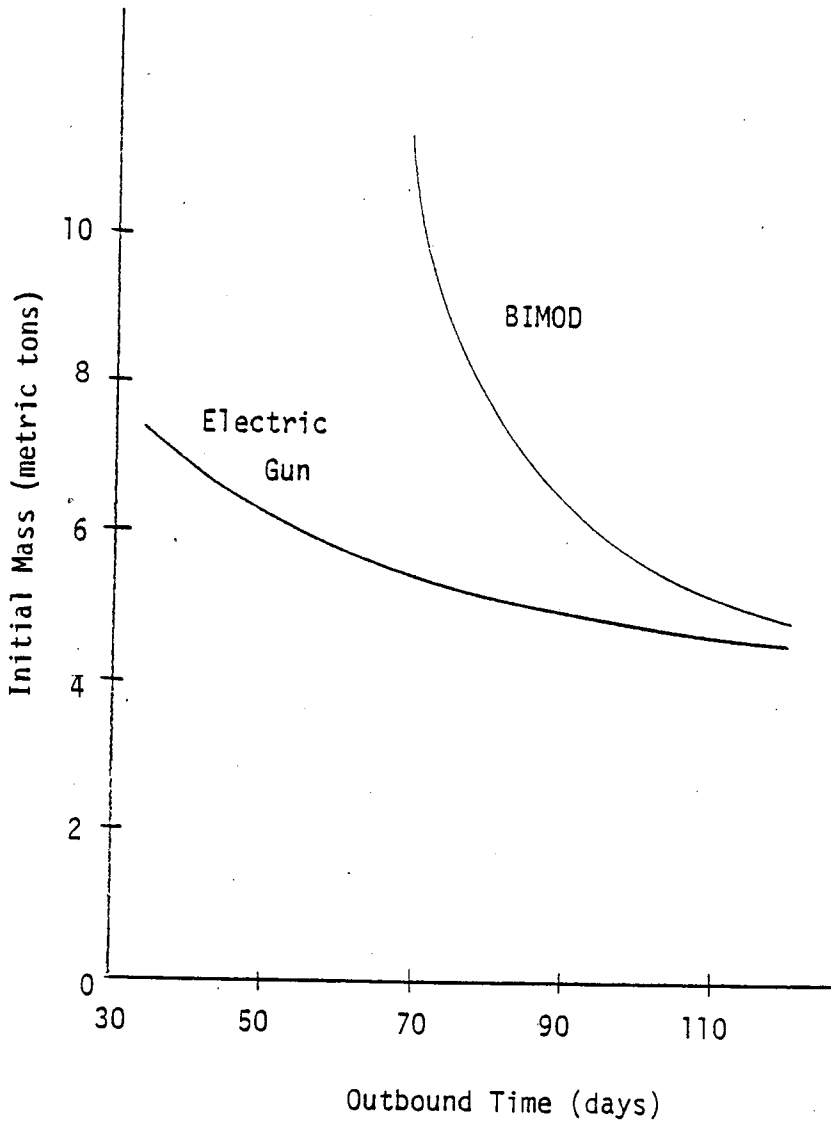


Figure 5-10 Initial Mass Requirements Comparison

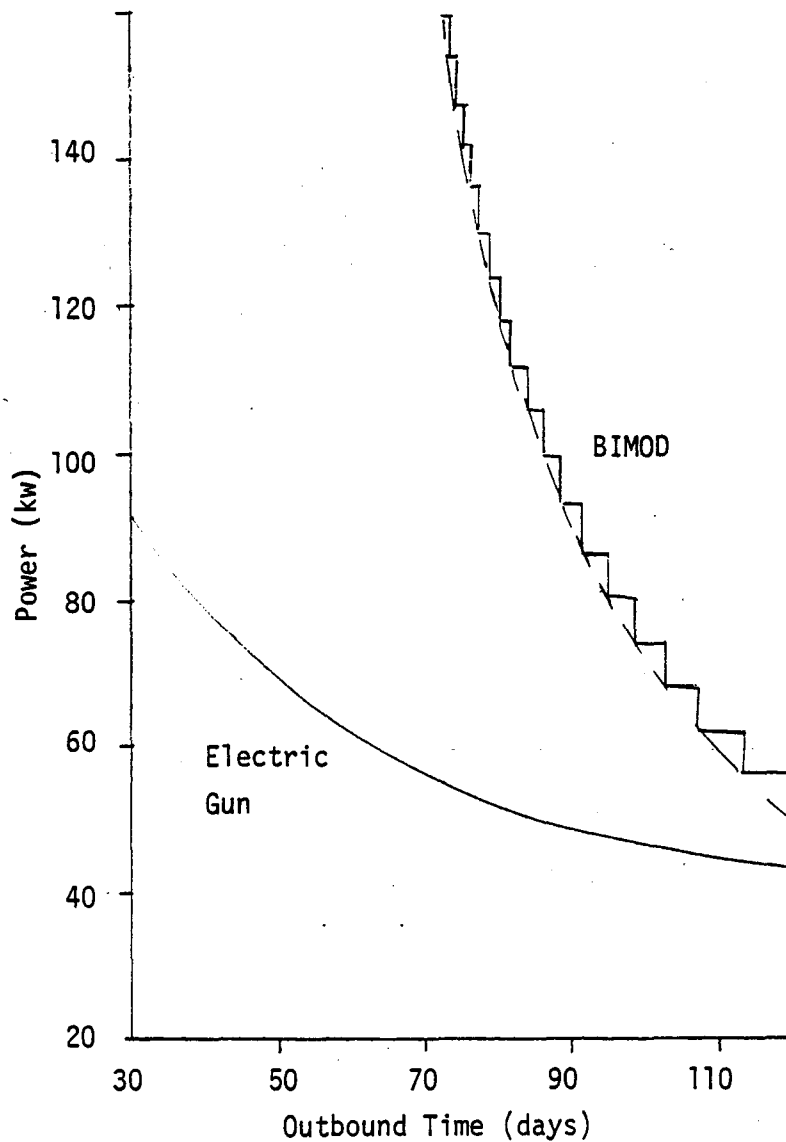


Figure 5-11 Propulsion System Requirements Comparison

### 5.3 Comparison with Inertial Upper Stage (IUS)

Another alternative propulsion system is the chemical-rocket Inertial Upper Stage (IUS). For coplanar transfers between circular orbits, the optimal transfer with the impulsive IUS is the classical Hohmann transfer with one impulse at perigee and a second impulse at apogee of an elliptic transfer orbit.

The "Two-Stage" IUS is basically sized for the transfer of a 2300 kg payload, the desired size for this study, from LEO to GEO with a plane change to equatorial orbit at GEO.

The basic energy equation for orbits

$$v^2 = \mu \left( \frac{2}{R} - \frac{1}{a} \right) \quad (5-1)$$

provides the information about the necessary IUS velocity increment at perigee,  $\Delta v_1$ , and apogee,  $\Delta v_2$ . The orbital parameters presented in Table 4-1 approximately represent the LEO to GEO parameters using  $\mu = 60$  (in the units of Table 4-1). The velocity on the initial circular orbit

$$v_o = \frac{\mu}{a_o} \quad (5-2)$$

must be increased to the intermediate elliptic orbit

$$v_1^2 = \mu \left( \frac{2}{a_o} - \frac{1}{a_1} \right) \quad (5-3)$$

Then the velocity at apogee on the elliptic orbit

$$v_2^2 = \mu \left( \frac{2}{a_f} - \frac{1}{a_1} \right) \quad (5-4)$$

must be increased to the final circular orbit velocity

$$v_f^2 = \frac{\mu}{a_f} \quad (5-5)$$

where

$$a_1 = \frac{(a_0 + a_f)}{2} .$$

The required velocity increments are

$$\Delta v_1 = v_1 - v_0 = 2.437 \text{ km/sec}$$

$$\Delta v_2 = v_f - v_2 = 1.471 \text{ km/sec}$$

The IUS with the parameters given in Table 5-3 , (as described in the documentation provided by NASA LeRC) is capable of providing

$$\Delta v_{2 \text{ IUS}} = 1.679 \text{ km/sec}$$

which is more than needed. However, provision is apparently not made to off-load fuel from the second stage, so some fuel would be wasted. The first stage would then only be able to yield

$$\Delta v_{1 \text{ IUS}} = 2.425 \text{ km/sec}$$

which is not quite the required amount.

It is thus concluded that the transfer parameters used for this study are not quite the same as the parameters used to establish the IUS as an adequate vehicle for LEO to GEO transfers. For comparison with the transfer considered in this report, compare the entire IUS first stage (10,886 kg), second stage (3856 kg) and payload (2300 kg) to yield

$$m_0 = 17,042 \text{ kg} .$$

The electric rail gun has a lower initial mass for all transfers longer than about 30 days. Further, for relatively small increases in

Table 5-3  
IUS Parameters

Stage	Designation	Rocket mass (kg)	Exhaust velocity (km/sec)	Total
1	SRM-1	1179	2.876	10,886
2	SRM-2	1134	2.869	3,856

the time of flight, the rail gun masses drop dramatically. Thus, it must be concluded that the IUS only has an advantage for very short transfer times or, in the event that there is a substantial capital cost differential.

For the rocket mass and exhaust velocities given, the initial mass would be given by

$$m_0 = (1179 + (2300 + 1134)e^{\frac{1.471}{2.869}}) e^{\frac{2.437}{2.876}}$$
$$= 16,132 \text{ kg}$$

if the IUS stages were free to be independently specified. Even for this lower initial mass, the rail gun provides superior performance for all but very short transfer times.



## 6.0 CONCLUSIONS AND RECOMMENDATIONS

All study objectives have been satisfied. The electric rail gun has been shown to provide a promising means of raising large payloads from LEO to GEO -- and in very short times relative to those achievable using BIMOD thrusters. The relatively small propulsion system mass more than compensates for a specific impulse and efficiency which are lower than for BIMOD. The rail gun provides a lower mass in LEO than the Inertial Upper Stage (IUS) for transfers longer than 15 days.

Further studies are clearly indicated. The effect upon propellant mass requirements of constraining the pellet exhaust velocity (so that no pellets remain in earth orbit) should be determined. In addition, there are a number of further investigations indicated which should explore the interrelationship between mission objectives and the characteristics of the rail gun. The studies to date have not fully explored and minimized the true costs of the system. The size and lifetime of a pellet processor are an important cost which has not been evaluated. Further, these studies have assumed the power supply and propulsion system were being reused many times. The finite (different) lifetimes of major components should be factored in. Finally, it has become apparent that, although theoretically possible, variation of rail gun exhaust velocity carries with it a penalty in efficiency. Thus, ways to vary the specific impulse without the efficiency penalty need to be explored. Once all of these effects have been modelled, optimization can be performed to determine the best choice of propulsion system parameters, given a more complete statement of cost involved.



7.0 REFERENCES

- (1) Barber, J. P., "Electric Rail Gun Application to Space Propulsion", AIAA Paper No. 79-2091, Princeton, NJ, 1979.
- (2) Sharp, G. R., J. E. Cake, J. C. Oglebay, and F. J. Shaker, Mass Study for Modular Approaches to a Solar Electric Propulsion Module, Technical Memorandum NASA TM X-3473, Lewis Research Center, March, 1977.
- (3) Vahlberg, C. Julian, Electric Gun Mission Analysis Results, Report BTS-FR-127, Business and Technological Systems, Inc., September 1980.
- (4) Vahlberg, C. J., and T. N. Edelbaum, "Transfers Between Coplanar Coaxial Ellipses Using the Combination of High- and Low-Thrust Propulsion", AIAA Paper No. 71-368, Ft. Lauderdale, 1971.
- (5) Leitmann, G., Ed., Optimization Techniques, Academic Press, N.Y., 1962.
- (6) Edelbaum, T. N., "Optimal Power Limited Orbit Transfer in Strong Gravity Fields", AIAA J., Vol. 3, No. 6, 1965.
- (7) Edelbaum, T. N., "Propulsion Requirements for Controllable Satellites", American Rocket Society Journal, August 1961.
- (8) Barber, J. P., and D. P. Bauer, Rail Gun Propulsion System Mass-Preliminary Estimates, Technical Memorandum IAP-TM-79-002, International Applied Physics Inc., October, 1979.
- (9) Bauer, D. P., personal communication, International Applied Physics Inc., October 1980
- (10) O'Neill, G. K., "The Low (Profile) Road to Space Manufacturing", Astronautics and Aeronautics, March 1978.

- (11) Sackett, L. L., H. L. Malchow, T. N. Edelbaum, Solar Electric Geocentric Transfer with Attitude Constraints: Analysis, NASA CR-134927 (Draper Lab R-901), The Charles Stark Draper Laboratory, Inc., August, 1975.
  
- (12) Sackett, L. L., and T. N. Edelbaum, Solar Electric Geocentric Transfer With Attitude Constraints: Program Manual, Report R-902, The Charles Stark Draper Laboratory, Inc., August, 1975.

Appendix AA

COMPARISON OF ANALYTIC PREDICTION WITH NUMERICAL INTEGRATIONS

In a previous study (Reference 3), the analytic results presented in Chapters 2 through 4 have been compared with the output of the Solar Electric Control Knob Setting Program for Optimal Trajectories (SECKSPOT). (References 11, 12) SECKSPOT numerically integrates the equations of motion under the assumption of fixed power and constant specific impulse. The program iterates to find the minimum time of flight which accomplishes the transfer. SECKSPOT also has the ability to include the oblateness effects upon gravity, the shadowing effects on solar cell power output, and the solar cell damage due to radiation.

The results of comparing SECKSPOT and the analytic results are shown in Table A-1. As expected, the two results are identical if there is no plane change and no shadowing. Results are surprisingly close when an inclination change is considered, given the approximations discussed in Section 3.3. Shadowing principally causes a longer transfer time with a small increase in  $\Delta u$  (propellant) required. Essentially the same change in  $\Delta u$  requirements were obtained over a range of flight times. Changes in time of flight were basically proportional to the nominal time of flight.

Although SECKSPOT has the ability to determine the effects of solar cell degradation due to radiation damage, no results have been obtained to date for these transfers. Initial attempts during the first phase of the referenced effort used shield thicknesses which, although reasonable for the newer GaAlAs solar cells, would result in almost instantaneous destruction of the silicon cells which are modeled in SECKSPOT. During the second phase, a solar cell shield thickness which would make silicon cell degradation equivalent to GaAlAs with a thinner shield was tried. That resulted in numerous underflows, overflows, and divide checks since the equivalent shield was so thick. Intermediate values were tried with only moderate success before the available resources were depleted.

Table A-1  
 Comparison of Analytic and SECKSPOT Results

Transfer	Parameter	Analytic Prediction	SECKSPOT Results	
			w/o Shadow	w/Shadow
No Inclination Change	$\Delta u$ (km/sec)	4.674	4.674	4.811
	$t_f$ (days)	40.0	40.0	51.5
Inclination Change	$\Delta u$ (km/sec)	5.757	5.802	5.814
	$t_f$ (days)	40.0	40.3	49.6

In both phases of that project the task was made more difficult due to problems with the iteration to find the minimum time solution. SECKSPOT requires an initial guess for the costates, it calculates the optimal transfer (to the wrong final conditions), and then iterates on the initial costate in order to reach the desired final condition. Two distinct problems have been encountered with the iteration. Although neither problem affects the final answer if the iteration converges (since the integration is correct), both problems affect the cost in obtaining convergence.

The first problem is with non-linearities in the optimal control problem being solved. The iterator is seeking the minimum (zero) of the sum of the squares of the errors in the orbit at the final time. However, the iterator gets trapped in local, non-zero minima which are not in the solution. Offsetting the initially guessed costates usually solves the problem. However, the program takes a lot of computer time to recognize that it is trapped and repeated trials have proven to be more expensive than expected.

The second problem is with the iteration algorithm itself. Although convergence is rapid once close to the solution, the algorithm has difficulty both in the early stages of the iteration and in recognizing when it is trapped at a local minimum. Other iterations are available which are, in fact, compatible with the SECKSPOT structure. They promise a solution to the above problems and should be able to find the minimum with fewer function evaluations (integrations along the optimal trajectory).

Although straightforward to implement, it cannot be guaranteed that other algorithms would resolve the problem of local minima. However, they would allow more trials to determine better initial costates. Unfortunately, such program changes are beyond the scope of this current effort and cannot be pursued within current project resources.



Appendix AB

PROPULSION SYSTEM MASS AND EFFICIENCY

The preliminary mass estimates provided by IAP in Reference 8 have been updated by Reference 9. Rather than providing a statement of the individual contributions to the mass, Reference 9 presents the following parametric model obtained by a curve fit to results from a more complex model. The power plant mass in kg is given by

$$25 + .0178 P_W \quad (B-1)$$

In addition, the efficiency is now given parametrically by

$$13.67 m_{\text{Pellet}}^{0.104} C_{\text{MAX}}^{-0.299} \quad (B-2)$$

where

$C_{\text{max}}$  = maximum exhaust velocity (km/sec)

$g$  = 0.009806 km/sec<sup>2</sup>

$P_W$  = solar cell output power (watts) (B-3)

$P$  = solar cell output power (MW)

The pellet mass is determined from the available energy

$$\eta P = \frac{1}{2} m_{\text{pellet}} C^2 f \quad (B-4)$$

where  $f = 9$  shot/sec is the optimum frequency for operation.

Following an algebraic manipulation and a change of units, the propulsion system mass and efficiency can alternatively be expressed as

$$m_e = 17,800P + 25 \quad (B-5)$$

$$\eta = 1.552 C_{\max}^{-0.566} p^{0.116} \quad (B-6)$$

Appendix AC

GLOSSARY OF SYMBOLS

The symbols used in this report are summarized in this appendix. They are logically grouped into three categories.

Orbital Parameters

A = Thrust acceleration from the propulsion system

a = semi-major axis of the orbit

i = inclination of the orbital plane

k = intermediate variable for description of the orbital elements

$t_f$  = total transfer time between orbits

v = mean orbital speed of the spacecraft in the orbit

$\Delta u$  = equivalent change in spacecraft velocity caused by the propulsion system

$\beta$  = the angle between the thrust vector and the orbital plane.

$\theta$  = the mean anomaly (position angle)

$\mu$  = gravitational constant

Propulsion System Parameters

$c$  = fuel exhaust velocity  $\geq 0$ .

$P$  = total power provided by power supply.

$\eta$  = propulsion system efficiency.

Mass Expressions

$$E = e^{\frac{\Delta u}{2c}}$$

= parameter used to describe mass change during constant exhaust velocity thrusting

$$L^2(t) = \frac{1}{2} \int_0^t \frac{A^2(s)}{\eta(s)} ds$$

= parameter used to describe mass change during optimal exhaust velocity thrusting

$m$  = total spacecraft mass

$\dot{m}$  = rate of depleting fuel

$m_0$  = initial total mass in LEO

$$= m_e + m_\pi + m_p$$

$m_e$  = mass of propulsion system including solar cells, power conditioning, rail gun, etc.

$m_p$  = total propellant mass expended for the mission

$m_{\pi}$  = mass of payload.





